



THE HONG KONG
POLYTECHNIC UNIVERSITY

香港理工大學

Pao Yue-kong Library

包玉剛圖書館

Copyright Undertaking

This thesis is protected by copyright, with all rights reserved.

By reading and using the thesis, the reader understands and agrees to the following terms:

1. The reader will abide by the rules and legal ordinances governing copyright regarding the use of the thesis.
2. The reader will use the thesis for the purpose of research or private study only and not for distribution or further reproduction or any other purpose.
3. The reader agrees to indemnify and hold the University harmless from and against any loss, damage, cost, liability or expenses arising from copyright infringement or unauthorized usage.

If you have reasons to believe that any materials in this thesis are deemed not suitable to be distributed in this form, or a copyright owner having difficulty with the material being included in our database, please contact lbsys@polyu.edu.hk providing details. The Library will look into your claim and consider taking remedial action upon receipt of the written requests.

The Hong Kong Polytechnic University
Department of Applied Physics

Solid Polymer Electrolyte and Its Composites with
Functional Ceramics

Submitted by

Chau Kam Hong

A thesis submitted in partial fulfilment of the requirements for
the degree of Master of Philosophy

August 2008

CERTIFICATE OF ORIGINALITY

I hereby declare that this thesis is my own work and that, to the best of my knowledge and belief, it reproduces no material previously published or written, nor material that has been accepted for the award of any other degree or diploma, except where due acknowledgement has been made in the text.

_____ (Signed)

CHAU Kam Hong (Name of student)

Abstract

Composite films consisting of lead zirconate titanate (PZT) inclusions dispersed in the polymer electrolyte polyethylene oxide (PEO) were prepared. Their piezoelectric coefficients d_{33} and pyroelectric coefficients p were measured. It is found that both coefficients are increased almost proportional to the volume fraction of the ferroelectric ceramic phase. For a 34% PZT composite, d_{33} and p are 170 pC/N and 120 $\mu\text{C}/\text{m}^2\text{K}$ respectively. The d_{33} is 7 times higher than the PZT/polyvinylidene fluoride (PVDF) composite and p is 30% higher than that of the PZT/polyurethane (PU) composite with similar ceramics content. It is believed that the enhancement is same as the PZT/PU, which is due to the high electrical conductivity of polymer electrolyte matrix. The conductive matrix helps stabilizing the poled PZT, and on the other hand, enhances amount of induced current between electrodes. Moreover, comparing with hours of poling procedure of ordinary ferroelectric/polymer composites, the poling time of PZT/PEO composites is reduced to the order of few minutes. This is also the advantage of choosing a conductive matrix. These results are confirmed by the theoretical models which take the conductivity of matrix into consideration.

In addition to the high piezoelectric and pyroelectric activities of PZT/PEO composites,

the magnetoelectric effects of the 3-phase composites with PEO matrix were also investigated. The composites, which are in 0-0-3 connectivity consisted of Terfenol-D particles and PZT particles blended in the PEO matrices. As an a.c. magnetic field applied to the samples, the induced electrical charges flow in external circuit under short circuit condition was measured. The piezoelectric PZT induced the surface charges while it was stressed by the magnetostrictive Terfenol-D as a result of the changing magnetic field. Compared with the samples with poly(methyl methacrylate) (PMMA) matrix, the magnetoelectric signals of the samples with PEO matrix are found to be greater. While samples of LiClO_4 doped PEO matrix exhibit the largest magnetoelectric signals. These results show that the large magnetoelectric signals should be attributed to the high ionic conductivity of the polymer electrolyte PEO.

Publications

Chau, K.H., Wong, Y.W. and Shin, F.G. "Enhancement of piezoelectric and pyroelectric properties of composite films using polymer electrolyte matrix". *Applied Physics Letters*, Vol.91(25), pp.2529-10 (2007)

Tsang, C.H., Chau, K.H., Wong, C.K., Wong, Y.W. and Shin, F.G. "Modeling of the Magnetoelectric Effect of Three-Phase Multiferroic Particulate Composites". *Integrated Ferroelectrics*, Vol.100 (1), pp.177-197 (2008).

Acknowledgements

I would like to acknowledge the support of my supervisor Dr Y. W. Wong for his excellent guidance, constant encouragement and invaluable advice throughout the project. My special thanks are also extended to Prof. F. G. Shin for his fruitful discussion and invaluable suggestion in my project.

I would like to deeply thank Dr. C. H. Tsang and Mr. B. Guan for their helpful assistance and discussion in theoretical aspect. It is my pleasure to thank Dr. C. W. Ong, Dr. Y. M. Poon and Prof. B. Ploss for their support and helpful suggestions. Ms. Y. Yeung, Mr. C. S. Lo, Mr. M. N. Yeung and Dr S. T. Lau, are especially thanked also for their generous assistance.

I appreciate for all my buddies Cathy, Harry, Sherman, Winkie, Water, Albert, Ching-Yee, Fai, Flora, Fred, Gary, Helios, Janet, Kai, Matthew, Ming, Pai, Pierre, Shing, Thomas, Victoria, Willy, Yao and Zhen-Ping for their continuous encouragement and support.

Finally, I would like to thank my parent, brother, uncle Kwok and Wallace for their

encouragement in the whole study period.

This research is supported by the Hong Kong Research Grants Council (A/C: G-RGRE). I am grateful for the award of the research studentship from the Hong Kong Polytechnic University.

Table of contents

| | |
|--|------|
| Abstract | I |
| Publications | III |
| Acknowledgements | IV |
| Table of contents | VI |
| List of Figures | VIII |
| List of Tables | XIII |
| Chapter 1 Introduction | 1 |
| 1.1 Background and Scope | 1 |
| 1.2 Literature Reviews | 3 |
| 1.2.1 Polymer Electrolyte | 3 |
| 1.2.2 Ferroelectric/Polymer Composites | 4 |
| 1.2.3 Magnetoelectric (ME) Composites | 6 |
| Chapter 2 Sample Preparation and Characterization | 10 |
| 2.1 Sample Preparation | 10 |
| 2.1.1 Preparation of PZT powder | 10 |
| 2.1.2 Preparation of pure PEO and LiClO ₄ doped PEO films | 12 |
| 2.1.3 Preparation of 0-3 PZT/PEO composites | 14 |
| 2.1.4 0-0-3 Terfenol-D/PZT/Polymer Composites | 15 |
| 2.2 Characterization Methods | 17 |
| 2.2.1 Determination of PZT Volume Fraction of 0-3 Composites | 17 |
| 2.2.2 X-ray Diffraction (XRD) Analysis | 19 |
| 2.2.3 Differential Scanning Calorimetry (DSC) | 20 |
| 2.2.4 Fourier Transform Infrared (FTIR) Spectroscopy | 21 |

| | |
|---|-----|
| 2.2.5 Microstructure Analysis | 22 |
| 2.3 Experimental | 24 |
| 2.3.1 Current-Voltage (I-V) Characteristics | 24 |
| 2.3.2 Dielectric Properties and Conductivity | 25 |
| 2.3.3 Voltage-Drop Scanning along Strip of PEO Samples | 27 |
| 2.3.4 Pyroelectric Property | 28 |
| 2.3.5 Piezoelectric Property | 29 |
| 2.3.6 Magnetoelectric Properties | 30 |
| Chapter 3 Properties of PEO | 32 |
| 3.1 General Properties of PEO | 32 |
| 3.2 Electrical Properties of PEO | 39 |
| Chapter 4 Pyroelectric and Piezoelectric Properties of 0-3 PZT/PEO Composites | 49 |
| 4.1 Theoretical Aspects | 49 |
| 4.1.1 Ferroelectric Ceramics | 49 |
| 4.1.2 0-3 Ferroelectric/Polymer Composites | 53 |
| 4.2 Results and Discussion | 60 |
| 4.2.1 0-3 Composites with LiClO ₄ Doped PEO Matrix | 67 |
| Chapter 5 Magnetoelectric Effect of 0-0-3 Terfenol-D/PZT/Polymer Composites | 70 |
| 5.1 Theoretical Aspects | 70 |
| 5.1.1 Magnetoelectric Effect | 70 |
| 5.1.2 0-0-3 Ferromagnetic/Ferroelectric/Polymer Composites | 71 |
| 5.2 Results and Discussion | 79 |
| Chapter 6 Conclusions | 100 |
| References | 103 |

List of Figures

| | | |
|------------|---|----|
| Figure 1.1 | Configurations of ME laminated composites reported in literature. [Nan, et al., 2008]..... | 8 |
| Figure 2.1 | Temperature profile of sintering process..... | 11 |
| Figure 2.2 | Schematic diagram of the cross-section of stack for hot pressing. | 13 |
| Figure 2.3 | Schematic diagram of X-ray diffraction by a crystal. | 19 |
| Figure 2.4 | Cross-sectional view of sample holder for current-voltage measurement. | 25 |
| Figure 2.5 | Circuit diagram of dielectric properties measurement. | 27 |
| Figure 2.6 | Experimental methodologies for measuring potential along PEO strip.. | 27 |
| Figure 2.7 | Schematic diagram of pyroelectric properties measurement | 29 |
| Figure 2.8 | Experimental setup of magnetoelectric measurement..... | 31 |
| Figure 3.1 | DSC thermogram of PEO powder..... | 33 |
| Figure 3.2 | FTIR spectra of solution cast PEO and LiClO ₄ films, with another PEO film has been elongated unidirectional. | 34 |
| Figure 3.3 | Wavenumber from 1400 to 800 of spectra in Figure 3.2. | 35 |
| Figure 3.4 | Wavenumber from 1400 to 800 of spectra in Figure 3.2. | 36 |
| Figure 3.5 | Conformations of PEO molecules. [Takahashi, et al., 1973]..... | 36 |
| Figure 3.6 | X-ray diffraction spectra of pure PEO and LiClO ₄ doped PEO..... | 37 |
| Figure 3.7 | Crystal structure of PEO. (Dark spheres refer to O, white spheres refer | |

| | | |
|-------------|---|----|
| | to CH ₂) [Takahashi and Tadokoro, 1973]..... | 38 |
| Figure 3.8 | Dielectric constants of pure PEO and LiClO ₄ doped PEO films with aluminium electrodes. | 40 |
| Figure 3.9 | Dielectric losses of pure PEO and LiClO ₄ doped PEO films with aluminium electrodes. | 41 |
| Figure 3.10 | Conductivities of pure PEO and LiClO ₄ doped PEO films with aluminium electrodes. | 42 |
| Figure 3.11 | Current-voltage relationship of PEO with gold electrodes, after various durations after annealing (sample thickness = 0.6 mm)..... | 43 |
| Figure 3.12 | Current-voltage relationship of PEO with gold electrodes, at ambient and vacuum (around 1 mTorr) (sample thickness = 0.065 mm). | 44 |
| Figure 3.13 | Current-voltage relationship of PEO with gold electrodes, with various cycling rates (sample thickness = 0.6 mm). | 45 |
| Figure 3.14 | Current against time of pure PEO under a constant voltage 10 V. | 46 |
| Figure 3.15 | Non-linear voltage drop along the direction of applied E-field. | 47 |
| Figure 4.1 | Structure of the perovskite PZT (a) above Curie temperature with cubic structure, (b) below Curie temperature with tetragonal structure. [Physik_Instrumente, 2008] | 50 |
| Figure 4.2 | Electric dipoles in domains; (a) unpoled ferroelectric ceramic, (b) during and (c) after poling. [Physik_Instrumente, 2008]..... | 51 |
| Figure 4.3 | A typical ferroelectric P-E hysteresis loop. [Jaffe, et al., 1971]..... | 51 |
| Figure 4.4 | SEM images of (a) surface of pure PEO and (b) cross-section of 34 | |

| | | |
|------------|--|----|
| | vol% PZT/PEO composite..... | 61 |
| Figure 4.5 | Transmission optical micrograph of 34 vol% PZT/PEO composite..... | 62 |
| Figure 4.6 | Pyroelectric coefficients of PZT/PEO composites against PZT volume fraction at 26 °C. The dots are experimental results, the dash line refers to the theoretical calculations that consider dilute inclusions, and solid line refers to calculation considered concentrated inclusions..... | 64 |
| Figure 4.7 | Piezoelectric charge coefficients of PZT/PEO composites against PZT volume fraction. The dots are experimental results, and the solid line refers to the theoretical calculations that consider both concentrated inclusion and conductivities..... | 67 |
| Figure 4.8 | Piezoelectric charge coefficients of PZT/polymer composites against PZT volume fraction. The dot and cross are experimental results with pure PEO matrix and LiClO ₄ doped PEO matrix respectively, and the lines refer to the theoretical calculations that consider both concentrated inclusion and conductivities..... | 69 |
| Figure 5.1 | Conductivity of matrices, PEO and LiClO ₄ doped PEO, as a function of frequency..... | 80 |
| Figure 5.2 | Dielectric constants of Terfenol-D/PZT/polymer composites, the matrices are PMMA, PEO and LiClO ₄ -PEO, as a function of frequency..... | 81 |
| Figure 5.3 | Magnetolectric coefficients, α_{p31} of Terfenol-D/PZT/polymer composites, the matrices are PMMA, PEO and LiClO ₄ -PEO, under 5 Oe at 100 Hz sinusoidal magnetic field as a function of biasing magnetic field..... | 83 |

-
- Figure 5.4 Magnetolectric voltage coefficients, α_{E31} of Terfenol-D/PZT/polymer composites, the matrices are PMMA, PEO and LiClO₄-PEO, under 5 Oe at 100 Hz sinusoidal magnetic field as a function of biasing magnetic field..... 84
- Figure 5.5 Magnetolectric coefficients, α_{P31} of Terfenol-D/PZT/polymer composites, the matrices are PMMA, PEO and LiClO₄-PEO, under 5 Oe sinusoidal magnetic fields superimposed with 1 kOe magnetic field in various frequencies. 86
- Figure 5.6 Magnetolectric coefficients, α_{E31} of Terfenol-D/PZT/polymer composites, the matrices are PMMA, PEO and LiClO₄-PEO, under 5 Oe sinusoidal magnetic fields superimposed with 1 kOe magnetic field in various frequencies. 87
- Figure 5.7 Magnetolectric coefficients, α_{P31} of Terfenol-D/PZT/polymer composites, the matrices are PEO and LiClO₄-PEO, under 5 Oe at 100 Hz sinusoidal magnetic field as a function of biasing magnetic field. The lines denoted as theoretical modelling..... 90
- Figure 5.8 Theoretical values of $|G|$ in Terfenol-D/PZT/polymer composites, the matrices are PEO and LiClO₄-PEO, under 5 Oe at 100 Hz sinusoidal magnetic field as a function of biasing magnetic field. 91
- Figure 5.9 Magnetolectric coefficients, α_{P31} of Terfenol-D/PZT/polymer composites, the matrices are PEO and LiClO₄-PEO, under 5 Oe sinusoidal magnetic fields superimposed with 1 kOe magnetic field in various frequencies. The lines denoted as theoretical modelling..... 93
- Figure 5.10 Theoretical values of F in Terfenol-D/PZT/polymer composites, the
-

-
- matrices are PEO and LiClO₄-PEO, under 5 Oe sinusoidal magnetic fields superimposed with 1 kOe magnetic field in various frequencies. 94
- Figure 5.11 Dielectric losses of Terfenol-D/PZT/polymer composites, the matrices are PMMA, PEO and LiClO₄-PEO, as a function of frequency. 95
- Figure 5.12 Magnetolectric voltage coefficients, α_{E31} of Terfenol-D/PZT/polymer composites, the matrices are PEO and LiClO₄-PEO, under 5 Oe at 100 Hz sinusoidal magnetic field as a function of biasing magnetic field. The lines denoted as theoretical modelling..... 96
- Figure 5.13 Magnetolectric coefficients, α_{P31} of Terfenol-D/PZT/LiClO₄-PEO composites, under 5 Oe at 100 Hz sinusoidal magnetic field as a function of biasing magnetic field..... 97
- Figure 5.14 Magnetolectric coefficients, α_{P31} of Terfenol-D/PZT/(LiClO₄-PEO) composites, under 5 Oe sinusoidal magnetic fields superimposed with 1 kOe magnetic field in various frequencies..... 99

List of Tables

| | | |
|-----------|--|----|
| Table 2.1 | Content of the 3-phase ME composites in volume fraction..... | 15 |
| Table 4.1 | Mechanical properties of constituents used in calculations. | 66 |
| Table 5.1 | Parameters of constituents used in calculations. | 88 |

Chapter 1 Introduction

1.1 Background and Scope

Composites of polymers blended with functional materials have been well studied and widely applied in various areas. Particulate composites with polymer matrices are easy to be fabricated by conventional polymer processing methods like extrusion and injection moulding. The pliant polymer matrices provide good protection for brittle inclusions, these composites can be fabricated into desire shapes for various applications, for example, sensors with large area or irregular dimensions.

A 0-3 composite with the ferroelectric ceramics lead zirconate titanate (PZT) in polyurethane (PU) matrix has been studied in previous project of my research group [Lam, et al., 2004]. The pyroelectric coefficient of 30% volume fraction of PZT of the PZT/PU composite was found to be $90 \mu\text{C}/\text{m}^2\text{K}$ at room temperature, which is about 30% higher than PZT/polyvinylidene fluoride-trifluoroethylene (PVDF-TrFE) composite of the similar ceramic volume fraction. This is found to be due to the comparatively high electrical conductivity of the matrix which effectively enhances the pyroelectric effect of the composites.

Polyethylene oxide (PEO) is a polymer electrolyte, its monomer unit is (CH₂-CH₂-O), its conductivity is higher than PU by three orders of magnitudes, and can be easily increased further by the introduction of inorganic salts such as lithium perchlorate (LiClO₄). This project aim at using the PEO as a substitute of PU and the PZT/PEO composite is expected to be more pyroelectric active than the PZT/PU composite. Other than the pyroelectric effect, piezoelectric effect of PZT/PEO composite is also interested in this study, since PEO has better mechanical properties than PU, d_{33} of the composite would also be benefited by mechanical and electrical properties of PEO.

The study of PZT/PEO has extended to a 3-phase composite, which is 0-0-3 Terfenol-D/PZT/PEO composite. Magnetoelectric (ME) effect of the composite is expected to be also enhanced by the conductivity of the PEO matrix. Therefore, as LiClO₄ doped into PEO matrix, obvious increase of ME signal will be observed in terms of current or charges.

1.2 Literature Reviews

1.2.1 *Polymer Electrolyte*

Polymer electrolytes are ionic conducting solid materials, its conductivity comes from the movement of ionic species and which is assisted by the motion of macromolecule [Gray, 1997; Scrosati, 1993]. Non-ohmic behaviour of polymer electrolyte can also be explained in terms of ionic conductivity. Comparing with insulating polymers, polymer electrolytes have much higher conductivity. Many works of solid polymer electrolytes were on batteries, fuel cells and electrochromic devices [Gray, 1991; Gray, 1997].

Liquid electrolyte in lithium-reversible battery can be replaced by solid polymer electrolyte, this replacement is called all-solid-state rechargeable lithium batteries. Benefited by using of polymer electrolyte, leakage can be prevented and the batteries are easy to be fabricated in compact and laminated geometries. Moreover, polymer electrolytes maintain good contact with electrodes, even they are under stress such as the volume change due to charging and discharging of the batteries. The most common used solid electrolyte is polyethylene oxide (PEO) doped with various lithium salts [Armand, 1987; Croce, et al., 1998; Gauthier, et al., 1987; Stephan and Nahm, 2006].

Transparent polymer electrolyte are used as source of ions in electrochromic devices,

the devices can be used as switchable windows, which is controlled by an applied voltage signal [Bohnke and Bohnke, 1991; Riande, 2004].

PEO is one of the most studied polymer electrolytes with high crystallinity and low glass transition temperature. For instance, PEO of molecular weight 6000 g/mol can have a crystallinity of 95% and a glass transition temperature at around -20 °C [Bailey and Koleske, 1976; Kirk and Othmer, 1991], therefore PEO is flexible at room temperature. Within the crystalline region, the conformation of PEO is likely to be helical [Takahashi, et al., 1973]. As mentioned before, the movement of ions is assisted by polymer chain motion, the conductivity of PEO in the amorphous phase was higher than in crystalline phase.

1.2.2 Ferroelectric/Polymer Composites

Ferroelectric/polymer composites have been well studied and widely applied in various areas. One of the most studied topics is the composites in 0-3 connectivity, which contain ferroelectric ceramic particles in a polymer matrix, for example, lead zirconate titanate (PZT)/polyvinylidene fluoride (PVDF) [Das-Gupta, 1991], PZT/polyvinylidene fluoride-trifluoroethylene (PVDF-TrFE) [Chan, et al., 1999; Furukawa, et al., 1986; Skinner, et al., 1978] and PZT/epoxy resin [Furukawa, et al.,

1976]. These researches were focused on dielectric, piezoelectric, pyroelectric, ferroelectric and poling studies.

For 0-3 PZT/PVDF with 70% by weight of PZT, it has piezoelectric coefficient d_{33} equal to 24 pN/C, [Son, et al., 2007] which is less than 10% in d_{33} of pure PZT. In another study, PZT/PVDF-TrFE was investigated, in fact, PVDF-TrFE copolymer is a ferroelectric materials, but the d_{33} of that composites are around 20 pC/N at maximum in a series of PZT compositions [Zeng, et al., 2002].

In pyroelectric coefficient p , lead titanate (PT)/PVDF-TrFE with 27% PT has p around 40 $\mu\text{C}/\text{m}^2\text{K}$ [Ploss, et al., 2000]. Another research group reported that 50 vol% PZT/PVDF-TrFE has p at around 150 $\mu\text{C}/\text{m}^2\text{K}$ [Abdullah and Das-Gupta, 1990], however, the PZT content of this composite was far higher than percolation limit, so that it could be classified as 3-3 instead of 0-3 connectivity. A composite of ferroelectric barium titanate particles with lithium perchlorate (LiClO_4) doped PEO matrix has investigated by Furukawa, et al. [Furukawa, et al., 2004], which has similar constituents to composites studied in this project, however, they were focus on dielectric and conductive studies but not pyroelectric and piezoelectric effects. In some other research, ferroelectric/polymer composites with 1-3 connectivity has also been

studied [Choy, et al., 2007; Kar-Gupta and Venkatesh, 2007].

In most of the practical polymer composites, the 0-3 connectivity ferroelectric/polymer composites were made with insulating polymer matrix, the pyroelectric coefficient of composite p could be represented by Maxwell-Wagner's equation [Das-Gupta, 1991; Lam, et al., 2004; Ploss, et al., 2000],

$$p = \phi B_E p_i \quad (1.1)$$

$$\text{where } B_E = \frac{3\varepsilon_m}{(2 + \phi)\varepsilon_m + (1 - \phi)\varepsilon_i} \quad (1.2)$$

where ϕ is the volume fraction of inclusion and ε is permittivity, subscript i and m represent the inclusion and matrix respectively. However, the conductivities of both inclusion and matrix have not been considered in this model. Due to the neglecting of conductivity, the p for this model was found significantly deviated from the experimental results of PZT/PU composites [Lam, et al., 2004], and the model for p with considering conductivities of constituents which is developed by my research group will be discussed in Chapter 4.

1.2.3 Magnetoelectric (ME) Composites

The first study of the ME effect of single phase crystal can be traced back to P. Curie in 1894, and not until in the sixties of last century, as mentioned by Van den Boomgaard

[Van den Boomgaard, et al., 1976], Cr_2O_3 was found to have significant ME voltage coefficient $\alpha_E = \frac{dE}{dH}$ of 20 mV/cm·Oe. Van den Boomgaard and co-workers had prepared ME composites by unidirectional solidification of eutectic melt, with certain amount of BaO, TiO_2 , CoO, Fe_2O_3 in final compositions, α_E of that composite was found as 130 mV/cm·Oe. Afterward, the attention has been attracted to composite materials which exhibit large ME coefficients in stead of the single phase materials.

In the past decade, laminated composites includes of piezoelectric and magnetostrictive materials layers were developing in various configurations (Figure 1.1). For example, laminated PZT/ CoFe_2O_4 (cobalt ferrite)/PZT composite has α_E 170 mV/cm·Oe [Zhou, et al., 2006]. In another research group, the α_E of Terfenol-D/PZT/Terfenol-D laminate is 5 V/cm·Oe at 4k Oe biasing field, by replacing PZT with single crystal $\text{Pb}(\text{Mg}_{1/3}\text{Nb}_{2/3})\text{O}_3\text{-PbTiO}_3$ (PMN-PT) can gives 10 V/cm·Oe of α_E , they also predicted theoretically that higher thickness ratio of Terfenol-D to PZT layers would produce larger α_E [Ryu, et al., 2002]. A composite of 0-3 Terfenol-D/epoxy combined with 0-3 PZT/epoxy to fabricate a hybrid composite has configuration shows in Figure 1.1(g), a resonance peak of $\alpha_E = 8$ V/cm·Oe appeared at 59.8 kHz and around 1 V/cm·Oe at other frequencies, at a bias magnetic field 0.7 kOe [Wan, et al., 2003]

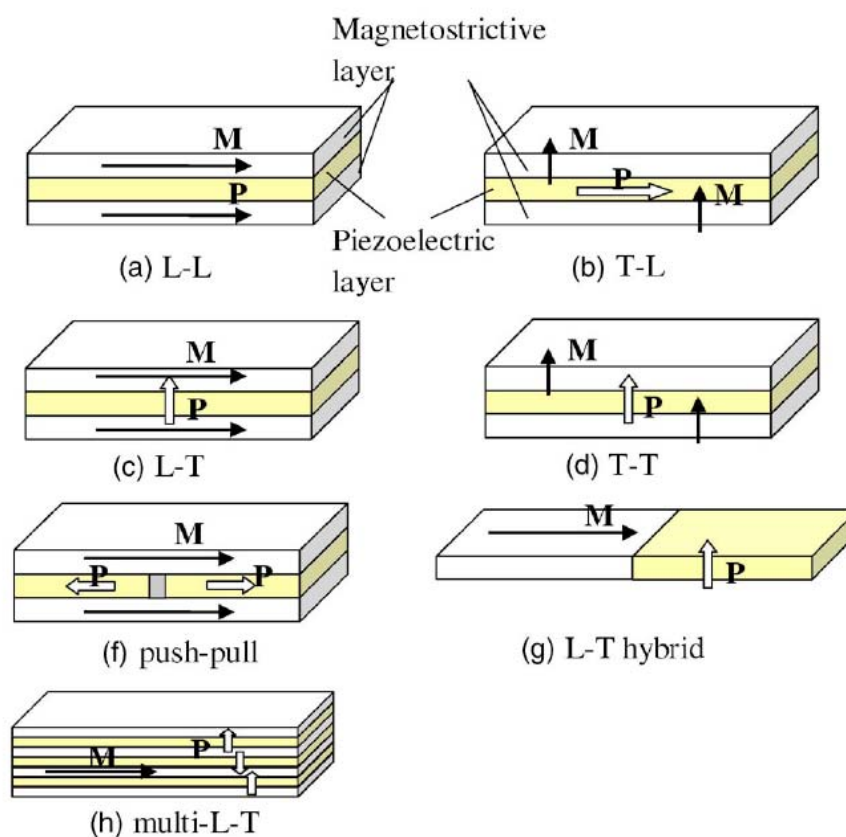


Figure 1.1 Configurations of ME laminated composites reported in literature. [Nan, et al., 2008]

In the practical sense, the piezoelectric/magnetostrictive laminates are too fragile for a wide range of applications, it also has adhesion problem between layers. Therefore, 0-0-3 magnetostrictive/piezoelectric/polymer composites are also developed [Nan, et al., 2003; Nan, et al., 2002; Shi, et al., 2004], even though the ME response of these 3-phase composites are not as strong as the laminated composites. Nan et al. [Nan, et al., 2002] fabricated Terfenol-D/PZT/PVDF particulate composites in 0-0-3

connectivity. The composites have a maximum α_E of 42 mV/cm·Oe, and they could also benefited by the simple fabrication methods.

Chapter 2 Sample Preparation and Characterization

2.1 Sample Preparation

In this study, PEO powder with molecular weight 6×10^5 and poly(methyl methacrylate) (PMMA) powders with molecular weight 1.2×10^5 was obtained from SIGMA-ALDRICH. Pre-sintered lead zirconate titanate (PZT) of Navy Type II 502 powders were bought from Piezo Kinetics, Terfenol-D discs were obtained from ETREMA and lithium perchlorate LiClO_4 was purchased from International Laboratory USA.

2.1.1 Preparation of PZT powder

The as-received PZT powder Navy Type II 502 were mixed with the polymer binder, therefore the binder should be removed from the PZT powder. The PZT powders were placed into an alumina crucible and heated up to $550\text{ }^\circ\text{C}$ for 2 hours, with temperature increased at a rate of $5\text{ }^\circ\text{C}/\text{minute}$. This binder removing process was performed in a high temperature furnace (Carbolite, RHF1600), and the crucible was not covered for the evaporation of the binder. After that, the PZT was furnace-cooled back to room

temperature.

After the binder burnout process, the PZT powder was put into the same furnace to perform sintering process. During sintering, the crucible of PZT powder was covered by alumina plate to isolating PZT from atmosphere, otherwise, excessive amount of lead will be lost from PZT at temperatures above 800 °C. Time profile for the process is shown in Figure 2.1, the PZT was first heated from room temperature with 5 °C/min rate until 850 °C, and kept for 2 hours, and then PZT was further heated up at 3 °C/min rate to 1280°C. After 1 hour, it was furnace cooling back to room temperature. Finally, the sintered PZT was hand milled into fine powder.

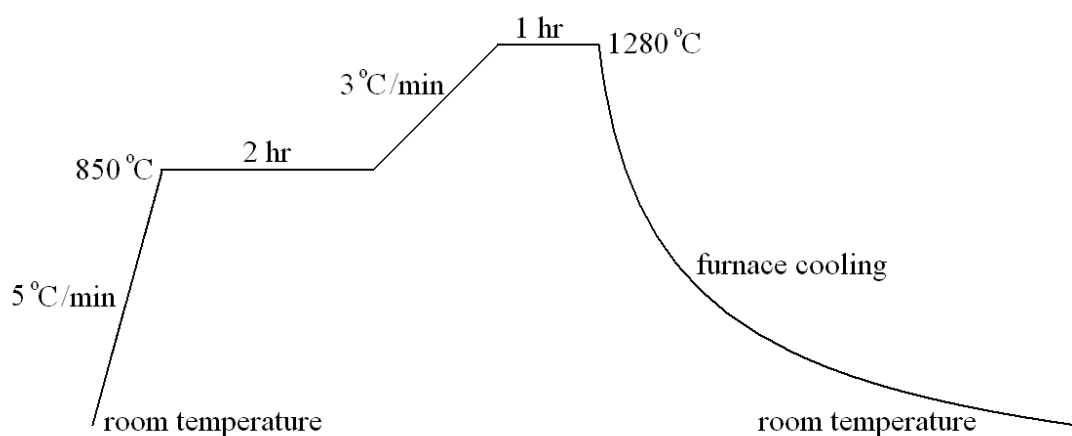


Figure 2.1 Temperature profile of sintering process.

2.1.2 Preparation of pure PEO and LiClO₄ doped PEO films

The pure PEO and LiClO₄ doped PEO films were prepared by solution casting, with dissolving PEO powder and LiClO₄ salt in de-ionized water. The thickness of the films were ranged from 6 μm to around 100 μm, the thickness can be controlled by varying the concentration of PEO in the solution. The solution should be quite dilute that to fabricate PEO films of 6 μm in thickness, this thickness is suitable for obtaining Fourier transform infrared (FTIR) spectra. However, for electrical measurement, the PEO and LiClO₄-PEO were fabricated to around 100 μm in thickness.

Before fabrication process, the PEO powder and LiClO₄ were oven-dried at 50°C for at least 12 hours, this process was aimed to remove moisture from the powder and salt. After the PEO and LiClO₄ dissolved, the solutions were cast on glass plates. The samples were then dried in oven at 48 °C for 12 hours, and then samples were detached from the glass plates.

In some of the cases, thick PEO strips, e.g. more than 100 μm should be used in some measurements. Hot pressing was applied to make those thick films. The PEO powder and spacer were placed between two poly(tetrafluoroethylene) (PTFE, or Teflon) sheets, and two parallel stainless steel plates are placed outside of Teflon sheets, and

the stack (Figure 2.2) was put into hot pressing machine (Carver 3856). Sample with final thickness around 600 μm were kept at 140°C for 30 minutes. At the same time, a moderate pressure was applied on the sample. Finally, the samples were cooled in the hot pressing machine with water. After hot pressing, the samples were annealed in oven at 50°C for at least 12 hours, this was done purposely to remove spatial charges trapped in the samples.

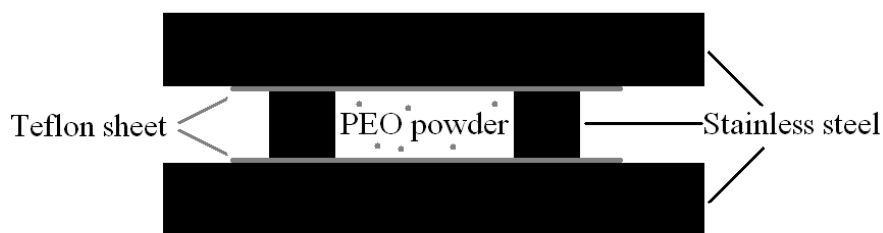


Figure 2.2 Schematic diagram of the cross-section of stack for hot pressing.

After the forming process, circular gold and aluminium electrodes were coated onto both surfaces of the samples by sputtering (Polaron Equipment, SEM-AUTOCOATING UNIT E5200) and thermal evaporation respectively. The diameter of electrodes is 10 mm for most of the samples.

2.1.3 Preparation of 0-3 PZT/PEO composites

In order to fabricate the PZT/PEO composite samples, PZT volume fractions of 10, 16, 20, 23, 34%. were mixed with PEO in de-ionized water initially. The mixtures in a viscous liquid form were placed in a vacuum chamber to remove trapped bubbles at pressure of a few mTorr, and then cast on the glass substrates to form thin films. The samples were then dried in oven at 48 °C for 12 hours. The thicknesses of the dried samples were ranged from 110 μm to 130 μm . Gold electrodes of 6 mm in diameter were coated on both sides of the samples by sputtering. d.c. poling was then performed at an applied field of 5 MV/m in silicon oil for one minute at room temperature. This poling process of the PZT phase that can be achieved in such short time which is benefited by the high conductivity of polymer matrix [Wong and Shin, 2006]. This is because charge from PEO will accumulate at the interface of PZT during poling, and depolarization field within PZT particles will be cancelled by that interfacial charge. The samples were then wrapped with an aluminium foil and grounded for one day to remove any residual spatial charges.

The fabrication process of PZT/PEO composites with LiClO_4 doped matrices was the same as the method mentioned above, with only replacing PEO powder by dried LiClO_4 -PEO films.

2.1.4 0-0-3 Terfenol-D/PZT/Polymer Composites

In this part of study, 0-0-3 composites were prepared, Terfenol-D (T-D) and PZT particles were chosen as inclusions, they were blended into 3 kinds of polymer matrices, they were PMMA, neat PEO and LiClO₄-PEO with a fixed molar ratio of [ethylene oxide]:[Li] = 1.24x10³:1. The content of each phase were listed in Table 2.1.

Table 2.1 Content of the 3-phase ME composites in volume fraction.

| Terfenol-D | PZT | Polymer |
|------------|--------|------------------------------|
| 4 volume % | 27 % | 69 % PMMA |
| 3 % | 27 % | 70 % PEO |
| 4 % | 27 % | 69 % LiClO ₄ -PEO |
| 8 % | 23 % | 69 % LiClO ₄ -PEO |
| 12 % | 19 % | 69 % PMMA |
| 12 % | 19 % | 69 % PEO |
| 12 % | 19 % | 69 % LiClO ₄ -PEO |
| 15.5 % | 15.5 % | 69 % LiClO ₄ -PEO |
| 20 % | 11 % | 69 % LiClO ₄ -PEO |

In order to fabricate the T-D/PZT/polymer composite samples, the PMMA, neat PEO and LiClO₄-PEO were dissolved into a mixture of chloroform and propan-2-ol solution respectively. The T-D and PZT particles were then mixed with the polymer solutions. The mixtures were casted into films on glass substrates. The films were then annealed at 45 °C for 12 hours. The films were further hot pressed to the controlled thickness, which were ranged from 200 μm to 280 μm. Aluminium electrodes were thermally evaporated on both sides of the samples, so that d.c. poling process can be conducted on the samples. The samples with PMMA matrices were poled at 5 MV/m for 3 hours, while the other composite samples with conductive matrices were poled at 5 MV/m for 1 minute. The residual trapped charges in the samples after poling were removed by holding the samples in short circuited condition and grounded for one day.

2.2 Characterization Methods

2.2.1 Determination of PZT Volume Fraction of 0-3 Composites

Archimedes's principle can be used to determine the volume as well as the density of an object. Therefore the density of 0-3 composites and its corresponding matrix and inclusion can be determined by applying this principle. Then the correct PZT volume fractions of the samples after forming are thus obtained.

Since PEO is water soluble, so that silicon oil was chosen as the liquid in the characterization process, its density was measured by density bottle (Technico, BS733). The volume of density bottle was calibrated by using distilled water, of which the density at 20 °C is found to be 0.9982 g/cm³ [Cohen, et al., 2003]. The density of silicon oil ρ_o for density measurement was found to be 1.064 g/cm³.

By applying Archimedes's principle, when composite sample is submerged in silicon oil, the weight of silicon oil W_o displaced is equal to the buoyant force on the object, so W_o will be the difference in weight of the sample measured in air F' and fluid F'' , i.e.

$$F' - F'' = W_o \quad (2.1)$$

we can write it in the form of mass m ,

$$m' - m'' = m_o \quad (2.2)$$

where m' , m'' and m_o are mass of sample in air, sample submerged in silicon oil and displaced silicon oil respectively. By substitute $\rho V = m$ into equation (2.2),

$$\frac{m' - m''}{\rho_o} = V = \frac{m}{\rho} \quad (2.3)$$

where V is the volume of sample and ρ is the density of sample, equation (2.3) can be rearranged as,

$$\rho = \frac{m\rho_o}{m' - m''} \quad (2.4)$$

The density of composites were measured, and the density of PEO ρ_m was found to be 1.207 g/cm^3 . On the other hand, the density of PZT powder ρ_i equal to 7.7 g/cm^3 was obtained from the manufacturer [Piezo_Kinetics, 2007]. Then, the volume fraction of PZT ϕ of PZT/PEO composites can be found by the following equation:

$$\phi = \frac{\rho - \rho_m}{\rho_i - \rho_m} \quad (2.5)$$

The content of PZT in composites can also be determined by considering the mass of used materials:

$$\phi = \frac{m_i / \rho_i}{m_m / \rho_m + m_i / \rho_i} \quad (2.6)$$

where m_i and m_m were mass of inclusion PZT and matrix PEO. The ϕ determined by the above methods are found to be closed to each other, and the latter one was used for

determine the content of 0-0-3 composites.

2.2.2 X-ray Diffraction (XRD) Analysis

When X-ray beam incident on a piece of crystal (Figure 2.3), the beam will be diffracted by different arrays of atoms in the crystal, there will be path difference between the different diffracted beams. If the phase shift due to the path difference between diffracted beams is a multiple of 2π , constructive interference will occur and results in a diffraction pattern, this pattern will satisfy the Bragg's law as given below,

$$2d \sin \theta = n\lambda \quad (2.7)$$

where n is an integer, λ is the wavelength of x-rays, d is the spacing between the lattice planes in the crystal, and θ is the incident angle.

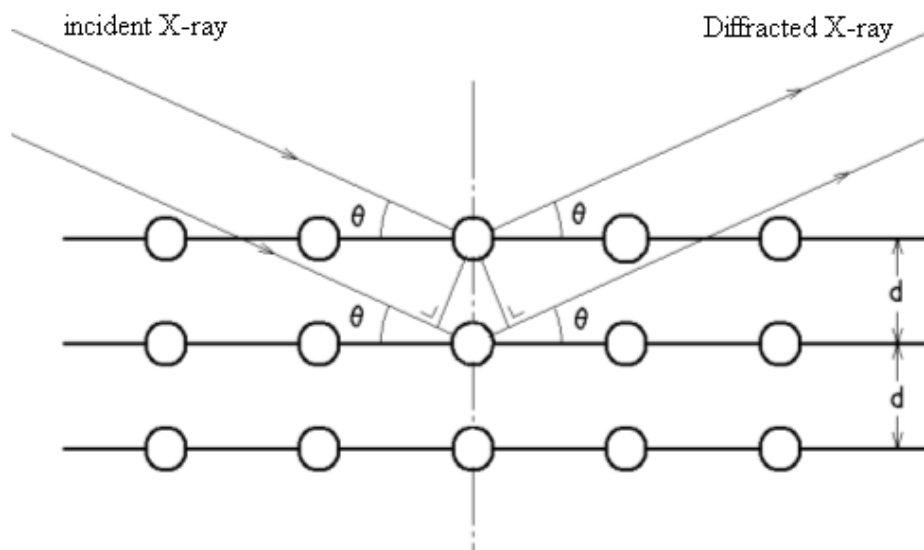


Figure 2.3 Schematic diagram of X-ray diffraction by a crystal.

In this project, the X-ray diffraction analyses of the samples prepared were performed by the X-ray Diffractometer (Philips, Xpert XRD System), the wavelength of its X-ray radiation is equal to 0.154 nm. 2 Theta-Omega ($2\theta-\omega$) scan was used in measurement.

2.2.3 Differential Scanning Calorimetry (DSC)

Calorimetry is a useful technique to characterize polymeric materials for finding its phase changes as a result of temperature change. From the results of calorimetric measurement, glass transition temperature, melting temperature or crystallization temperature can be determined.

Differential scanning calorimeter (DSC) is one of the calorimetric techniques designed to measure the enthalpy H change of a sample within a temperature range. Enthalpy H was defined as,

$$H = U + PV \tag{2.8}$$

where U is internal energy, P is pressure and V is volume of sample. From the change in temperature of sample, phase changes would be induced, and the phase changes will result in change of internal energy ΔU . For infinitesimal reversible process, change in work $dW = -PdV$ can be obtained [Finn, 1998; Mathot and Benoist, 1994], and applying first law of thermodynamics $\Delta U = Q + W$, following relations are obtained,

$$dH = dU + PdV + VdP \quad (2.9)$$

$$dH = dU - dW + VdP \quad (2.10)$$

$$dH = dQ + VdP \quad (2.11)$$

where dQ is the heat flow to the sample, since the process is in constant pressure,

$$dH = dQ \quad (2.12)$$

therefore, the change in enthalpy can be represented by the heat flow to the sample.

In this study, the DSC (Perkin Elmer, DSC7) is using power-compensation method in the measurement. For this method, two aluminium pans are placed in two nitrogen rich furnaces individually, as one of the pans is filled with sample around 10 mg in weight and the another pan is empty as a reference. The pans are heated and cooled in thermal cycles at a 10 °C/minute rate, the temperature of pans are kept at equal by compensating the heat flow from heater to the pans, and monitoring temperature by using thermometer.

2.2.4 Fourier Transform Infrared (FTIR) Spectroscopy

Fourier Transform Infrared (FTIR) Spectroscopy is to study the absorption characteristics of infrared (IR) by materials. When the frequency of irradiating IR is equal to natural vibration frequency of chemical bonds of the molecules, the IR will be

absorbed by the corresponding molecules. The natural vibration frequencies of polymeric molecules are commonly within the frequency range of IR, so that FTIR is one of the major characterization techniques for polymer.

FTIR spectrometer (Nicolet, Magna-IR 760) is used to analyze the structure of polymers. IR beam is transmitted through a Michelson interferometer and then the sample, and finally detected by an IR detector. Therefore, interferogram is obtained as a result of intensity against optical path difference. Finally, the interferogram is Fourier transformed into absorbance against wavenumber W , where W is defined as the number of waves per unit distance (in cm^{-1}) [Smith, 1979; Stuart and Ando, 1996]. A plot of absorbance versus wavenumber is called the IR spectrum.

2.2.5 Microstructure Analysis

The morphologies of samples were studied by a field emission scanning electron microscope (SEM) (Cambridge, Stereoscan 440). Its resolution can be better than 10 nm in optimum condition. An EDX elemental analyser is installed for the benefit of sample element analysis in micron-sized regions. In addition to the SEM, optical microscope (Nikon, Microphot-FXA) was also used to investigate the morphologies of samples, the distribution of constituents in macroscopic view of composite was

observed in transmission mode.

2.3 Experimental

2.3.1 Current-Voltage (*I-V*) Characteristics

From the measurement of the relationship between current I and voltage V , the conductivity of the samples can be estimated. In order to investigate the current voltage characteristics of the samples, a sample holder was built as shows in Figure 2.4.

In the sample holder, guard ring is used to eliminate any current going through the surface of samples, and a piece of Teflon is used to isolate electrode and guard ring.

The measurements were preformed by using an electrometer (Keithley, 6517A Electrometer/High-Resistance Meter), with a built-in voltage source, and it was applied as the voltage source during the *I-V* measurements.

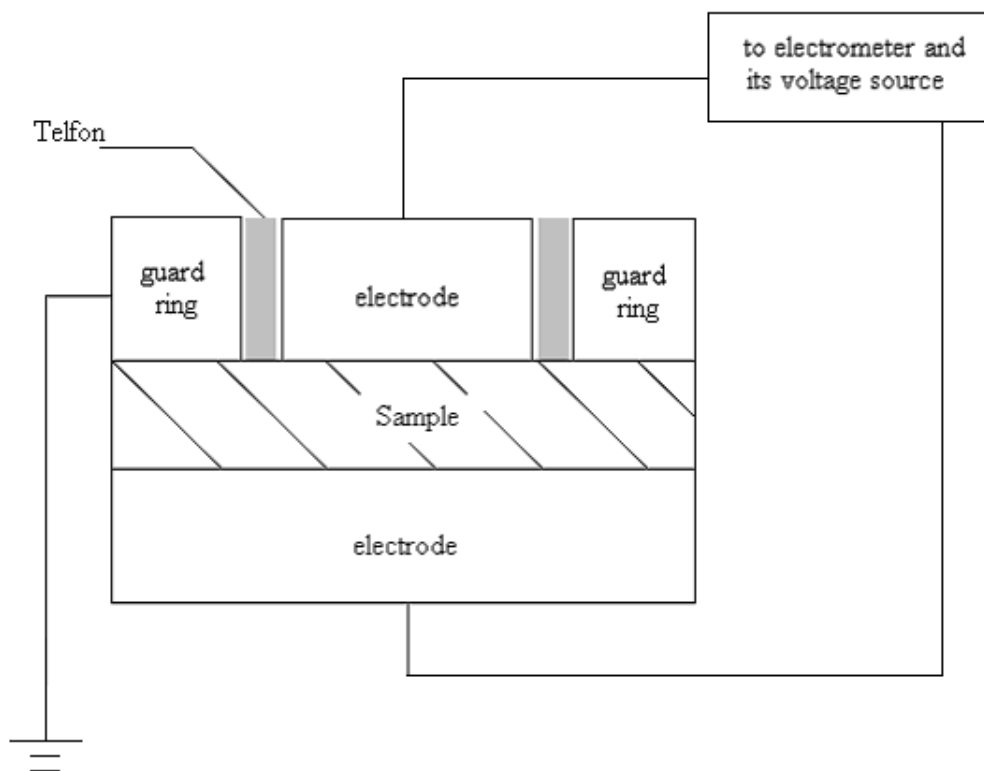


Figure 2.4 Cross-sectional view of sample holder for current-voltage measurement.

2.3.2 Dielectric Properties and Conductivity

The a.c. conductivities and dielectric properties of composites and their corresponding matrices polymers were determined by applying a 1 V sinusoidal signal on the samples in series with a standard resistor, and the samples were regarded as parallel plate capacitors. The in phase V_X^R and out of phase V_Y^R signal across the standard resistor were measured by a lock-in amplifier (Stanford Research System, SR 810 DSP), thus the a.c. conductivities and dielectric properties of samples were obtained by substituting the results to the equation:

$$\frac{V^R}{V^C} = \frac{V^R}{V - V^R} = \frac{I \cdot R}{I \cdot \left(\frac{1}{i2\pi f C^*} \right)} = i2\pi f R C^* \quad (2.13)$$

where f is frequency and C^* is the complex capacitance of sample. Considering

$V^R = V_X^R + iV_Y^R$, and a parallel plate capacitor, equation (2.13) changes into

$$\frac{V_X^R + iV_Y^R}{V - V_X^R - iV_Y^R} = i\omega R \epsilon_0 \frac{A}{d} (\epsilon_r' - i\epsilon_r''). \quad (2.14)$$

where A and d are area of electrode and thickness of sample respectively. By separating

the real and imaginary parts from the equation (2.14), dielectric constant ϵ_r' and the

dielectric loss ϵ_r'' are determined.

$$\epsilon_r' = \frac{V V_Y^R d}{2\pi f R \epsilon_0 A [(V - V_X^R)^2 + V_Y^{R2}]} \quad (2.15)$$

$$\epsilon_r'' = \frac{[(V - V_X^R) V_X^R - V_Y^{R2}] d}{2\pi f R \epsilon_0 A [(V - V_X^R)^2 + V_Y^{R2}]} \quad (2.16)$$

Subsequently the real and imaginary parts of conductivity, σ' and σ'' will be

obtained from the relations:

$$\sigma' = 2\pi f \epsilon_0 \epsilon_r'' \quad (2.17)$$

$$\sigma'' = 2\pi f \epsilon_0 \epsilon_r' \quad (2.18)$$

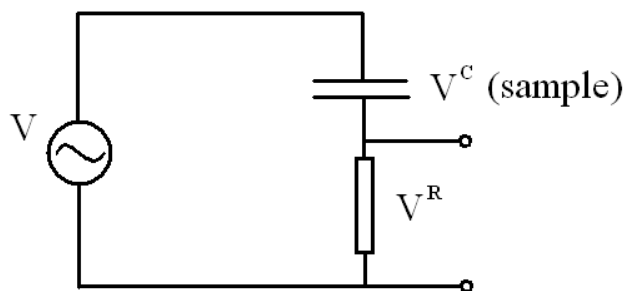


Figure 2.5 Circuit diagram of dielectric properties measurement.

2.3.3 Voltage-Drop Scanning along Strip of PEO Samples

The PEO strip was coated with gold electrodes at its both ends, one of the electrodes was connected to the ground of electrometer (Keithley, 6517A), then a 100 V constant voltage was applied on the electrode. After the constant voltage was applied for 15 minutes, the sample had reached equilibrium, a metal probe which was connected to the electrometer, for voltage measurement was scanned along the length between the pairs of electrodes.

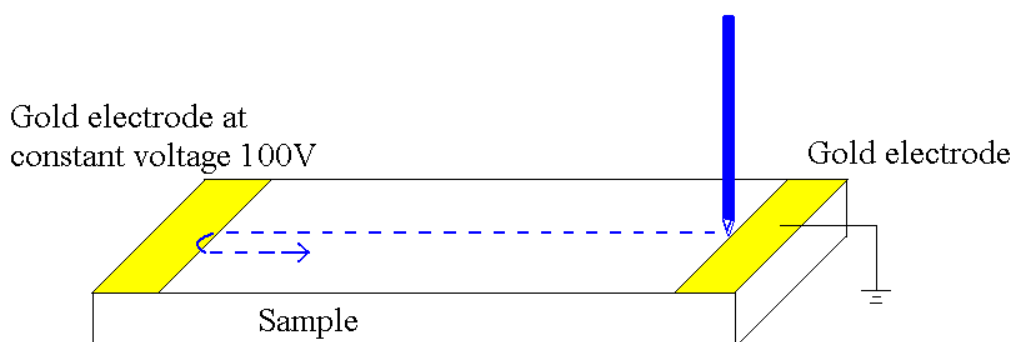


Figure 2.6 Experimental methodologies for measuring potential along PEO strip.

2.3.4 Pyroelectric Property

The pyroelectric coefficients of the series of poled 0-3 PZT/PEO composites were determined by a dynamic method in short circuit condition. The setup of measurement is shown in Figure 2.7, a sinusoidal 5 mHz reference signal from lock-in amplifier (Stanford Research System, SR 830 DSP) and thermocouple feedback was controlling a PID control with Peltier element. The thermocouple mentioned was used to monitor the temperature of the Peltier element, and the samples were placed on the Peltier element. By using this setup, the samples were driven in a 5 mHz sinusoidal heating and cooling cycle, with the amplitude of temperature modulation $T_{\Delta} = 1$ K at temperature $T_0 = 299$ K, therefore the temperature of samples $T(t)$ is

$$T(t) = T_0 + T_{\Delta} \sin \omega t . \quad (2.19)$$

The thermally induced current was measured by a digital electrometer (Keithley, 617), and was fed to a lock-in amplifier for phase analysis. The current 90° out of phase with the temperature modulation (in phase with the heating rate, $\frac{\partial T}{\partial t}$) was the pyroelectric current I_p , and then the measured pyroelectric coefficient p can be found

from the equation (2.19) and current density $J = \frac{I_p}{A}$:

$$p = -\frac{I_p}{\omega A T_{\Delta} \cos \omega t} \quad (2.20)$$

where A was the area of electrode.

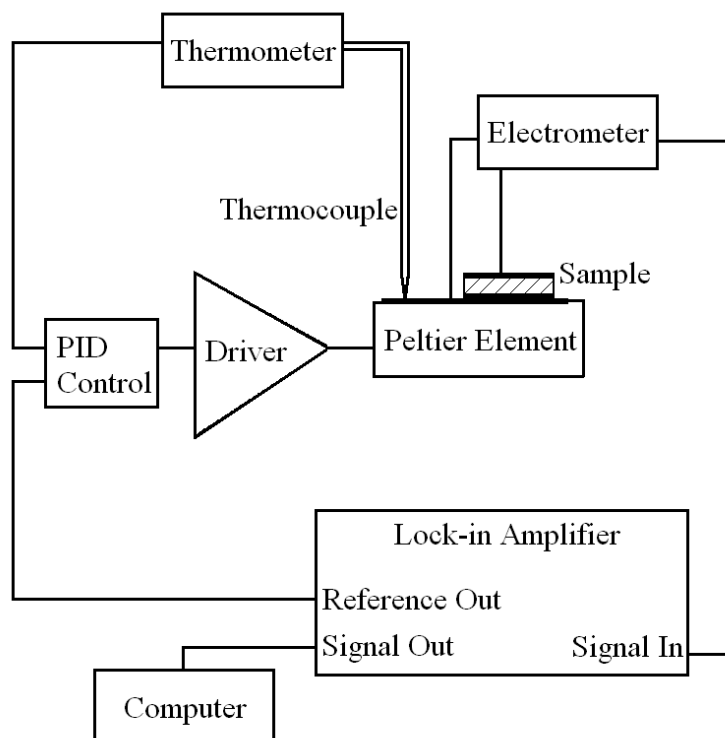


Figure 2.7 Schematic diagram of pyroelectric properties measurement

2.3.5 Piezoelectric Property

The piezoelectric property of the samples in term of piezoelectric coefficients d_{33} was measured by using a piezo-tester (Institute of Acoustics Academia Sinica, ZJ-3D).

Samples with top-down electrode were subjected to sinusoidal compressive stress and which the vibration frequency is 60 Hz.

2.3.6 Magnetoelectric Properties

The magnetoelectric (ME) measurements was conducted under short circuit condition, the setup is depicted in Figure 2.8. The ME signals of the 3-phase composites were measured by applying a 5 Oe a.c. magnetic field with a biased d.c. magnetic fields. The magnetic field was measured by a Gauss-meter (Hirst Magnetic Instruments LTD, GM05), the a.c. field was measured as root-mean-square value. All of the magnetic fields were applied parallel to the samples surface, i.e. in-plane configuration, and the changes in amount of induced charges were measured by using a charge amplifier (Kistler, 5011). The samples were gently held within a sample holder by using plastic screws, and the metal contact of the holder to the sample electrodes were in shape of thin lines, this can suppress the eddy current induced. The output signals from charge amplifier were then fed to a lock-in amplifier (Stanford Research System, SR 810 DSP) for signal recovery, and the charge output was displayed as the root-mean-square value.

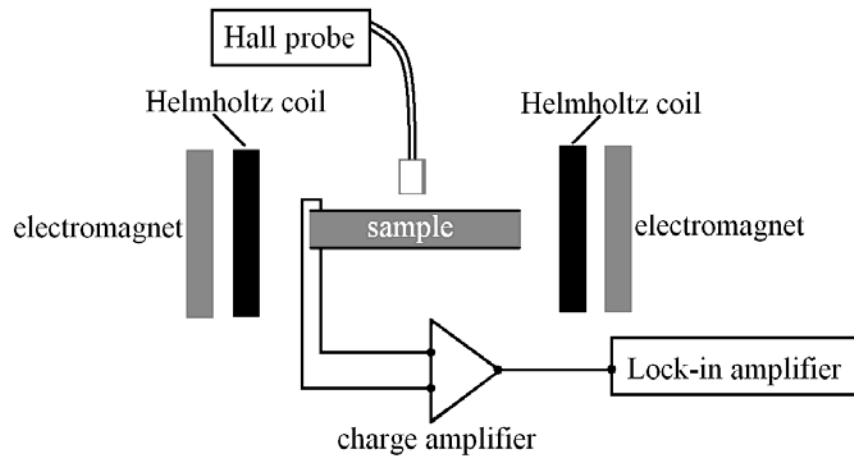


Figure 2.8 Experimental setup of magneto-electric measurement.

Chapter 3 Properties of PEO

3.1 General Properties of PEO

This section is mainly focus on the structure analysis of PEO by using various characterization techniques mentioned in the last Chapter. Differential scanning calorimeter (DSC) thermogram of PEO powder is shown in Figure 3.1. A peak of crystalline melt is found in the heating curve, where the peak begin at 37 °C, the onset temperature at 61 °C, then fall to the peak minimum at 67 °C and the melting process finish at 70 °C. These values agree with the specification of melting point from 61.7 to 66.6 °C [Sigma-Aldrich, 2007]. For the cooling curve, the recrystallization start at 50 °C, onset temperature appear at 49 °C, the maximum of the peak locate at 44 °C and the recrystallization finish at 23 °C. In this DSC thermogram, the glass transition temperature have not been observed, this is because the glass transition of PEO with molecular weight 600 kg/mol is around -50 °C [Kirk and Othmer, 1991].

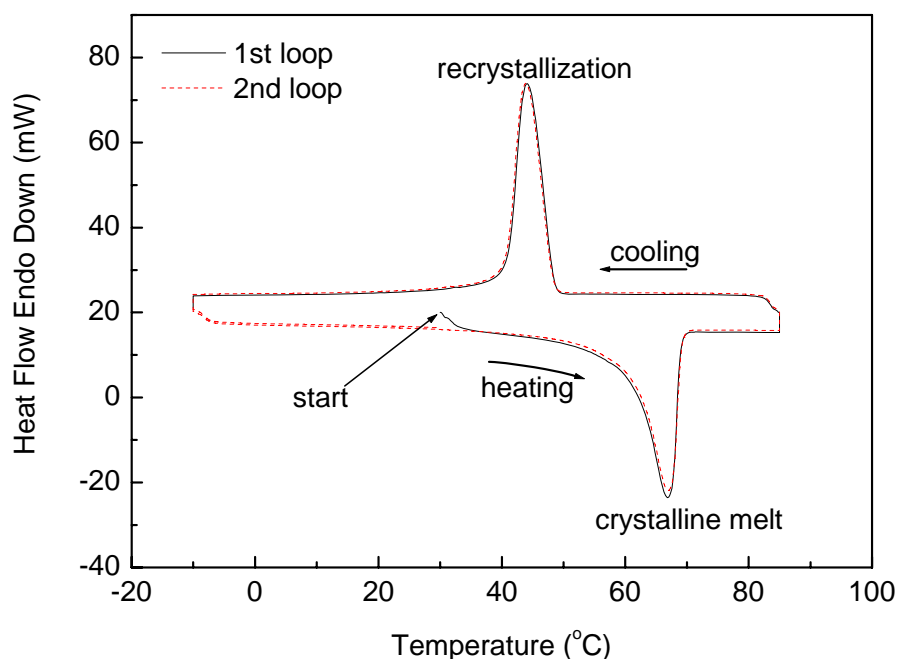


Figure 3.1 DSC thermogram of PEO powder.

Fourier Transform Infrared (FTIR) spectra of various solution cast PEO films are shown in Figure 3.2, they are PEO film with 6 to 7 μm in thickness, PEO sample was stressed in a single direction, and its thickness was drawn from 50 down to 25 μm , and the last sample is a LiClO_4 doped PEO film with 4mm in thickness. Due to the difference in thickness, the transmittance of 4 μm film is the highest, and the 25 μm film is the smallest. By comparing with correlations charts [Smith, 1979; Stuart and Ando, 1996], the broad absorption peak around 2900 cm^{-1} would be corresponded to the C-H stretching of CH_2 molecules. Most of the absorption peaks locate between 1400 and 800 cm^{-1} , so that this part of the spectra are enlarged for further investigation.

According to the literature [Marcos, et al., 1990], the peaks are assigned and identified as two conformations, the characters “H” and “T” represented helical and all-trans structure respectively in Figure 3.3 and 3.4.

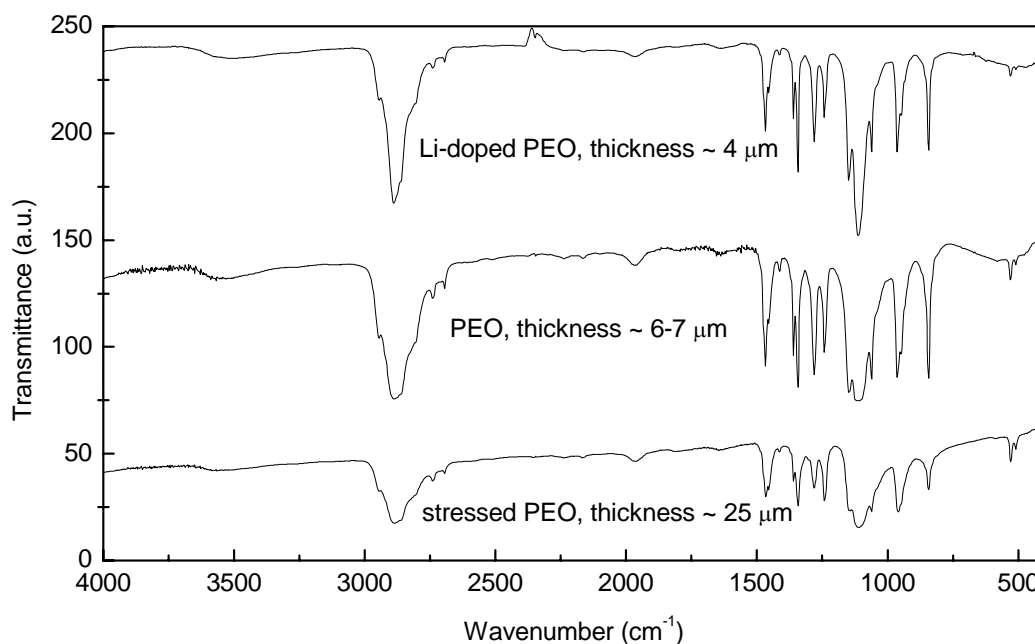


Figure 3.2 FTIR spectra of solution cast PEO and LiClO₄ films, with another PEO film has been elongated unidirectional.

In the stressed PEO film, taking CH₂ twisting as an example, its 1241 cm⁻¹ is stronger than 1281 cm⁻¹, and this reverse for the untreated PEO film. Similar observation can also be found in CH₂ wagging (1342 cm⁻¹ and 1360 cm⁻¹) and CH₂ rocking (962 cm⁻¹ and 949 cm⁻¹). Therefore, the stressed PEO contains more molecules in all-trans

structure than in the helical structure, this result match with previous research stated that [Takahashi, et al., 1973], all-trans structure is only stable under tension and corresponding to zigzag conformation (Figure 3.5). The most stable helical structure of PEO is represented as a 7/2 helix conformation, and denote the trans-trans-gauche conformation.

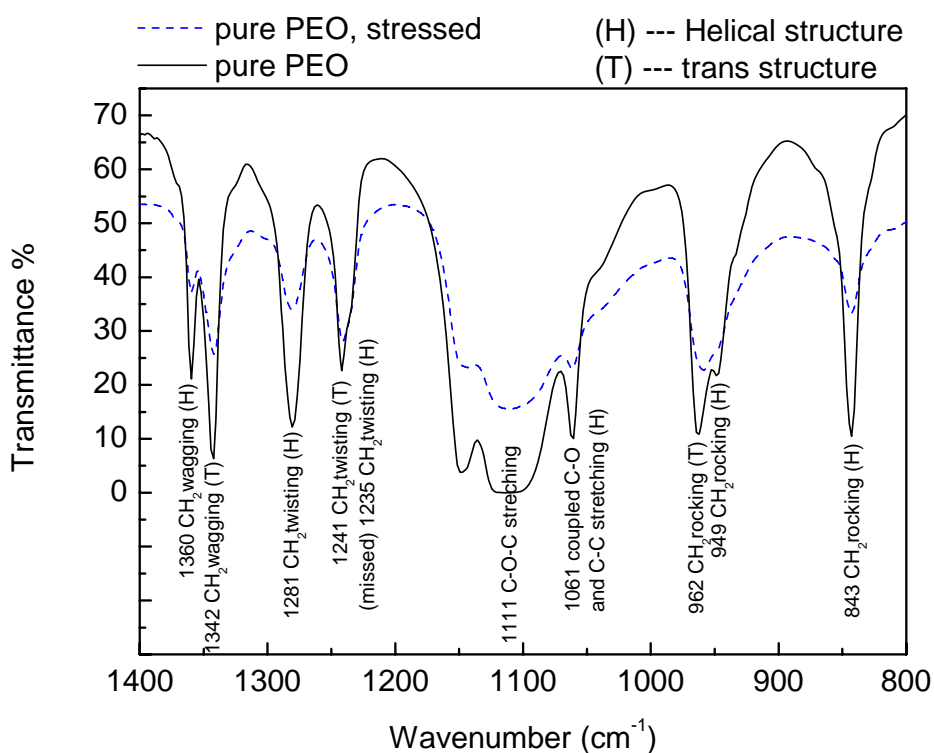


Figure 3.3 Wavenumber from 1400 to 800 of spectra in Figure 3.2.

In Figure 3.4, no change in FTIR spectrum can be observed as LiClO₄ salt doped in PEO, including the positions of peaks and generally the relative intensities between the

two structures. Therefore, the doping level of LiClO_4 (molar ratio [ethylene oxide]:[Li] = $1.24 \times 10^3:1$) do not affect the structure of PEO.

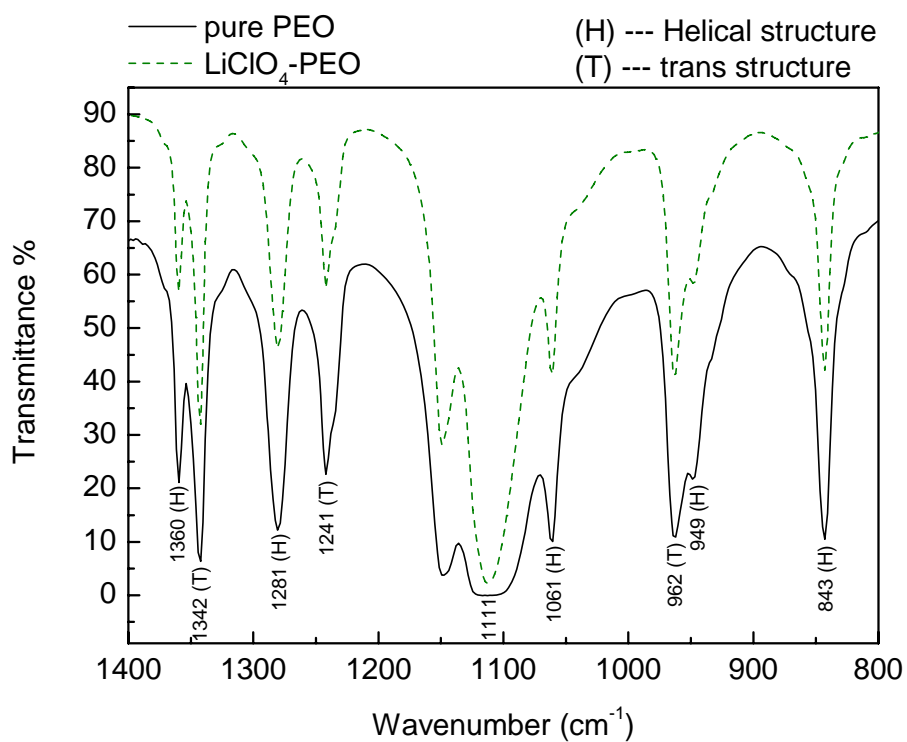


Figure 3.4 Wavenumber from 1400 to 800 of spectra in Figure 3.2.

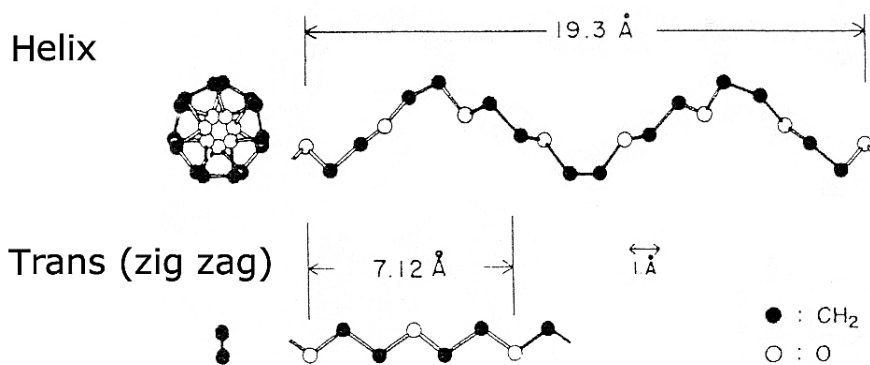


Figure 3.5 Conformations of PEO molecules. [Takahashi, et al., 1973]

In X-ray diffraction (XRD) study of pure PEO and LiClO_4 -PEO, well defined and identical diffraction peaks are found at 2θ equal to 19° and 23° (Figure 3.6), so that PEO from crystalline phase in significant proportion, this result is consistent with some previous studies [Deitzel, et al., 2001]. The 19° and 23° correspond to (120) and (112) crystal plane respectively. The crystal structure of PEO can be referred to Takahashi and Tadokoro's work (Figure 3.7). The identical diffraction peaks also implied that the low doping concentration of LiClO_4 do not change the crystallinity of PEO.

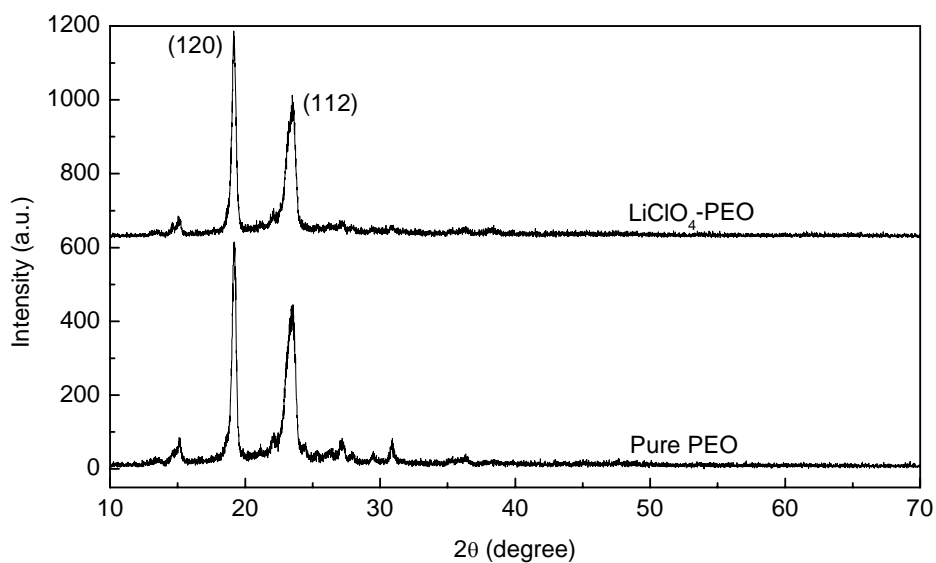


Figure 3.6 X-ray diffraction spectra of pure PEO and LiClO_4 doped PEO.

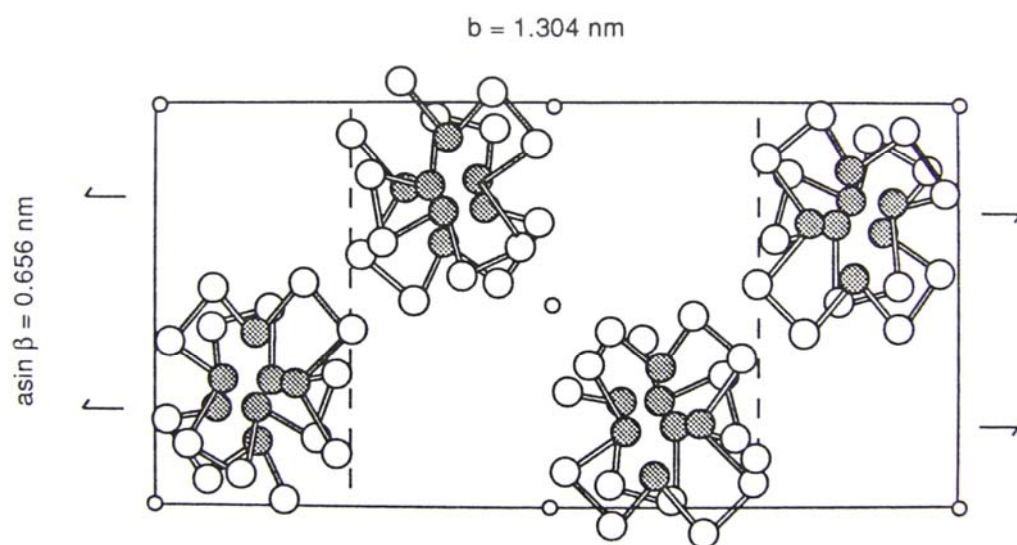


Figure 3.7 Crystal structure of PEO. (Dark spheres refer to O, white spheres refer to CH_2) [Takahashi and Tadokoro, 1973]

3.2 Electrical Properties of PEO

In this section, the results of a series of electrical measurements are discussed, these help to understand the ionic conduction of PEO, and also provide basic information for studies in coming chapters. Figure 3.8 shows the dielectric constants ϵ_r' of PEO and LiClO₄ doped PEO which were measured against various frequencies at ambient condition. The ϵ_r' of PEO is highly frequency dependent, for example, the pure PEO film with aluminium electrodes has ϵ_r' from 1 to 10^6 as frequency varies from 100k Hz to 1 mHz. This phenomenon is a common characteristic of PEO and even solid polymer electrolytes [Furukawa, et al., 2004; Natesan, et al., 2006; Wagner and Kliem, 2002], this is mainly due to the mobile charge motion. The ϵ_r' of LiClO₄ doped PEO with molar ratio [EO]:[Li] = 1.24×10^3 :1 was also investigated, the ϵ_r' is between 1 to 2 order higher than the pure PEO sample, but these two spectra are quite similar in shape.

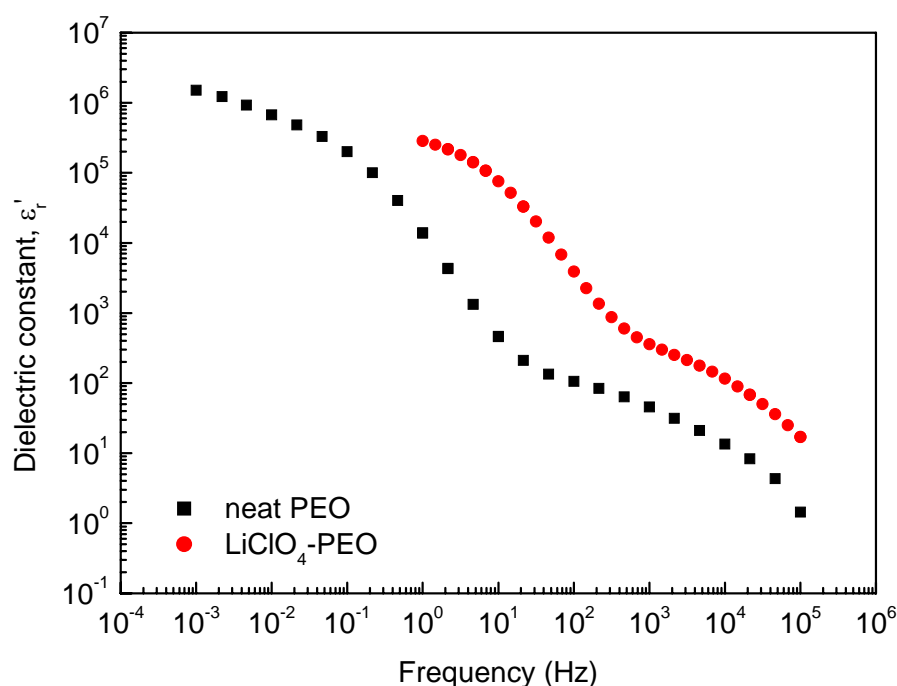


Figure 3.8 Dielectric constants of pure PEO and LiClO₄ doped PEO films with aluminium electrodes.

Correspondingly, dielectric loss ϵ_r'' (Figure 3.9) and conductivity σ' (Figure 3.10) of the samples mentioned are also calculated from the same measurements. The spectra of dielectric losses have similar trend to their dielectric constants. For example, pure PEO with aluminium electrodes has ϵ_r'' from 10 to 10⁶ as frequency varied from 100 kHz to 1 mHz. This large ϵ_r'' is caused by the high σ' of polymer electrolyte, since dielectric materials are defined as insulator, the measured dielectric properties of PEO would not be appeared as the ordinary values of dielectric materials. As doping LiClO₄ into PEO, the conductivity is enhanced for around 1 to 2 orders.

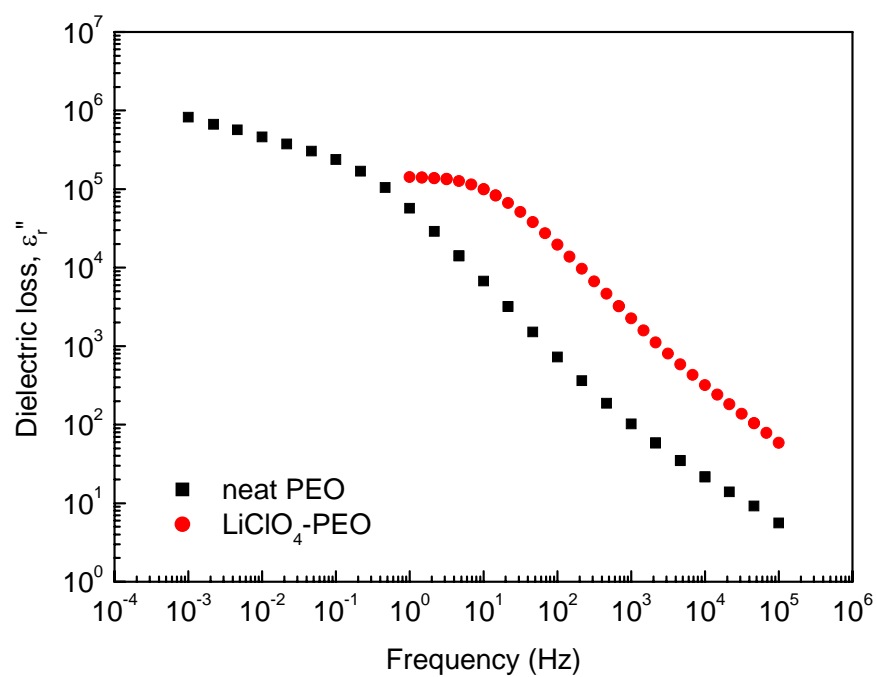


Figure 3.9 Dielectric losses of pure PEO and LiClO_4 doped PEO films with aluminium electrodes.

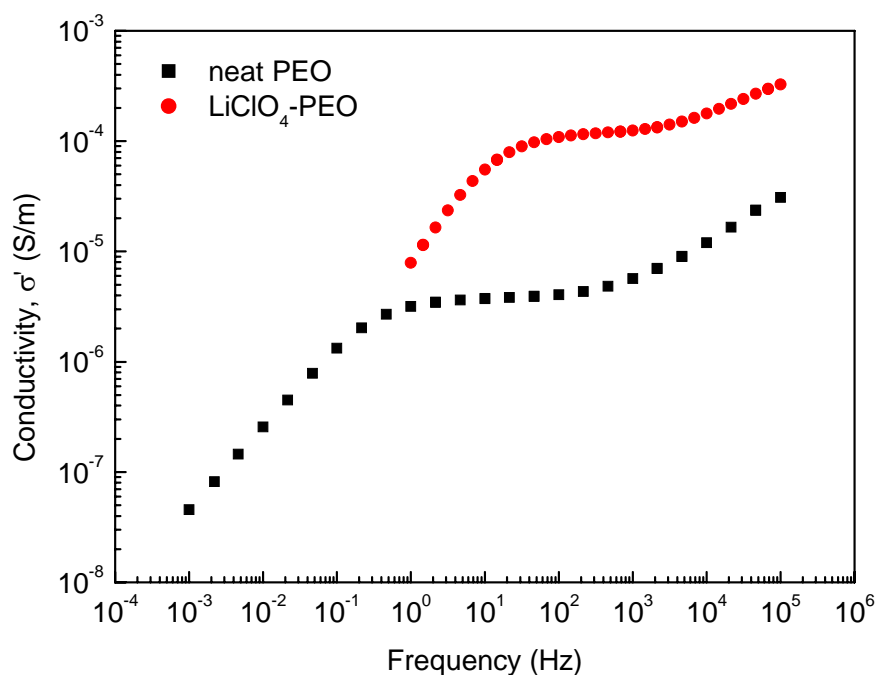


Figure 3.10 Conductivities of pure PEO and LiClO_4 doped PEO films with aluminium electrodes.

The current-voltage (I - V) relationships of pure PEO are shown in Figure 3.11, gold electrodes was coated on both sides of the sample with 1 cm diameter, and the thickness of sample is 0.6 mm. Applied voltage was started from 0 V and stepping down to -5 V with 0.1V step size, and each steps were kept at constant voltage for 0.25 s before data logging, the voltage were performed for three cycles between ± 5 V. The first measurement was conducted in ambient just after one day annealing, the I - V relation is quite linear and maximum current is around 0.15 μA . The sample was then placed in ambient, the experiment was repeated at the 6th and 24th hr, and it is found

that the maximum current increase to 4.3 μA and 7.8 μA respectively. This is because water in the air are absorbed by PEO, more H^+ ions could act as charge carriers to increase ionic conductivity of PEO. The I - V relationship is found to be unchanged after 24 hr stay in ambient, this is due to the water content has been saturated. Moreover, as the electrical properties of PEO dominated by the ionic conduction, the I - V curves become non-linear, the current do not equal to zero at zero voltage.

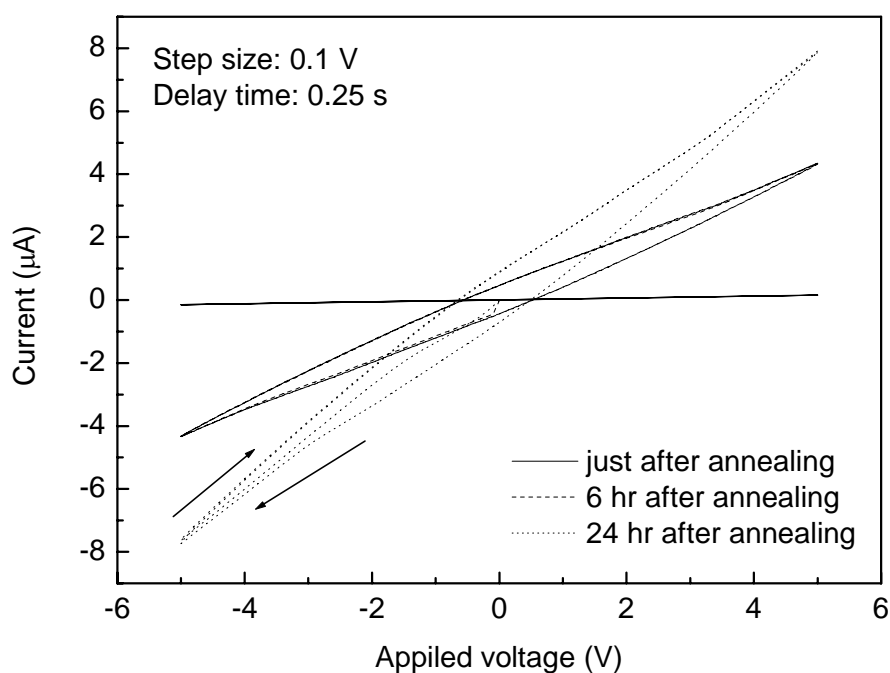


Figure 3.11 Current-voltage relationship of PEO with gold electrodes, after various durations after annealing (sample thickness = 0.6 mm).

Figure 3.12 can further illustrate the effect of moisture within PEO, ambient

measurement was followed by the vacuum measurement. The results show that, conduction of PEO in vacuum is much lower than in ambient, this can be due to water molecules leaving PEO at low pressure. On the other hand, first cycle of I - V loops differing to its following loops, this indicates that PEO is sensitive to its history. In the ambient measurement, a maximum (minimum) current is observed as the applied voltage increase (decrease), some stated that these peaks are oxidation and reduction of ions [Armand, 1983; Scrosati, 1993].

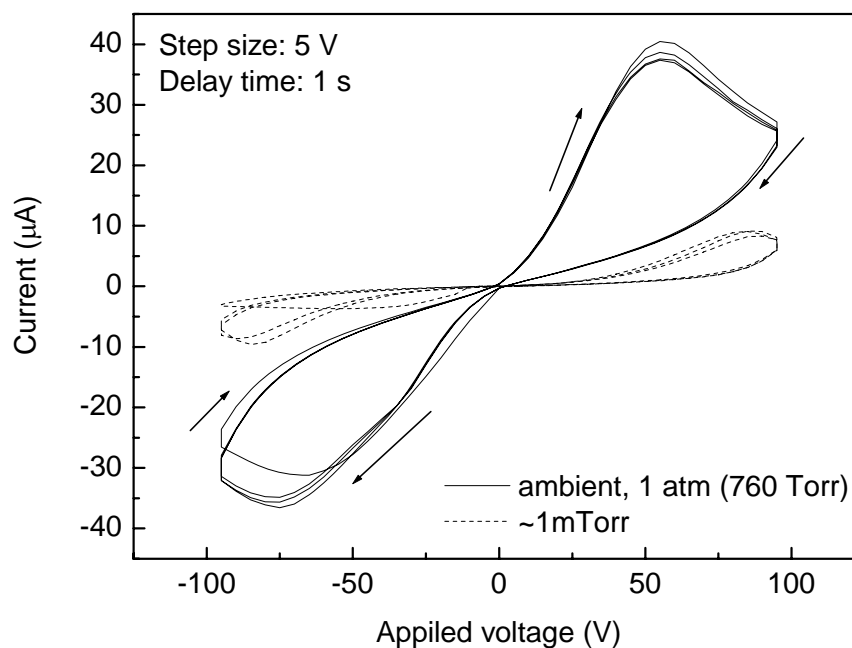


Figure 3.12 Current-voltage relationship of PEO with gold electrodes, at ambient and vacuum (around 1 mTorr) (sample thickness = 0.065 mm).

Figure 3.13 has shown that the I - V relations of PEO are affected by the rate of applied voltage cycles. The results were obtained in the same conditions, excepted that they had different delay time at each step of applied voltage, the delay time 2.5, 8 and 25 s are corresponding to 200, 640 and 2000 s per cycle respectively. The shifts in oxidation and reduction peaks as well as current are depending on the rate of voltage cycles, the slower in cycling rate, PEO is less conductive, which is consistent to conductivity measurement (Figure 3.10).

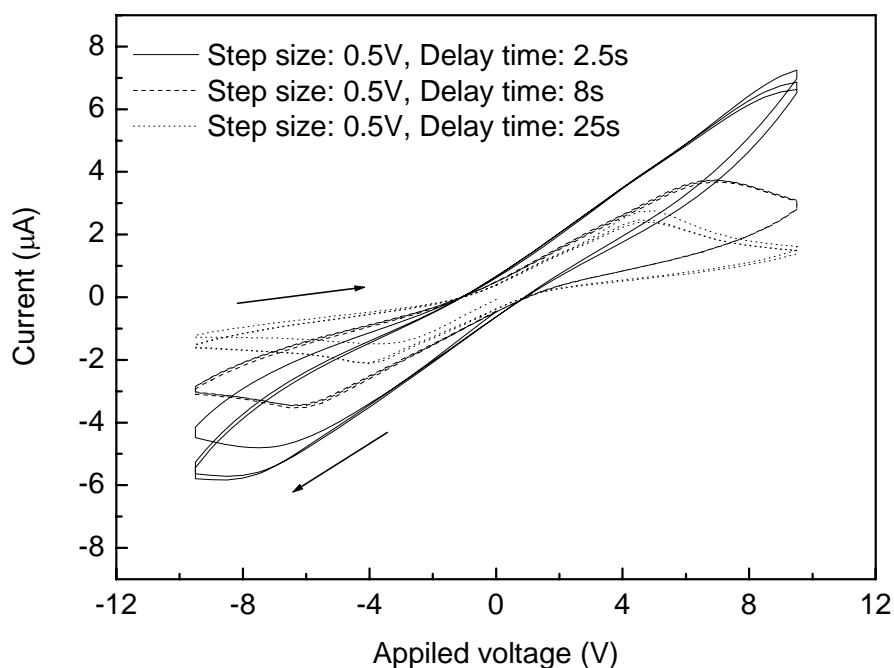


Figure 3.13 Current-voltage relationship of PEO with gold electrodes, with various cycling rates (sample thickness = 0.6 mm).

Together with the I - V relationship, measurement had also made on the current flow through PEO as a constant voltage 10 V applied on it (Figure 3.14). The current drops for around 10 times at first 1000 seconds, this shows the blocking of charges by gold electrodes, for example, H^+ ions is mobile in PEO but not in gold, so that the ions accumulate at the boundary of electrodes. An electric field that is in opposite direction to the applied E-field will be built up by the accumulated charges, therefore, current is suppressed as the voltage continuously applied. The accumulation of charges can also appear at low frequency a.c. measurement, however, the drop in current is not obvious, this is because the accumulated charges are brought away by the applied a.c. E-field.

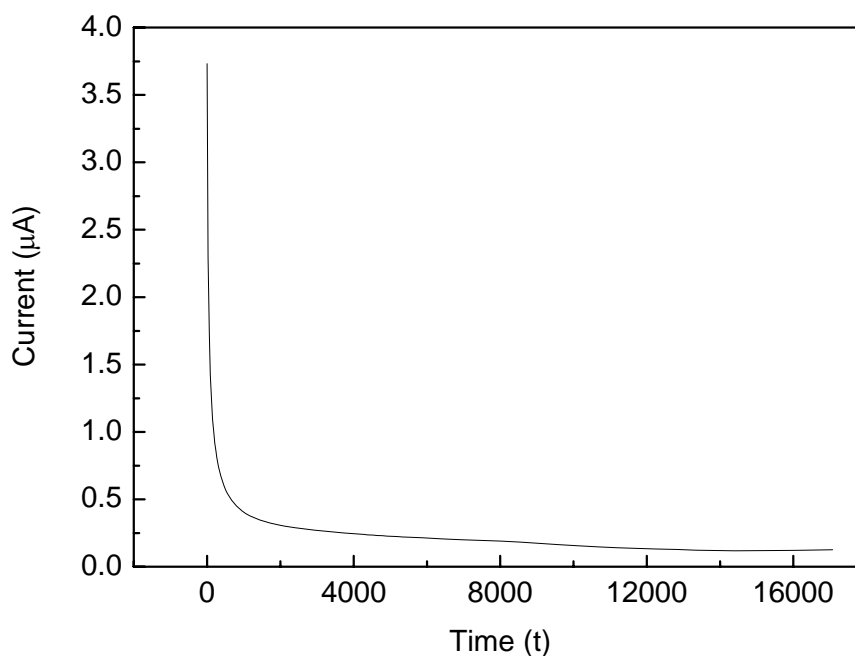


Figure 3.14 Current against time of pure PEO under a constant voltage 10 V.

In order to further study the accumulating of charges in PEO under a constant E-field, potential scanning of PEO strip (Figure 2.6) was performed, and the result shows in Figure 3.15. It is found that the voltage along PEO strip is not linear along its length. For example, voltage drops sharply at the 100 V end, this due to a layer of charges accumulated as described in last paragraph.

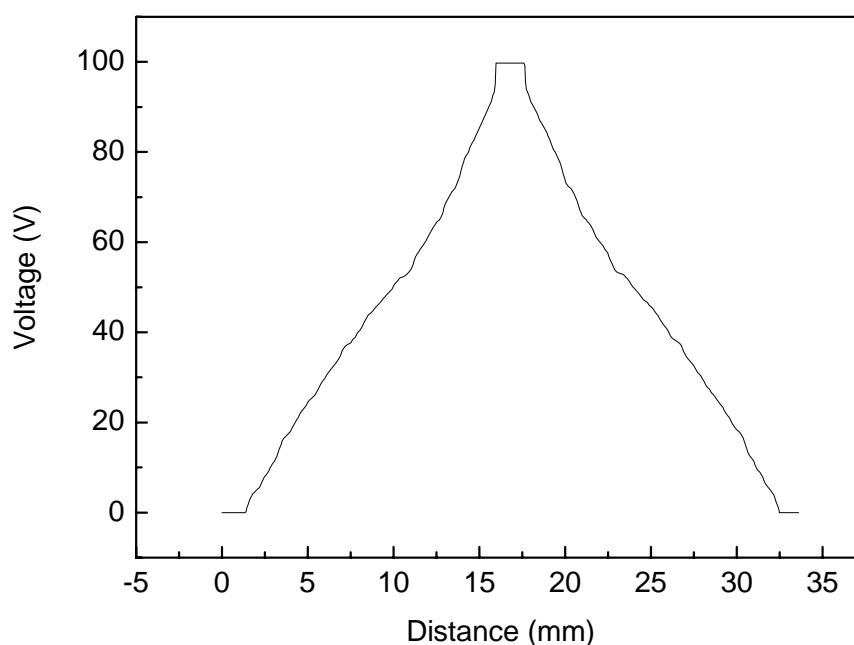


Figure 3.15 Non-linear voltage drop along the direction of applied E-field.

In summary on the properties of PEO, its dielectric constant and dielectric loss are highly frequency dependent, and quite high value at low frequency is observed. Due to the charge accumulation at interface of electrodes, conductivity of PEO decrease as

frequency decrease, conductivity of PEO is also found to be sensitive to moisture and inorganic salt LiClO_4 , however, the structure of PEO do not affected by the low doping concentration of LiClO_4 .

Chapter 4 Pyroelectric and Piezoelectric Properties of 0-3 PZT/PEO Composites

4.1 Theoretical Aspects

4.1.1 Ferroelectric Ceramics

Ferroelectric ceramics meant that the materials exhibit spontaneous polarization in the absence of external electric field [Callister, 2003]. This phenomenon can be explained by the structure of ferroelectric ceramics, lead zirconate titanate (PZT), or $\text{Pb}(\text{Zr}_x\text{Ti}_{1-x})\text{O}_3$ is one of the common ferroelectric ceramics materials with perovskite structure (Figure 4.1). It has cubic structure at temperature higher than Curie temperature, due to the symmetry in structure, it do not exhibit any spontaneous polarization. Below Curie temperature, the PZT has tetragonal structure, the Ti^{4+} or Zr^{4+} are then shift away from the centre along the c-axis. Therefore, non-zero dipole moment has induced as Figure 4.1(b). Before any treatment on the PZT, the dipole moments are randomly orientated (Figure 4.2(a)) and the net polarization P is zero, when electric field E is applied on the PZT, the electric dipole will be aligned along the applied E -field. If the field is large enough, all of the dipoles will be aligned straight to

the same direction like Figure 4.2(b), this process is named as poling, and the polarization in ferroelectric ceramic will be at maximum, i.e. saturated polarization P_s .

When the applied E -field is removed, the dipoles will spring back a little but generally remain in the same direction (Figure 4.2(c)), therefore, a remnant polarization P_r can be obtained, and this is also the working condition for pyroelectric and piezoelectric applications. If the PZT is cycled by E -field, P - E hysteresis loop can be observed as Figure 4.3.

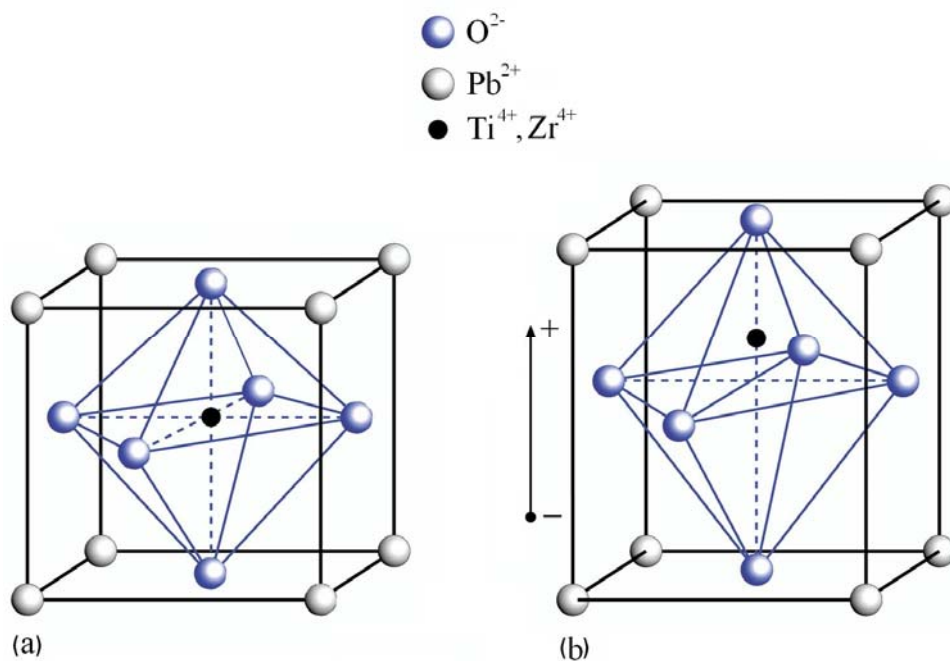


Figure 4.1 Structure of the perovskite PZT (a) above Curie temperature with cubic structure, (b) below Curie temperature with tetragonal structure. [Physik_Instrumente, 2008]

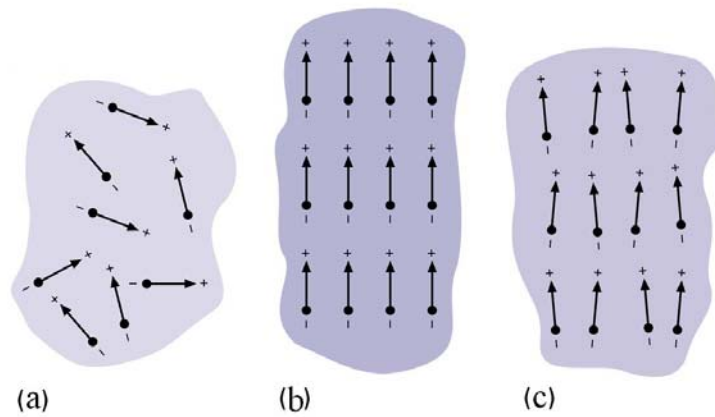


Figure 4.2 Electric dipoles in domains; (a) unpoled ferroelectric ceramic, (b) during and (c) after poling. [Physik_Instrumente, 2008]

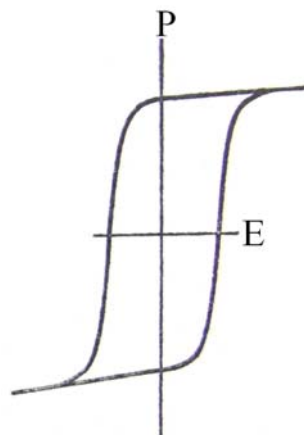


Figure 4.3 A typical ferroelectric P-E hysteresis loop. [Jaffe, et al., 1971]

As the PZT being poled, a non-zero P_r will be observed. When temperature T change in the PZT, the length of c-axis will be changed and the position of Ti^{4+} or Zr^{4+} will also be changed along the c-axis. As a result of change in structure, the polarization in PZT will be varied with the temperature modulation, this phenomenon is called pyroelectric effect and pyroelectric coefficient p defined as [Das-Gupta, 1991],

$$p = -\frac{\partial P}{\partial T} \quad (4.1)$$

In this study, the pyroelectric coefficient measurements for the samples were varied in a sinusoidal temperature $T(t) = T_0 + T_{\Delta} \sin \omega t$ in short circuit condition. The current density of ferroelectric ceramics J can be written as

$$J = \frac{\partial D}{\partial t} \quad (4.2)$$

where D is electric displacement, for electroactive dielectric materials,

$$D = \varepsilon_0 E + P \quad [\text{Anderson, 1964; Reitz and Milford, 1960}]. \quad (4.3)$$

as the measurements were in short circuit condition, E can be set to be zero and put equation (4.3) into (4.2),

$$J = \frac{\partial D}{\partial t} = \frac{\partial P}{\partial t} = \frac{\partial P}{\partial T} \frac{\partial T}{\partial t} \quad (4.4)$$

and applying equation (4.1), J and p are related as follows:

$$J = -p T_{\Delta} \omega \cos \omega t. \quad (4.5)$$

The direct piezoelectric effect is the change in the electric charge which is induced by the applied stress [Jaffe, et al., 1971], this can also be explained by the asymmetric perovskite structure in tetragonal phase. For the converse piezoelectric effect, mechanical deformation will be induced by the applied electric field,

$$e = sS + dE \quad (4.6)$$

$$D = dS + \varepsilon' \varepsilon_0 E \quad (4.7)$$

where e is strain tensor, s is elastic compliance tensor, S is the elastic stress tensor, d is the piezoelectric coefficient tensor and D is electric displacement tensor. Equation (4.6) refer to converse and (4.7) direct piezoelectric effect [Hom, et al., 1994].

The piezoelectric coefficient d is a common measure of piezoelectric activity [Wong and Shin, 2006],

$$d = \frac{\partial P}{\partial S} \quad (4.8)$$

d equal to charge density induced by applied tensile stress S in direct piezoelectric effect, and equal to strain induced by applied E -field in converse piezoelectric effect.

4.1.2 0-3 Ferroelectric/Polymer Composites

In the discussion of 0-3 ferroelectric/polymer composites, subscripts i and m denote inclusion and matrix respectively.

As PEO is conducting polymer, in this part of discussion, theoretical model on the effect of conductivities σ on the pyroelectric coefficient of composites p will be introduced. The following theoretical model was developed by Lam, et al [Lam, et al., 2004], which can be applied equally well to the samples fabricated for this project. In

fact, this project is an extension study of the Lam's project previously in our research group.

In the model, similar to equation (4.3) relations are obtained for inclusion and matrix,

$$D_i = \varepsilon_i E_i + P_i \quad (4.9)$$

$$D_m = \varepsilon_m E_m + P_m \quad (4.10)$$

Current density of the whole composite J is the sum of conduction current densities j of both phases and displacement current $\frac{\partial D}{\partial t}$, therefore J can be written as,

$$J = \phi j_i + (1 - \phi) j_m + \frac{\partial D}{\partial t} \quad (4.11)$$

according to Ohm's law, the conduction current densities j are [Wong, et al., 2002],

$$j_i = \sigma_i E_i \quad (4.12)$$

$$j_m = \sigma_m E_m \quad (4.13)$$

The boundary conditions can be taken into account [Wong, et al., 2002] by considering a single sphere inclusion under a uniform electric field applied at a far distance, then the following equations can be obtained:

$$D_i + 2\varepsilon_m (E_i - E_m) = D_m + q_0 \quad (4.14)$$

$$j_i + 2\sigma_m (E_i - E_m) = j_m - \frac{\partial q_0}{\partial t} \quad (4.15)$$

where q_0 is the surface charge density at the interface, which at the pole of inclusion

along the polarizing direction ($\theta = 0$) with a distribution given by $q_0 = \cos \theta$.

The average electric field E and electric displacement D of the composites can be described by,

$$E = \phi E_i + (1 - \phi) E_m \quad (4.16)$$

$$D = \phi D_i + (1 - \phi) D_m \quad (4.17)$$

By using equations (4.9), (4.10), (4.12) to (4.16), and putting $P_m = 0$ for non-ferroelectric PEO together with some manipulation

$$\frac{\partial E_i}{\partial t} + \frac{E_i}{\tau} = \frac{3 \left(\sigma_m E + \varepsilon_m \frac{\partial E}{\partial t} \right) - (1 - \phi) \frac{\partial P_i}{\partial t}}{\phi 3 \varepsilon_m + (1 - \phi) (\varepsilon_i + 2 \varepsilon_m)} \quad (4.18)$$

$$\text{where } \tau = \frac{\phi 3 \varepsilon_m + (1 - \phi) (\varepsilon_i + 2 \varepsilon_m)}{\phi 3 \sigma_m + (1 - \phi) (\sigma_i + 2 \sigma_m)} \quad (4.19)$$

Since the pyroelectric measurements were performed at a short circuit condition, the electric field on the composites are zero, i.e. $E = 0$ and equations (4.18) and (4.16) can be reduced to

$$\frac{\partial E_i}{\partial t} + \frac{E_i}{\tau} = \frac{-(1 - \phi) \frac{\partial P_i}{\partial t}}{\phi 3 \varepsilon_m + (1 - \phi) (\varepsilon_i + 2 \varepsilon_m)} \quad (4.20)$$

$$\text{and } E_i = \frac{-(1 - \phi)}{\phi} E_m \quad (4.21)$$

by substituting equation (4.21) into (4.20)

$$\frac{\partial E_m}{\partial t} + \frac{E_m}{\tau} = \frac{\frac{\partial P_i}{\partial t}}{\phi 3\varepsilon_m + (1-\phi)(\varepsilon_i + 2\varepsilon_m)} \quad (4.22)$$

In the pyroelectric coefficient measurement, samples were varied in a sinusoidal temperature $T(t) = T_0 + T_\Delta \sin \omega t$, substitute $\frac{\partial T(t)}{\partial t}$ and equation (4.1) into equation

(4.4), $\frac{\partial P_i}{\partial t}$ will be obtained as

$$\frac{\partial P_i}{\partial t} = -p_i T_\Delta \omega \cos \omega t, \quad (4.23)$$

and solve the first order differential equations (4.20) and (4.22) together with (4.23),

solutions of E_i and E_m are found as,

$$E_i = \frac{(1-\phi)p_i T_\Delta}{\phi 3\varepsilon_m + (1-\phi)(\varepsilon_i + 2\varepsilon_m)} \frac{\omega \tau}{1 + \omega^2 \tau^2} (\cos \omega t + \omega \tau \sin \omega t) \quad (4.24)$$

$$\text{and } E_m = -\frac{\phi p_i T_\Delta}{\phi 3\varepsilon_m + (1-\phi)(\varepsilon_i + 2\varepsilon_m)} \frac{\omega \tau}{1 + \omega^2 \tau^2} (\cos \omega t + \omega \tau \sin \omega t) \quad (4.25)$$

By using (4.9), (4.10) and (4.17), $\frac{\partial D}{\partial t}$ will be obtained as

$$\frac{\partial D}{\partial t} = \phi \left(\varepsilon_i \frac{\partial E_i}{\partial t} + \frac{\partial P_i}{\partial t} \right) + (1-\phi) \varepsilon_m \frac{\partial E_m}{\partial t} \quad (4.26)$$

By substituting equations (4.12), (4.13), (4.24) (4.25) and (4.26) into (4.11), with only

considering the $\cos \omega t$ terms of J ,

$$J^{\cos} = -\phi p_i T_\Delta \omega \cos \omega t \left[1 - \frac{(1-\phi)}{\phi 3\varepsilon_m + (1-\phi)(\varepsilon_i + 2\varepsilon_m)} F \right] \quad (4.27)$$

$$\text{where } F = \frac{\omega^2 \tau^2}{1 + \omega^2 \tau^2} (\varepsilon_i - \varepsilon_m) + \frac{\tau}{1 + \omega^2 \tau^2} (\sigma_i - \sigma_m). \quad (4.28)$$

Equation (4.5) is also applicable for composites sample, therefore pyroelectric

coefficient p can be expressed as:

$$p = \phi p_i \left[1 - \frac{(1-\phi)}{3\phi\varepsilon_m + (1-\phi)(\varepsilon_i + 2\varepsilon_m)} F \right] \quad (4.29)$$

this p is compared with the experimental results (Figure 4.5), theoretical p is deviated from experimental results at high PZT concentration. Therefore, another theoretical model from Wong and Shin [Wong and Shin, 2006] is introduced.

In the theoretical model below, the interaction among inclusion particles have been taken into consideration in the theoretical model of pyroelectric coefficient of composites p . The interaction mentioned is that the electric displacement as seen by a particular single inclusion is the sum of two parts: the first is due to the pure medium and the other due to the total polarization of all other inclusions [Poon and Shin, 2004]. Therefore, according to [Wong and Shin, 2006] equations (4.14) and (4.15) are rewritten for higher volume fraction as

$$D_i + 2\varepsilon_m(E_i - E_m) = \tilde{D}_m + q_0 \quad (4.30)$$

$$j_i + 2\sigma_m(E_i - E_m) = j_m + \phi(\sigma_i - \sigma_m)E_i - (1-\phi)\frac{\partial q_0}{\partial t} \quad (4.31)$$

where $\tilde{D}_m = D_m + \phi\tilde{P}_i$ and $\tilde{P}_i = P_i - P_m + q_0 + (\varepsilon_i - \varepsilon_m)E_i$

Similar to pervious model, by using (4.9), (4.10), (4.12), (4.13), (4.16), (4.30), (4.31)

and putting $P_m = 0$ for non-ferroelectric PEO, following equation will be obtained:

$$\frac{\partial E_i}{\partial t} + \frac{E_i}{\tau'} = \frac{3\left(\sigma_m E + \varepsilon_m \frac{\partial E}{\partial t}\right) - (1-\phi)^2 \frac{\partial P_i}{\partial t}}{\phi 3\varepsilon_m + (1-\phi)[\varepsilon_i + 2\varepsilon_m - \phi(\varepsilon_i - \varepsilon_m)]} \quad (4.32)$$

$$\text{where } \tau' = \frac{\phi 3\varepsilon_m + (1-\phi)[\varepsilon_i + 2\varepsilon_m - \phi(\varepsilon_i - \varepsilon_m)]}{\phi 3\sigma_m + (1-\phi)[\sigma_i + 2\sigma_m - \phi(\sigma_i - \sigma_m)]} \quad (4.33)$$

and the solutions are found to be

$$E_i = \frac{(1-\phi)^2 p_i T_\Delta}{\phi 3\varepsilon_m + (1-\phi)[\varepsilon_i + 2\varepsilon_m - \phi(\varepsilon_i - \varepsilon_m)]} \frac{\omega \tau'}{1 + \omega^2 \tau'^2} (\cos \omega t + \omega \tau' \sin \omega t) \quad (4.34)$$

$$\text{and } E_m = -\frac{\phi(1-\phi) p_i T_\Delta}{\phi 3\varepsilon_m + (1-\phi)[\varepsilon_i + 2\varepsilon_m - \phi(\varepsilon_i - \varepsilon_m)]} \frac{\omega \tau'}{1 + \omega^2 \tau'^2} (\cos \omega t + \omega \tau' \sin \omega t) \quad (4.35)$$

Finally, by substituting equations (4.5), (4.12), (4.13), (4.34) (4.35) and (4.26) into

(4.11)

$$p = \phi p_i \left[1 - \frac{(1-\phi)^2}{\phi 3\varepsilon_m + (1-\phi)[\varepsilon_i + 2\varepsilon_m - \phi(\varepsilon_i - \varepsilon_m)]} F' \right] \quad (4.36)$$

$$\text{where } F' = \frac{\omega^2 \tau'^2}{1 + \omega^2 \tau'^2} (\varepsilon_i - \varepsilon_m) + \frac{\tau'}{1 + \omega^2 \tau'^2} (\sigma_i - \sigma_m). \quad (4.37)$$

In the discussion of piezoelectric coefficient d_{33} , the conductivities of constituents and the concentration of inclusion are considered in the theoretical aspect, follows the considerations of Wong and Shin [Wong and Shin, 2006].

The resultant electric field in the constituents can be obtained from the analogy of pyroelectric calculation, as the applied tensile stress $S = S_\Delta \sin \omega t$:

$$E_i = \frac{(1-\phi)^2 d_i S_\Delta}{\phi 3\varepsilon_m + (1-\phi)[\varepsilon_i + 2\varepsilon_m - \phi(\varepsilon_i - \varepsilon_m)]} \frac{\omega \tau'}{1 + \omega^2 \tau'^2} (\cos \omega t + \omega \tau' \sin \omega t) \quad (4.38)$$

$$\text{and } E_m = -\frac{\phi(1-\phi) d_i S_\Delta}{\phi 3\varepsilon_m + (1-\phi)[\varepsilon_i + 2\varepsilon_m - \phi(\varepsilon_i - \varepsilon_m)]} \frac{\omega \tau'}{1 + \omega^2 \tau'^2} (\cos \omega t + \omega \tau' \sin \omega t) \quad (4.39)$$

from the result of Wong and Shin [Wong and Shin, 2006], with non-piezoelectric matrix

$$d_{33} = \phi[1 - \Gamma_d(1 - L_E)]\{F_S^{\parallel} d_{33i} + 2F_S^{\perp} d_{31i}\} \quad (4.40)$$

$$\text{where } \Gamma_d = \frac{\tau' \left(\frac{\sigma_i - \sigma_m}{\varepsilon_i - \varepsilon_m} \right) + \omega^2 \tau'^2}{1 + \omega^2 \tau'^2}, \quad (4.41)$$

$$\text{electric field factor } L_E = \frac{3\varepsilon_m}{\phi 3\varepsilon_m + (1 - \phi)[\varepsilon_i + 2\varepsilon_m - \phi(\varepsilon_i - \varepsilon_m)]}, \quad (4.42)$$

$$\text{stress field factors } F_S^{\perp} = \frac{1}{\phi} \left(\frac{1}{3} \frac{k^{-1} - k_m^{-1}}{k_i^{-1} - k_m^{-1}} - \frac{1}{3} \frac{\mu^{-1} - \mu_m^{-1}}{\mu_i^{-1} - \mu_m^{-1}} \right), \quad (4.43)$$

$$F_S^{\parallel} = \frac{1}{\phi} \left(\frac{1}{3} \frac{k^{-1} - k_m^{-1}}{k_i^{-1} - k_m^{-1}} + \frac{2}{3} \frac{\mu^{-1} - \mu_m^{-1}}{\mu_i^{-1} - \mu_m^{-1}} \right), \quad (4.44)$$

$$\text{effective bulk modulus } k = k_m + \frac{\phi(k_i - k_m)}{1 + \frac{(1 - \phi)(k_i - k_m)}{k_m + \frac{4\mu_m}{3}}} \quad (4.45)$$

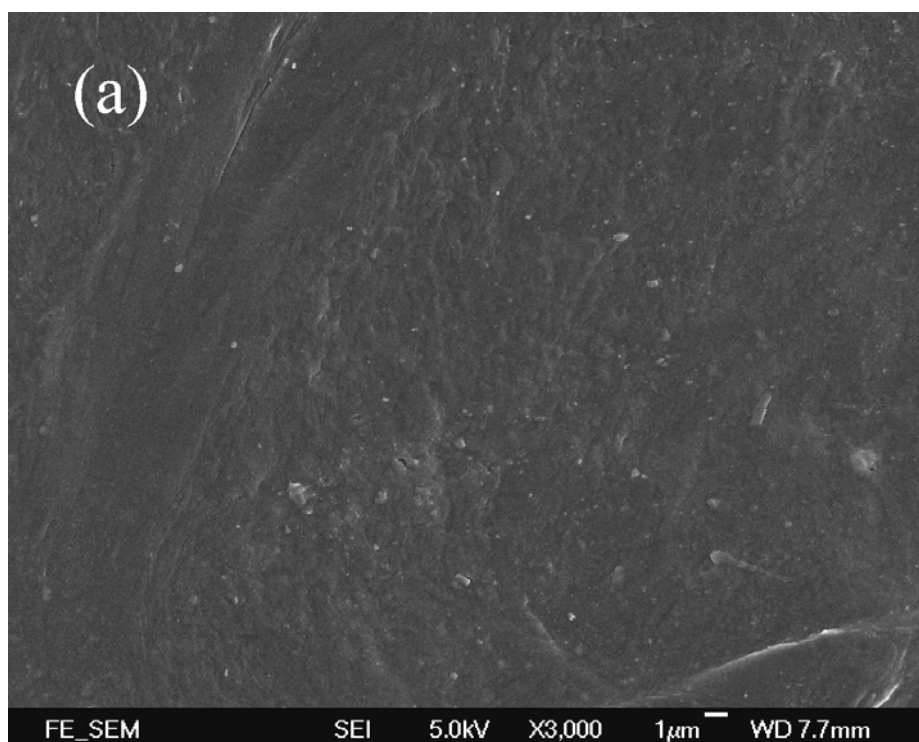
and lower bound of effective shear modulus

$$\mu = \mu_m \left\{ 1 + \frac{15(1 - \nu_m) \left(\frac{\mu_i}{\mu_m} - 1 \right) \phi}{7 - 5\nu_m + 2(4 - 5\mu_m) \left[\frac{\mu_i}{\mu_m} - \left(\frac{\mu_i}{\mu_m} - 1 \right) \phi \right]} \right\} \quad (4.46)$$

where ν_m is the Poisson's ratio of matrix material. The upper and lower bound of effective shear modulus were reported by Hashin [Hashin, 1962], and the calculated d_{33} by using upper and lower bound are closed to each other.

4.2 Results and Discussion

The morphology of pure PEO and 34vol% PZT/PEO composite was captured by using SEM and Figure 4.4 shows their SEM images. The image of pure PEO was taken at sample surface, and image of PZT/PEO was taken at the cross-section by cutting up the sample. In the SEM picture, smooth background is the PEO matrix. At the top-right corner of picture (b), a few PZT particles are located out of the PEO matrix, therefore, the size of PZT particles are estimated as around 3 to 4 μm . PZT particles can also be observed though out the cross-section surface, as they were partially embedded in PEO matrix.



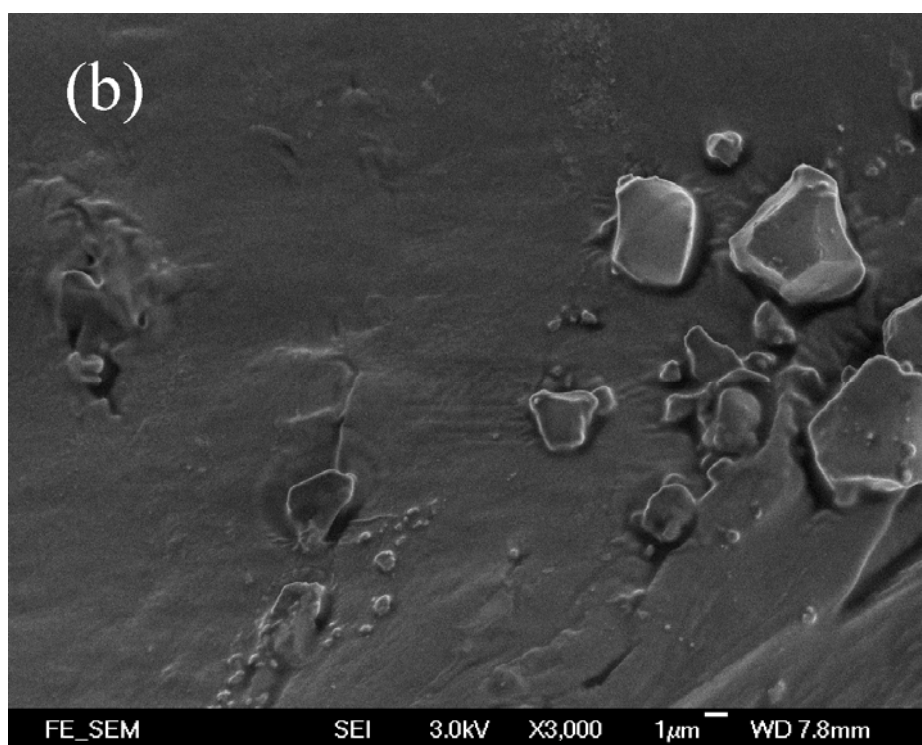


Figure 4.4 SEM images of (a) surface of pure PEO and (b) cross-section of 34 vol% PZT/PEO composite.

In addition to the SEM picture, optical micrograph of the 34 vol% PZT/PEO composite was also taken in a transmission mode. As shown in figure 4.5, the large shadows are the crystalline regions of PEO, whereas the solid dots with size of a few microns are PZT inclusions, it is evident that they dispersed quite homogeneously throughout the inspected region.

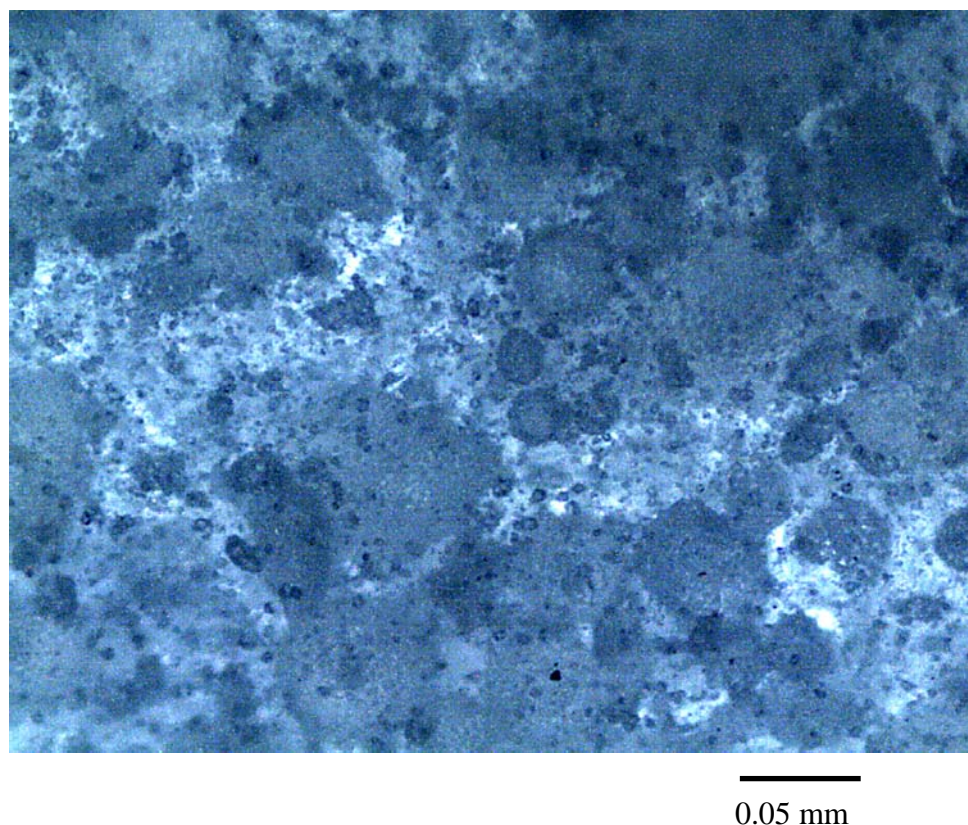


Figure 4.5 Transmission optical micrograph of 34 vol% PZT/PEO composite.

The pyroelectric coefficients of the composite samples measured by the dynamic method versus PZT volume fractions are plotted as shows in Figure 4.6. It can be clearly seen that the pyroelectric coefficients of the samples are increased almost proportionally with the PZT contents. At 34% volume fraction of PZT, the pyroelectric coefficient reaches about $120 \mu\text{C}/\text{m}^2\text{K}$, which is 36% of pure PZT, and 30% higher than PZT/PU composites [Lam, et al., 2004].

The model discussed in last section is applied [Lam, et al., 2004], it points out that the

polarization of the poled ferroelectric particles in the matrix are stabilized by the spatial charges adhered. Under a short-circuit measurement, any change in polarization of the particles thus changing the adhered charge density which contributes to the displacement current of the samples, and also the conduction current through the constituents. Therefore, the electrical conductivity of both inclusion and matrix respectively should be taken into account in the derivation of the pyroelectric coefficients. As a result, the pyroelectric coefficients of the composite system at different volume fractions of inclusion, p has to be expressed in terms of the σ_i and σ_m as shows in the equation (4.29).

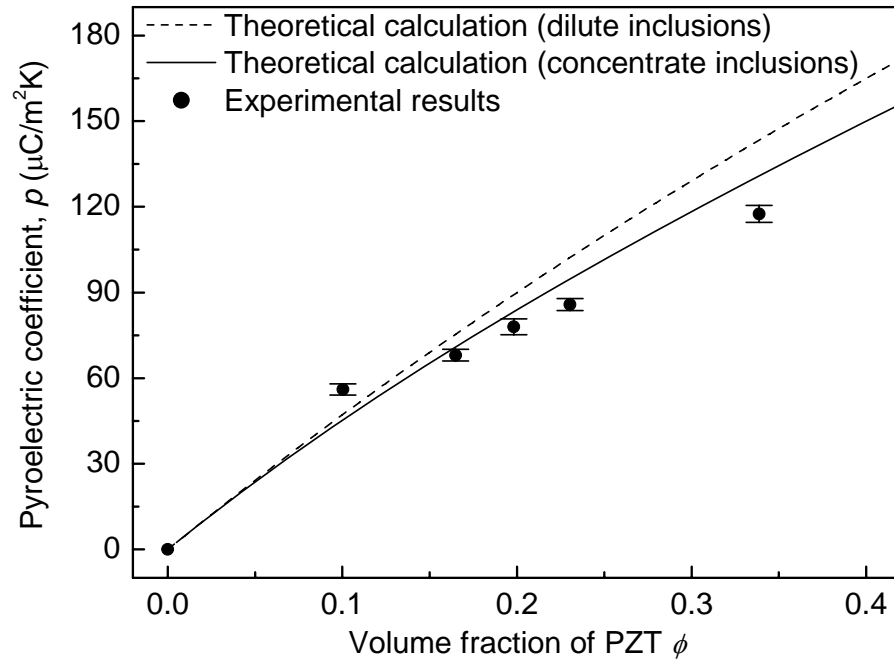


Figure 4.6 Pyroelectric coefficients of PZT/PEO composites against PZT volume fraction at 26 °C. The dots are experimental results, the dash line refers to the theoretical calculations that consider dilute inclusions, and solid line refers to calculation considered concentrated inclusions.

As shows in Figure 4.6, the dash line is the theoretical values at 5 mHz thermal cycles calculated by the equation (4.29) with $p_i = 330 \mu\text{C}/\text{m}^2\text{K}$ [Piezo_Kinetics, 2007], $\sigma_m = 2.5 \times 10^{-7} \text{ S/m}$, $\sigma_i = 5 \times 10^{-12} \text{ S/m}$ [Chan, et al., 1995], $\varepsilon_m = 3.1 \times 10^5 \varepsilon_o$ and $\varepsilon_i = 1800 \varepsilon_o$ [Piezo_Kinetics, 2007], where ε_o is the permittivity in vacuum, it matches fairly well with the experimental results. This suggests the role played by the conductivity of the samples as emphasized in the model is correct. Nevertheless, this

model assumes only dilute dispersion of particle inclusions in a continuous matrix, it explains the calculated curve exhibit a larger deviation from the experimental results at higher PZT contents. In the more recent work given by Wong and Shin [Wong and Shin, 2006], composite of high inclusion content is considered in their model. The pyroelectric coefficient of the composite can be obtained from equation (4.36), solid line plotted in Figure 4.6 shows its corresponding calculation. It shows a better agreement with the measured data. It indicated that this latter model is more satisfactory to describe the enhancement of the composite samples. Regarding the success of the modelling to describe the high pyroelectric performance of composites with either PU or PEO matrix, this will widen the study of composites with many other matrices with high conductivity and on the other hand to extend applications of composite materials with functional inclusions.

Other than the pyroelectric coefficients, the piezoelectric coefficients of the PZT/PEO composites were measured. The results are shown in Figure 4.7. Same as the pyroelectric coefficients, d_{33} are also enhanced significantly as a result of the higher conductivity of the matrix. At 34% of PZT, the d_{33} of the composite was found to be 167 pC/N, which is much larger than the 24 pC/N for 70% by weight of PZT in a PZT/PVDF composite as given in Son, et al. [Son, et al., 2007]. In the same model as

mentioned by Wong and Shin [Wong and Shin, 2006], it has also illustrated the formulation of d_{33} of the composite to high inclusion content as shows in the equation (4.40). The $\sigma_m = 1.68 \times 10^{-6}$ S/m and $\varepsilon_m = 203 \varepsilon_o$ at 60 Hz, $d_{33} = 400$ pC/N, $d_{31} = -175$ pC/N [Piezo_Kinetics, 2007] and mechanical properties of constituents (Table 4.1) were substituted into equation (4.40). The solid line in Figure 4.7 show the theoretical d_{33} with the conductivities of the constituents taken into consideration. The model is in good agreement with the experimental results. It further confirms that the piezoelectricity of the 0-3 composites can also be enhanced by the considerable large conductivity of the matrix.

Table 4.1 Mechanical properties of constituents used in calculations.

| | Y (GPa) | ν | K (GPa) | μ (GPa) |
|-----|-------------------|-------------------|-----------|-------------|
| PZT | 71 ^a | 0.31 ^a | 62 | 27 |
| PEO | 0.40 ^b | 0.35 ^c | 0.74 | 0.25 |

^a [Piezo_Kinetics, 2007].

^b [Bartolotta, et al., 1992].

^c Commonly, the Poisson's ratio ν of polymers are between 0.35 and 0.45.

^d Calculated from Y and ν by using $K = \frac{Y}{3(1-2\nu)}$ and $\mu = \frac{Y}{2(1+\nu)}$.

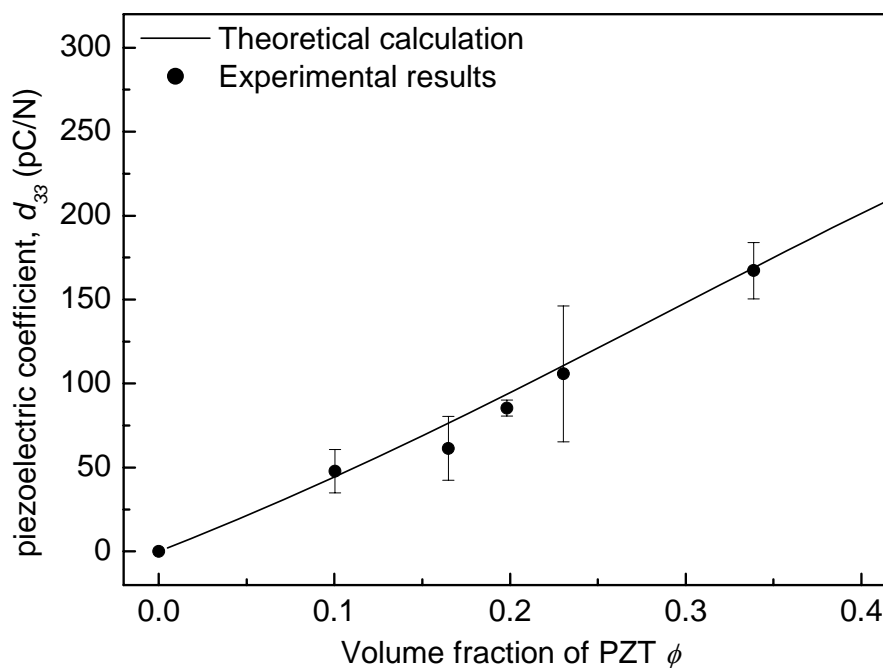


Figure 4.7 Piezoelectric charge coefficients of PZT/PEO composites against PZT volume fraction. The dots are experimental results, and the solid line refers to the theoretical calculations that consider both concentrated inclusion and conductivities.

4.2.1 0-3 Composites with LiClO_4 Doped PEO Matrix

As mentioned in previous Chapter, suitable content of lithium perchlorate LiClO_4 can enhance the conductivity of PEO. Therefore, the PZT/ $(\text{LiClO}_4\text{-PEO})$ composite, with molar ratio [ethylene oxide]:[Li] = 1.3×10^3 :1, will further confirm the enhancement of pyroelectric and piezoelectric properties by increasing the conductivity of matrix.

In this part of study, a PZT/(LiClO₄-PEO) sample with 20% of PZT in volume fraction was fabricated and supported with the theoretical model [Wong and Shin, 2006] discussed in last section. By using equation (4.36) with varying the conductivity of matrix material and all other parameters are kept at the same as previous discussion, the theoretical result indicated that PZT/PEO composites have achieved the highest pyroelectric coefficient at $\sigma_m = 2.5 \times 10^{-7}$ S/m, therefore discussion was only focus on piezoelectric properties.

As the conductivity of matrix measured at 60 Hz increases from 1.68×10^{-6} S/m to 3.88×10^{-5} S/m, the $d_{33} = 185$ pC/N of the PZT/(LiClO₄-PEO) sample together with previous result (Figure 4.7), which is larger than $d_{33} = 85$ pC/N of PZT/PEO with the same inclusion content. Theoretical calculations of different matrix conductivities are also shown in Figure 4.8, the d_{33} was quite sensitive to conductivity from 10^{-7} S/m to 10^{-5} S/m. Moreover, the d_{33} of matrix conductivity at 1.68×10^{-5} S/m and 1.68×10^{-4} S/m are the same in the entire PZT volume fraction, therefore, the d_{33} achieved its highest value in 0-3 PZT/PEO composite system with matrix conductivity higher than 1.68×10^{-5} S/m.

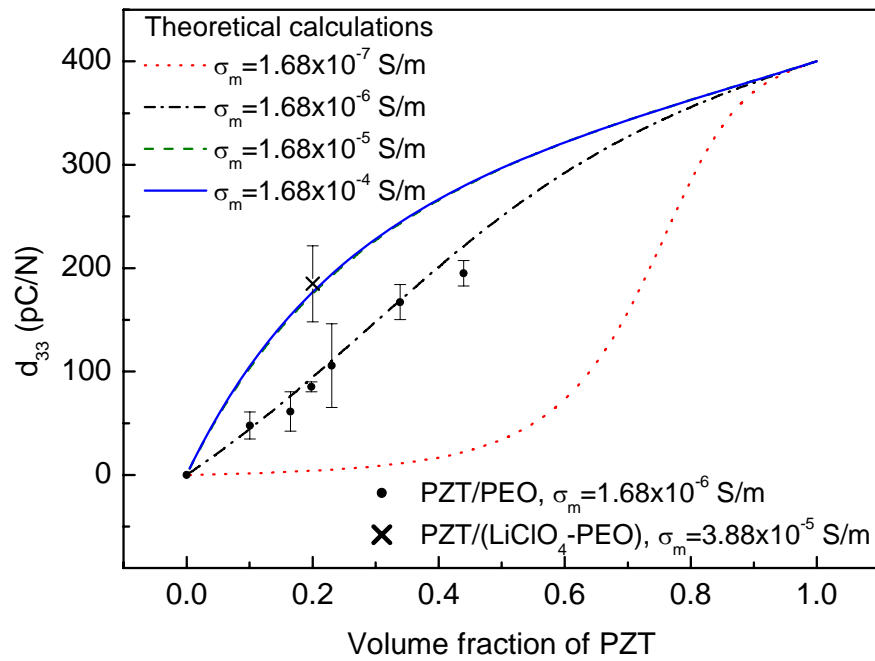


Figure 4.8 Piezoelectric charge coefficients of PZT/polymer composites against PZT volume fraction. The dot and cross are experimental results with pure PEO matrix and LiClO₄ doped PEO matrix respectively, and the lines refer to the theoretical calculations that consider both concentrated inclusion and conductivities.

Chapter 5 Magnetoelectric Effect of 0-0-3

Terfenol-D/PZT/Polymer Composites

5.1 Theoretical Aspects

5.1.1 Magnetoelectric Effect

Magnetoelectric (ME) effect is the coupling effect between electric and magnetic fields in matter [Fiebig, 2005]. The direct magnetoelectric (ME) effect of materials has long been studied for its interesting fundamental physics and potential applications in both electric and magnetic areas. This effect is the response of materials in electric polarization P to the applied magnetic field H_a and can be described by the equation [Fiebig, 2005; Grössinger, et al., 2008; Nan, et al., 2008; Zhou and Shin, 2006]

$$\text{ME effect} = \frac{\text{magnetic}}{\text{mechanical}} \times \frac{\text{mechanical}}{\text{electric}} \quad (5.1)$$

In general, the ME voltage coefficient $\alpha_E = \frac{dE}{dH_a}$ [Ryu, et al., 2002] is used to describe the effectiveness of the materials which can be obtained from the measured induced charges Q as a result of the polarization change:

$$\alpha_E = \frac{dE}{dH_a} = \left(\frac{dQ}{dH_a} \right) \left(\frac{1}{\varepsilon' A} \right) = \left(\frac{dD}{dH_a} \right) \left(\frac{1}{\varepsilon'} \right) \quad (5.2)$$

where A is the area of electrode, ε' is the permittivity of composite.

However, there is another ME coefficient $\alpha_p = \frac{dP}{dH_a}$ described by the change in polarization with respect to change in magnetic field, which is related to the voltage coefficient with a permittivity [Nan, et al., 2008; Ryu, et al., 2002], similarly this can be expressed in terms of the measured charge as:

$$\alpha_p = \frac{dP}{dH_a} = \frac{dD}{dH_a} = \left(\frac{dQ}{dH_a} \right) \left(\frac{1}{A} \right) \quad (5.3)$$

The α_p can directly represent ME output signal in a short circuit measurement, it can be in terms of charge or current induced from samples. On the other hand, α_E is the better coefficient for denoting open circuit measurement.

5.1.2 0-0-3 Ferromagnetic/Ferroelectric/Polymer Composites

In general, when magnetic field applied on the 0-0-3 ME composites, strain will be induced on the ferromagnetic phase, and stress couple via the polymer matrix to the ferroelectric ceramic phase. Therefore, amount of charges on the surface of ferroelectric particles and also on the surface of composites will be changed.

Since many of the theoretical models of ME effect focused on layer structured

composites, there are only a limited models work on the 0-0-3 particulate composites, in particular we found almost no one for conductive matrix. Recently as we have discovered the significant ME effect of the particulate PEO composites, Tsang et al. of our research group has purposely developed a model for this specific system and the results fit reasonable good to the experimental data. Therefore, in the following section, we will give a brief introduction to this model and the fitting to the experimental data will be illustrated in the next section.

The theoretical modelling starts from the relation between applied magnetic field H_a to apparent magnetic field on ferromagnetic phase H_f , followed by its magnetostriction λ_1 and then the induced stress applied on the ferroelectric phase S_2 . Finally, the change in dielectric displacement of composite D induced by piezoelectric effect.

For magnetic materials and also magnetic composites, a general relation could be written as

$$B = \xi H + M \quad [\text{Zhou and Shin, 2006}] \quad (5.4)$$

where B , ξ , H and M are the magnetic flux density, permeability, magnetic field, and magnetization respectively. The magnetic properties of the 0-0-3 composite can start from these constitutive relations

$$\begin{cases} B_1 = \xi_1 H_1 + M_1 \\ B_2 = \xi_2 H_2 \\ B_3 = \xi_3 H_3 \end{cases} \quad (5.5)$$

where the subscripts “1”, “2” and “3” denote magnetostrictive inclusion, piezoelectric inclusion and matrix respectively. In considering demagnetization of magnetic materials, the volumetric average of magnetic field H is given by

$$H = H_a - D_0 M = \phi_1 H_1 + \phi_2 H_2 + \phi_3 H_3 \quad (5.6)$$

$$\text{and } B = \phi_1 B_1 + \phi_2 B_2 + \phi_3 B_3 \quad (5.7)$$

where ϕ_j is the volume fraction of the constituent materials. D_0 is the demagnetization factor and H_a is the applied magnetic field acting on the composite.

In this study, the constituents are assumed to be a single inclusion and embedded in a homogeneous matrix, and which the matrix proceeds effective physical properties of all constituents, this assumption is named as effective medium approximation (EMA).

Then the boundary conditions in equation (4.14) can be borrowed to magnetic cases,

$$\begin{cases} B_1 + 2\xi(H_1 - H) = B \\ B_2 + 2\xi(H_2 - H) = B \\ B_3 + 2\xi(H_3 - H) = B \end{cases} \quad (5.8)$$

By combining equations (5.5) to (5.8), relation between H_1 and H_a will be found as

$$\frac{dH_1}{dH_a} = \frac{3}{3 + (1 + (3D_0 - 1)\phi_1)dM_1/dH_1} \quad (5.9)$$

$$\text{where } M_1 = M_{s1} \left\{ 1 - \frac{\pi - 2 \tan^{-1}[(H_1 - \bar{H}_1)/\chi_1]}{\pi + 2 \tan^{-1}[\bar{H}_1/\chi_1]} \right\} \quad (5.10)$$

where M_{s1} is the saturated magnetization with subscript s represent x , y or z directions and χ_1 was a relaxation factor. \bar{H}_1 corresponds to the field at which dM_1/dH_1 was maximum.

We adopt the following expression to describe the magnetostriction strain λ_1^{\parallel} in a polycrystalline material parallel to a magnetic field H_1 :

$$\lambda_1^{\parallel} = \lambda_{s1} \left\{ 1 - \frac{\pi - 2 \tan^{-1}[(H_1 - \bar{H}_{\lambda 1})/\chi_{\lambda 1}]}{\pi + 2 \tan^{-1}[\bar{H}_{\lambda 1}/\chi_{\lambda 1}]} \right\}^2 \quad (5.11)$$

where λ_{s1} is the saturated magnetostriction strain. Following Wong and Shin [13], λ_1^{\perp} is assumed to be $-\beta\lambda_1^{\parallel}$, where β is a positive constant called the magnetostrictive strain ratio.

According to the theory of elasticity, for elastically isotropic materials, the relation of stress S and strain e in the constituents in the x , y and z directions are given by

$$\begin{cases} e_{x1} = S_{x1}/Y_1 - \nu_1 (S_{y1} + S_{z1})/Y_1 + \lambda_{x1}(H_1) \\ e_{y1} = S_{y1}/Y_1 - \nu_1 (S_{x1} + S_{z1})/Y_1 + \lambda_{y1}(H_1), \\ e_{z1} = S_{z1}/Y_1 - \nu_1 (S_{x1} + S_{y1})/Y_1 + \lambda_{z1}(H_1) \end{cases} \quad (5.12)$$

$$\begin{cases} e_{x2} = S_{x2}/Y_2 - \nu_2 (S_{y2} + S_{z2})/Y_2 \\ e_{y2} = S_{y2}/Y_2 - \nu_2 (S_{x2} + S_{z2})/Y_2 \text{ and} \\ e_{z2} = S_{z2}/Y_2 - \nu_2 (S_{x2} + S_{y2})/Y_2 \end{cases} \quad (5.13)$$

$$\begin{cases} e_{x3} = S_{x3}/Y_3 - \nu_3 (S_{y3} + S_{z3})/Y_3 \\ e_{y3} = S_{y3}/Y_3 - \nu_3 (S_{x3} + S_{z3})/Y_3 \cdot [\text{Wong and Shin, 2007}] \\ e_{z3} = S_{z3}/Y_3 - \nu_3 (S_{x3} + S_{y3})/Y_3 \end{cases} \quad (5.14)$$

where Y and ν are the Young's modulus and Poisson's ratio of constituents respectively, and λ is magnetostrictive induced strains of ferromagnetic inclusions described in equation (5.11).

In the experiment, the samples was gently held in the sample holder, so the external stress applied on the sample can assumed to be negligible, therefore the stress components of composite S_x , S_y and S_z are written as

$$\begin{cases} S_x = \phi_1 S_{x1} + \phi_2 S_{x2} + \phi_3 S_{x3} = 0 \\ S_y = \phi_1 S_{y1} + \phi_2 S_{y2} + \phi_3 S_{y3} = 0. \\ S_z = \phi_1 S_{z1} + \phi_2 S_{z2} + \phi_3 S_{z3} = 0 \end{cases} \quad (5.15)$$

The strains of the composite can be given by

$$\begin{cases} e_x = \phi_1 e_{x1} + \phi_2 e_{x2} + \phi_3 e_{x3} \\ e_y = \phi_1 e_{y1} + \phi_2 e_{y2} + \phi_3 e_{y3} . \\ e_z = \phi_1 e_{z1} + \phi_2 e_{z2} + \phi_3 e_{z3} \end{cases} \quad (5.16)$$

According to Wong and Shin [Wong and Shin, 2007], the elastic boundary value problem can be written as

$$\begin{pmatrix} S_{xj} - S_x \\ S_{yj} - S_y \\ S_{zj} - S_z \end{pmatrix} = \begin{pmatrix} A & B & B \\ B & A & B \\ B & B & A \end{pmatrix} \begin{pmatrix} e_{xj} - e_x \\ e_{yj} - e_y \\ e_{zj} - e_z \end{pmatrix} \quad (5.17)$$

where j stands for 1, 2 and 3, $A = 10\mu\{2\mu/(k+2\mu)-3\}/9$ and $B = -\mu\{10\mu/(k+2\mu)+3\}/9$; k and μ are bulk modulus and shear modulus respectively. By solving equations (5.12) to (5.17), the relation of S_{x2} , S_{y2} and S_{z2}

together with $\lambda_{x1}(H_1)$, $\lambda_{y1}(H_1)$ and $\lambda_{z1}(H_1)$ will be obtained.

Same as discussion in Chapter 4, the dielectric properties of constitues are given by

$$\begin{cases} D_1 = \varepsilon_1 E_1 \\ D_2 = \varepsilon_2 E_2 + P_2 \\ D_3 = \varepsilon_3 E_3 \end{cases} \quad (5.18)$$

However, the permittivity ε_j in this section is defined as $\varepsilon'_j - i\varepsilon''_j$ with $\varepsilon''_j = \frac{\sigma_j}{2\pi f}$, this

is taken as the consideration of conductivity. The volumetric average of the electric

field E and electric displacement D of the composite are given by

$$E = \phi_1 E_1 + \phi_2 E_2 + \phi_3 E_3 \quad (5.19)$$

$$\text{and } D = \phi_1 D_1 + \phi_2 D_2 + \phi_3 D_3. \quad (5.20)$$

Using EMA in the boundary value problem and the interfacial surface charge is not

considered in this problem, equation (4.14) can be modified as

$$\begin{cases} D_1 + 2\varepsilon(E_1 - E) = D \\ D_2 + 2\varepsilon(E_2 - E) = D \\ D_3 + 2\varepsilon(E_3 - E) = D \end{cases} \quad (5.21)$$

Solving equation (5.18) to (5.21):

$$D = \varepsilon E + \phi_2 \frac{3\varepsilon}{\varepsilon_2 + 2\varepsilon} P_2. \quad (5.22)$$

It is known that in a ferroelectric material, external stresses are also contributing to its

polarization, which is actually the part of relevance here. This part is represented by

$$P_2 = d_{31,2} S_{x2} + d_{32,2} S_{y2} + d_{33,2} S_{z2}. \quad (5.23)$$

Here $d_{31,2}$, $d_{32,2}$ and $d_{33,2}$ are the ferroelectric coefficients of the ferroelectric phase.

Therefore, the dielectric displacement D and stress S can also related by combining

equation (5.22) and (5.23), with $E = 0$ under short circuit condition,

$$D = \phi_2 \frac{3\varepsilon}{\varepsilon_2 + 2\varepsilon} (d_{31,2} S_{x2} + d_{32,2} S_{y2} + d_{33,2} S_{z2}) \quad (5.24)$$

In the experiment, the root-mean-square value of charge output and the magnetic field

are measured, so the dielectric displacement and magnetic field are written as $H_{a,rms}$

and D_{rms}

$$\begin{aligned} \alpha_p &= \frac{dD}{dH_a} = \frac{dD_{rms}}{dH_{a,rms}} \\ &= 3\phi_2 \sqrt{\frac{\varepsilon'^2 + \varepsilon''^2}{(2\varepsilon' + \varepsilon'_2)^2 + (2\varepsilon'' + \varepsilon''_2)^2}} \left(d_{31,2} \frac{dS_{x2}}{dH_1} + d_{32,2} \frac{dS_{y2}}{dH_1} + d_{33,2} \frac{dS_{z2}}{dH_1} \right) \frac{dH_1}{dH_a} \end{aligned} \quad (5.25)$$

Similarly,

$$\begin{aligned} \alpha_E &= \frac{1}{\varepsilon'} \frac{dD}{dH_a} = \frac{1}{\varepsilon'} \frac{dD_{rms}}{dH_{a,rms}} \\ &= \frac{3\phi_2}{\varepsilon'} \sqrt{\frac{\varepsilon'^2 + \varepsilon''^2}{(2\varepsilon' + \varepsilon'_2)^2 + (2\varepsilon'' + \varepsilon''_2)^2}} \left(d_{31,2} \frac{dS_{x2}}{dH_1} + d_{32,2} \frac{dS_{y2}}{dH_1} + d_{33,2} \frac{dS_{z2}}{dH_1} \right) \frac{dH_1}{dH_a} \end{aligned} \quad (5.26)$$

For example, from the experimental setup, applied magnetic field H_a was always

parallel to the electrodes of the composites films (x - y plane), and the change in charge

or D was measured in the z -direction. Then, equations (5.25) and (5.26) can represent α_{P31} and α_{E31} . Moreover, as the width of the films are much larger than their thickness, then the demagnetization effects can assumed to be negligible, so the demagnetization factor D_0 is set to be zero in equation (5.6). Because of the geometry, we can write $\lambda_{x1} = \lambda_1^{\parallel}$ and $\lambda_{y1} = \lambda_{z1} = \lambda_1^{\perp}$ in equation (5.12) to denote the magnetostriction in the magnetostrictive inclusions parallel and perpendicular to H_1 , respectively. Also, $e_{yj} = e_{zj}$, $e_y = e_z$ and $S_{yj} = S_{zj}$ in equations (5.12) to (5.17). Hence, from equation (5.25), the measured “in-plane” ME coefficient of a three-phase multiferroic particulate composite becomes

$$\alpha_{P31} = 3\phi_2 \sqrt{\frac{\varepsilon'^2 + \varepsilon''^2}{(2\varepsilon' + \varepsilon'_2)^2 + (2\varepsilon'' + \varepsilon''_2)^2}} \times \left[d_{31,2} \frac{dS_{x2}(\lambda_1^{\parallel}, \lambda_1^{\perp})}{dH_1} + (d_{31,2} + d_{33,2}) \frac{dS_{z2}(\lambda_1^{\parallel}, \lambda_1^{\perp})}{dH_1} \right] \frac{dH_1}{dH_a} \quad (5.27)$$

$$\equiv FG$$

$$\text{where } F = 3\phi_2 \sqrt{\frac{\varepsilon'^2 + \varepsilon''^2}{(2\varepsilon' + \varepsilon'_2)^2 + (2\varepsilon'' + \varepsilon''_2)^2}} \quad (5.28)$$

$$\text{and } G = \left[d_{31,2} \frac{dS_{x2}(\lambda_1^{\parallel}, \lambda_1^{\perp})}{dH_1} + (d_{31,2} + d_{33,2}) \frac{dS_{z2}(\lambda_1^{\parallel}, \lambda_1^{\perp})}{dH_1} \right] \frac{dH_1}{dH_a}. \quad (5.29)$$

5.2 Results and Discussion

In this chapter, the main focus is to study the effect of matrix conductivity of composites to its ME properties. Therefore the discussion will begin from the conductivity of matrix materials. The conductivity of PMMA is the lowest, it is of the order of 10^{-9} S/m at 100 Hz [McCrum, et al., 1967; Shukla and Gupta, 1987], and is almost frequency independent, so that it is regarded as an insulating matrix. On the other hand, the conductivities against frequency of the neat and doped PEO are given in Figure 5.1. For polymer electrolyte PEO, its conductivity at 100 Hz is 4.1×10^{-6} S/m, where the LiClO₄ doped PEO at the same frequency is about 1.1×10^{-4} S/m, around one to two orders of magnitude higher than neat PEO.

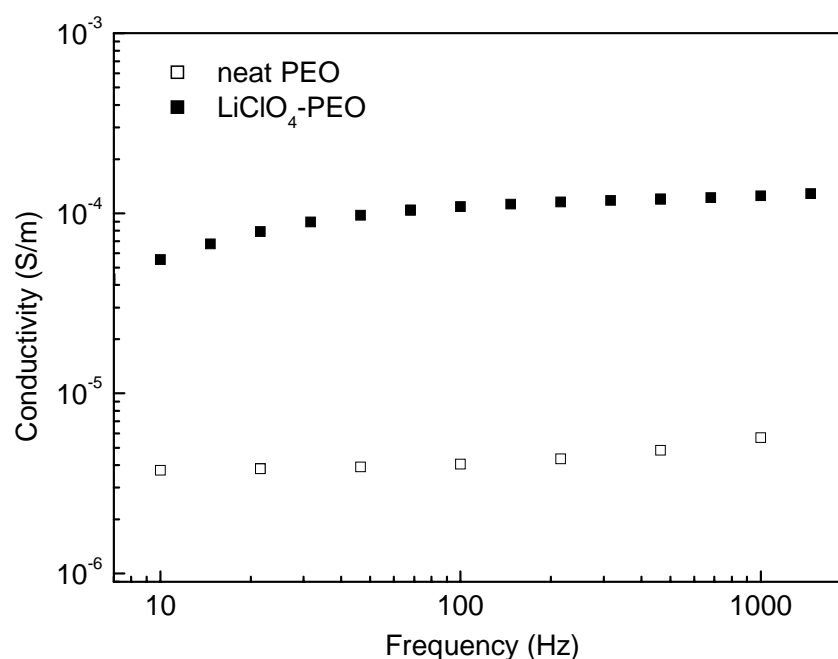


Figure 5.1 Conductivity of matrices, PEO and LiClO₄ doped PEO, as a function of frequency.

The frequency dependence of dielectric constant of the composites were measured for calculating the corresponding ME voltage coefficient. As shows in Figure 5.2, the dielectric constant of composites with PEO and Li⁺ doped PEO matrices are highly frequency dependent, which increase with frequency decreasing. This feature reflects the ionic conducting characteristic of the PEO as described in Chapter 3.2. On the other hand, the sample of PMMA matrix shows almost no frequency dependence and it has the lowest dielectric constant. These set of data are used to calculate ME voltage coefficient $\alpha_E = \frac{dE}{dH}$ in the coming section.

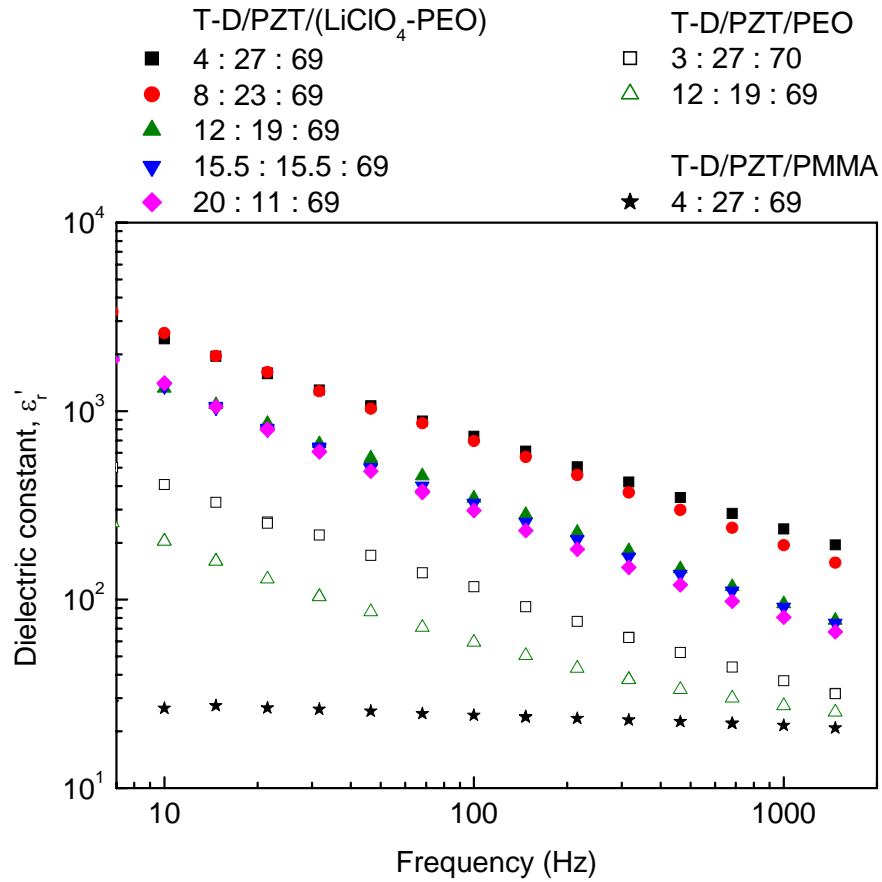


Figure 5.2 Dielectric constants of Terfenol-D/PZT/polymer composites, the matrices are PMMA, PEO and LiClO₄-PEO, as a function of frequency.

Since the ME properties of the composites were measured in a short-circuit configuration via a charge amplifier, the ME coefficient $\alpha_p = \frac{dP}{dH}$ is more appropriate to describe the charge induced by ME effect than the ME voltage coefficient $\alpha_E = \frac{dE}{dH}$. Figure 5.3 shows the α_{p31} under 5 Oe sinusoidal magnetic field at 100 Hz, and various d.c. bias magnetic field H_{dc} of the three samples, the α_{p31} of the Li-doped PEO sample is the highest among all samples, its α_{p31} is around 950

pC/m²·Oe at bias magnetic field H_{dc} equal to 1100 Oe, and the undoped PEO sample has a value 330 pC/m²·Oe at the H_{dc} equal to 1200 Oe. Similarly, the α_{p31} of PMMA sample is found as 100 pC/m²·Oe at bias magnetic field H_{dc} equal to 1400 Oe. According to the experimental results given in Figure 5.3, the following conclusion can be drawn. The change in charge density due to the change in magnetic field can be enhanced by increasing the conductivity of matrix in a 0-0-3 magnetoelectric composite, and therefore conducting matrix can benefit the ME effect of composites samples for magnetic sensing applications. In addition, the T-D/PZT/PMMA achieves its own maximum α_{p31} at higher H_{dc} (1400 Oe) than other samples, this might be due to the higher elastic modulus of PMMA broadens the magnetostrictive strain profile of Terfenol-D. In fact the difference between Li-doped PEO sample (at 1100 Oe) and undoped PEO sample (at 1200 Oe) can be explained by the experimental fluctuations, because the values of α_{p31} are very close to each other when α_{p31} approach to their maximum.

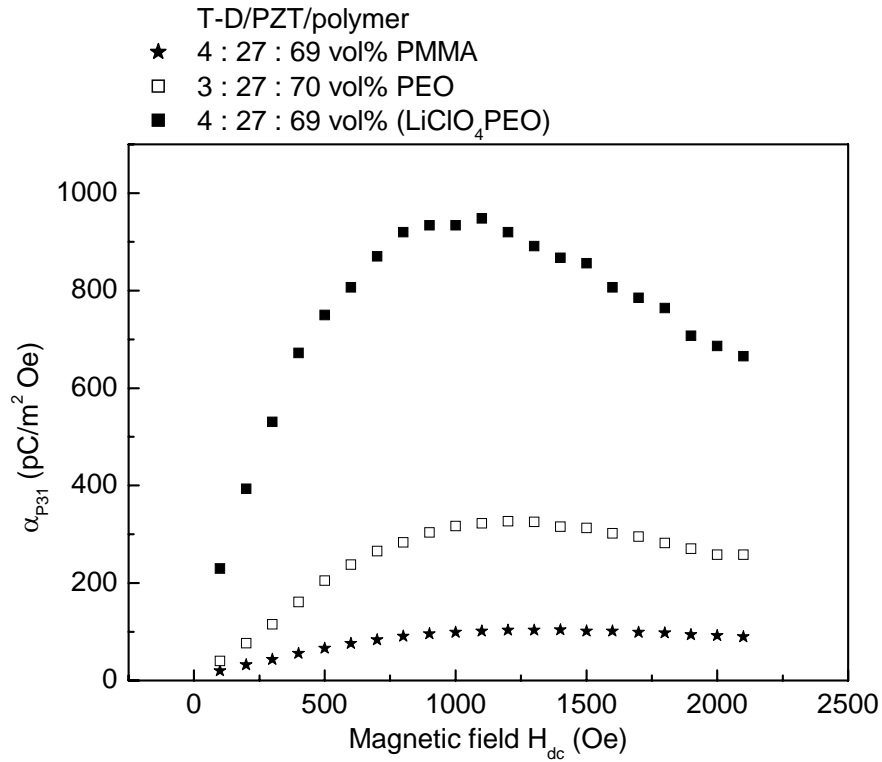


Figure 5.3 Magnetolectric coefficients, α_{p31} of Terfenol-D/PZT/polymer composites, the matrices are PMMA, PEO and LiClO₄-PEO, under 5 Oe at 100 Hz sinusoidal magnetic field as a function of biasing magnetic field.

On the other hand, the ME voltage coefficients α_{E31} of the three samples are shown in Figure 5.4. Due to the large permittivity of the polymer electrolyte matrix, α_{E31} of T-D/PZT/LiClO₄-PEO becomes the smallest, and the peak of α_{E31} of T-D/PZT/LiClO₄-PEO and T-D/PZT/PEO are found to be 1.5 and 3.2 mV/cm·Oe respectively at H_{dc} equal to 1100 and 1200 Oe. It can be seen that the α_E of T-D/PZT/PMMA approaches a peak value of 4.8 mV/cm·Oe at 1400 Oe.

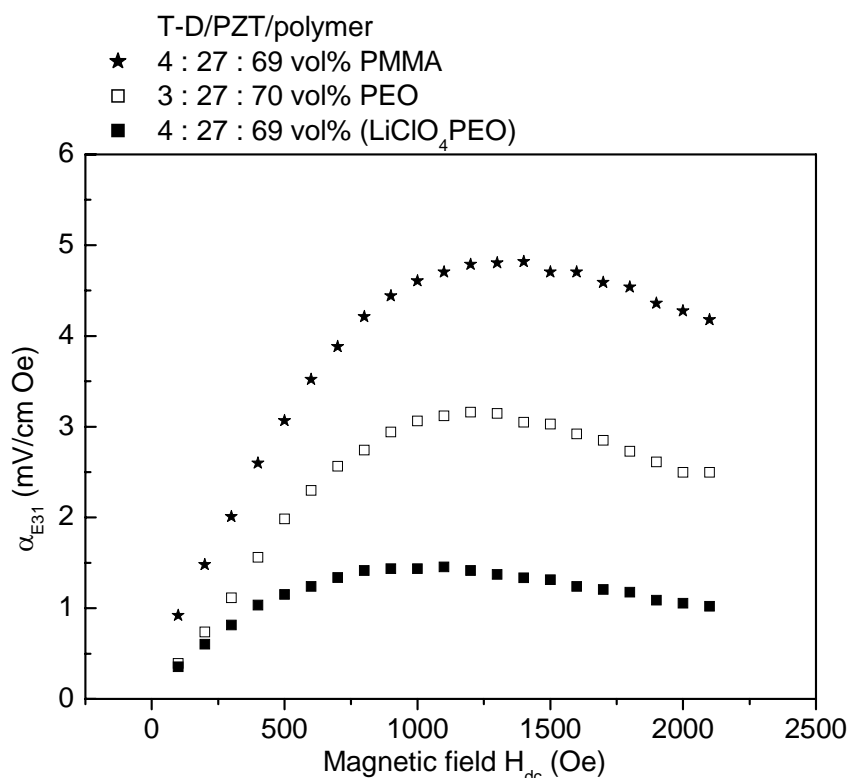


Figure 5.4 Magnetolectric voltage coefficients, α_{E31} of Terfenol-D/PZT/polymer composites, the matrices are PMMA, PEO and LiClO₄-PEO, under 5 Oe at 100 Hz sinusoidal magnetic field as a function of biasing magnetic field.

The α_{P31} and α_{E31} of T-D/PZT/polymer composites measured under 1 kOe bias magnetic field superimposed with 5 Oe sinusoidal magnetic field at various frequency are shown in Figure 5.5 and 5.6 respectively. Composite with LiClO₄-PEO matrix has the smallest α_{E31} but largest α_{P31} , and for composite with PMMA matrix is on the reverse. There are quite obvious frequency dependence of α_{P31} in LiClO₄-PEO and PEO samples, this phenomenon is due to the frequency dependence of dielectric

properties of matrices, and will be discussed in latter paragraph with a factor F (Figure 5.10). These confirm the effect of conductivity of matrix on the ME properties of the 0-0-3 composites. In addition, there are spikes found at around 20 and 300 Hz of PEO sample as shows in Figure 5.5 and 5.6. At such a low frequency range, it cannot be due to the resonance effect. The causes of these repeatable measured results are worth for a further investigation.

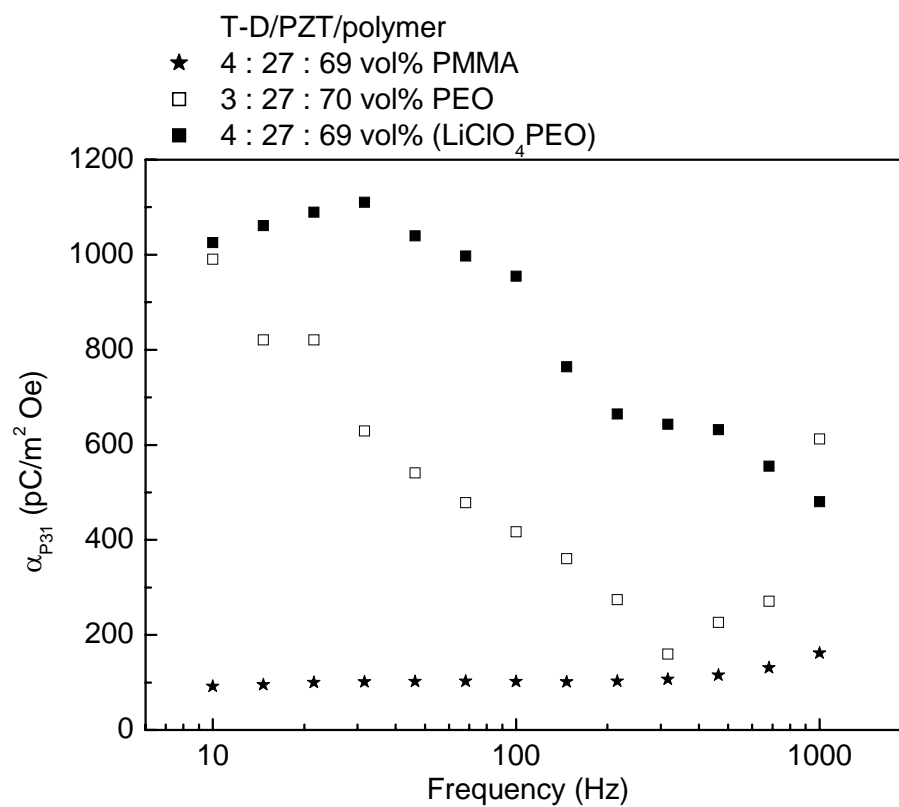


Figure 5.5 Magnetolectric coefficients, α_{p31} of Terfenol-D/PZT/polymer composites, the matrices are PMMA, PEO and LiClO₄-PEO, under 5 Oe sinusoidal magnetic fields superimposed with 1 kOe magnetic field in various frequencies.

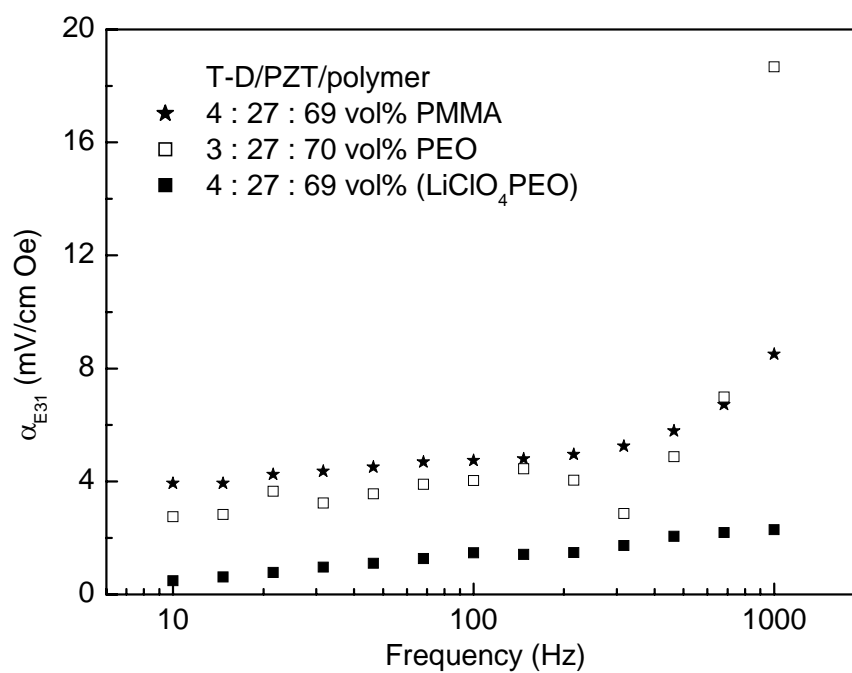


Figure 5.6 Magnetolectric coefficients, α_{E31} of Terfenol-D/PZT/polymer composites, the matrices are PMMA, PEO and LiClO₄-PEO, under 5 Oe sinusoidal magnetic fields superimposed with 1 kOe magnetic field in various frequencies.

Table 5.1 Parameters of constituents used in calculations.

| | ξ_r/ξ_0 | Y (GPa) | ν | d_{31} (pC/N) | d_{33} (pC/N) | | |
|-------------------------|------------------------------------|---------------------|-------------------|-------------------------|-------------------------------|----------------------------|---------|
| Terfenol-D | 5 ^a | 30 ^b | 0.3 ^b | 0 | 0 | | |
| PZT | 1 | 71 ^c | 0.31 ^c | -175 ^c | 400 ^c | | |
| PEO | 1 | 0.40 ^d | 0.35 ^e | 0 | 0 | | |
| LiClO ₄ -PEO | 1 | 0.40 ^f | 0.35 ^f | 0 | 0 | | |
| | M_{s1} (emu/cm ³) | \bar{H}_1 (Oe) | χ_1 (Oe) | λ_{s1} (ppm) | $\bar{H}_{\lambda 1}$ (Oe) | $\chi_{\lambda 1}$ (Oe) | β |
| Terfenol-D | 700 ^g | 50 | 1200 | 1000 | 140 | 470 ^g | 0.45 |

^a [Shi, et al., 2004].

^b [Armstrong, 2002; Chen, et al., 1999].

^c [Piezo_Kinetics, 2007].

^d [Bartolotta, et al., 1992].

^e Commonly, the Poisson's ratio ν of polymers are between 0.35 and 0.45.

^f The LiClO₄-PEO polymer was doped with small amount of LiClO₄. The molar ratio was fixed to be [ethylene oxide]:[Li] = 1.24x10³:1. This amount of LiClO₄ would affect on Young's modulus Y and Poisson's ratio ν very little. Therefore Y and ν were assumed to be the same as the values of PEO.

^g [Cai, et al., 2003]

Figure 5.7 shows another set of composites samples which have more T-D content (12% T-D/19% PZT/69% polymer). The theoretical curve fitting as described in the last section are also shown in the graph. The parameters required for equation (5.25) are given in Table 5.1. The α_{p31} of sample with PMMA matrix do not shown in Figure 5.7, this is because the poling process of that sample with 12% T-D was not success. The experimental data and modelling are quite match with each other, excepted that 4% T-D/27% PZT/69% (LiClO₄-PEO) observed some deviations, the reason for the difference is still under investigation. As other experimental and theoretical results are in good match, we can state that the modelling results verify the effect of matrix's conductivity on the ME effect of the composites. Same as the findings in previous discussion, composite with LiClO₄ doped matrix has higher α_{p31} than the composite with pure PEO matrix. The result also shows that, even though the 4% T-D/27% PZT/69% (LiClO₄-PEO) has less T-D content and smaller factor $|G|$ (equation (5.29)) than 12% T-D/19% PZT/69% PEO (Figure 5.8), the former one still has higher α_{p31} than the latter. The highest α_{p31} can obtain for sample 12% T-D/19% PZT/69% (LiClO₄-PEO), it is equal to 2760 pC/m²·Oe at H_{dc} of 900 Oe. Similar to α_{p31} in Figure 5.7, the $|G|$ in Figure 5.8 show peaks at around H_{dc} of 1000 Oe, but the position of peaks of each content are differ from each other, this is caused by the difference in dielectric and magnetic properties of constituents.

Moreover, factor $|G|$ of the composites are frequency independent.

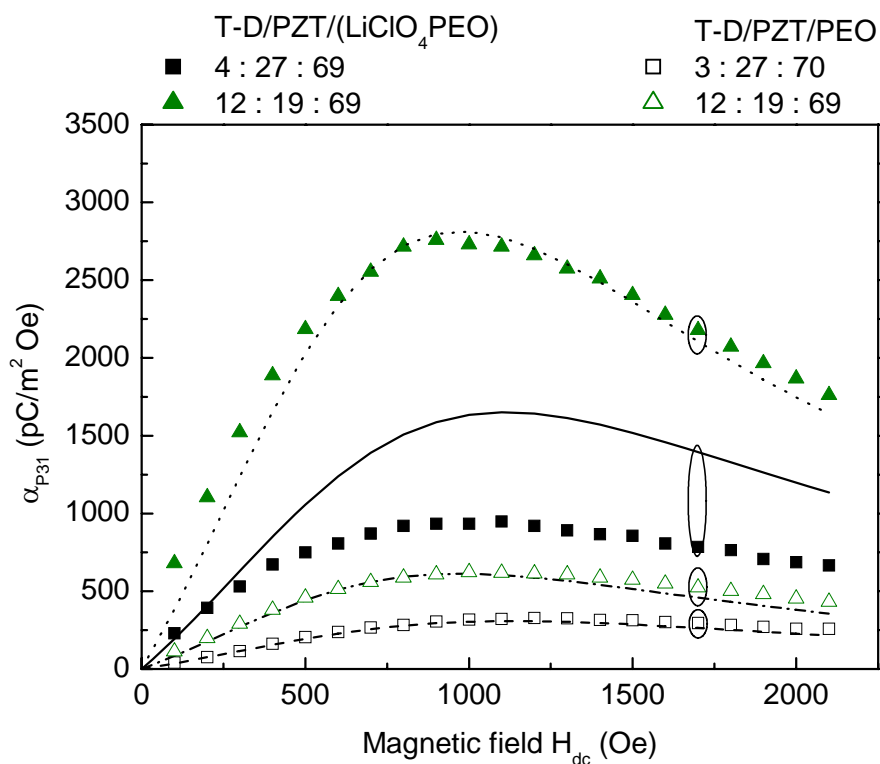


Figure 5.7 Magnetolectric coefficients, α_{p31} of Terfenol-D/PZT/polymer composites, the matrices are PEO and LiClO_4 -PEO, under 5 Oe at 100 Hz sinusoidal magnetic field as a function of biasing magnetic field. The lines denoted as theoretical modelling.

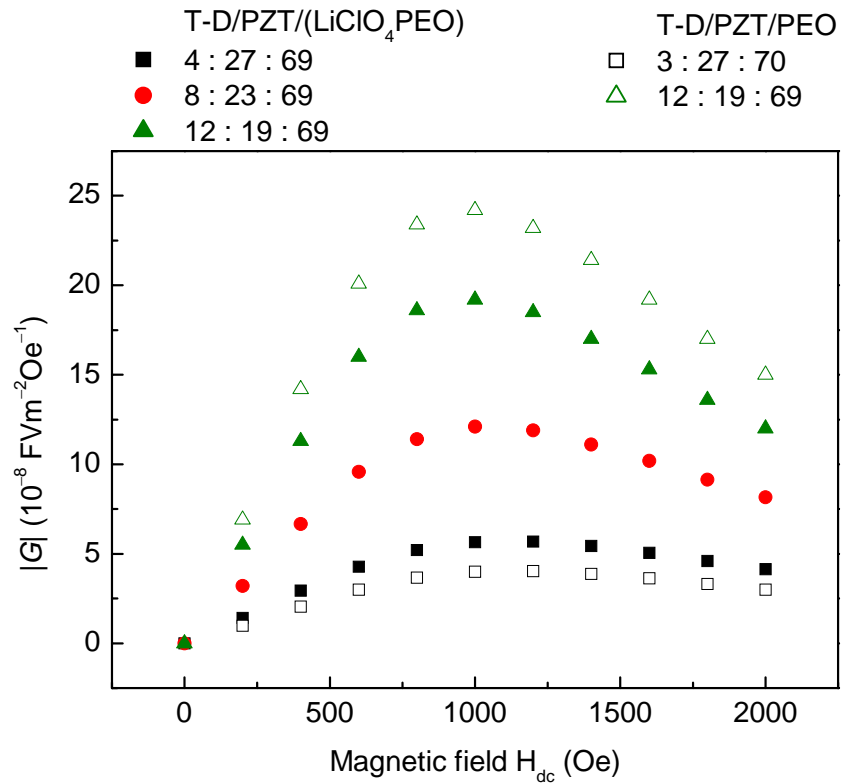


Figure 5.8 Theoretical values of $|G|$ in Terfenol-D/PZT/polymer composites, the matrices are PEO and LiClO₄-PEO, under 5 Oe at 100 Hz sinusoidal magnetic field as a function of biasing magnetic field.

Figure 5.9 shows the α_{p31} against frequency of composites mentioned in Figure 5.7, the experimental and theoretical results consist with each other, as same as Figure 5.7, experimental and theoretical results of the 4% T-D/27% PZT/69% (LiClO₄-PEO) also has some mismatch. The α_{p31} of composites drop as frequency increases, this can be explained by the dielectric properties with factor F in equation (5.28). F of the composites decrease when frequency increases (Figure 5.10), this is due to the

frequency dependency of ε' and ε'' (Figure 5.2 and 5.11), with $\varepsilon'_2 = 1800 \varepsilon_o$. and $\varepsilon''_2 = 27 \varepsilon_o$ [Piezo_Kinetics, 2007] are frequency independent, therefore, the factor F of composites decrease when frequency increases. F is sensitive to the ratio of dielectric constant and dielectric loss, when the conductivity $\sigma = 2\pi f\varepsilon''$ and ε' are higher than $\sigma_2 = 2\pi f\varepsilon''_2$ and ε'_2 , the factor F of composites will achieve fruitful values. Therefore, multiplying F with the frequency independent $|G|$, α_{p31} can be enhanced by increasing the conductivity of composites or matrices.

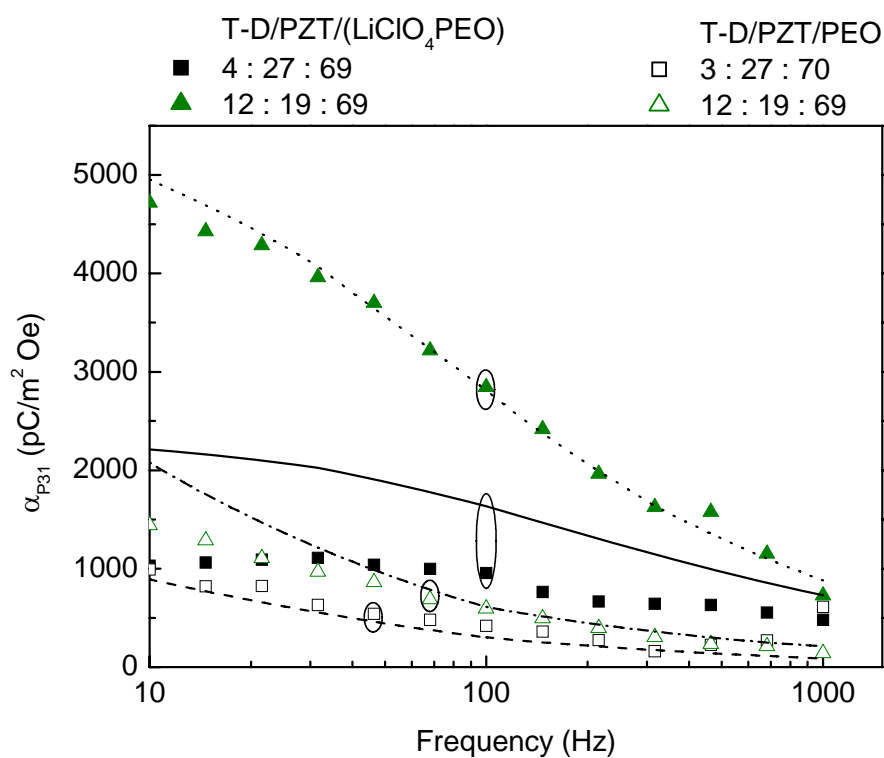


Figure 5.9 Magnetolectric coefficients, α_{p31} of Terfenol-D/PZT/polymer composites, the matrices are PEO and LiClO₄-PEO, under 5 Oe sinusoidal magnetic fields superimposed with 1 kOe magnetic field in various frequencies. The lines denoted as theoretical modelling.

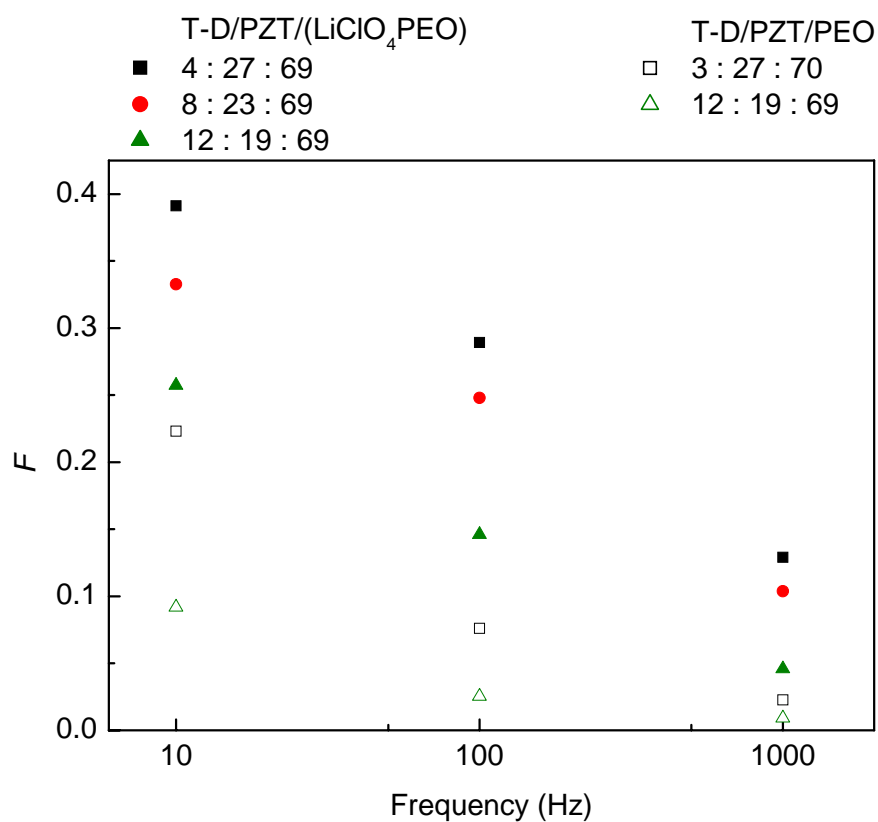


Figure 5.10 Theoretical values of F in Terfenol-D/PZT/polymer composites, the matrices are PEO and LiClO₄-PEO, under 5 Oe sinusoidal magnetic fields superimposed with 1 kOe magnetic field in various frequencies.

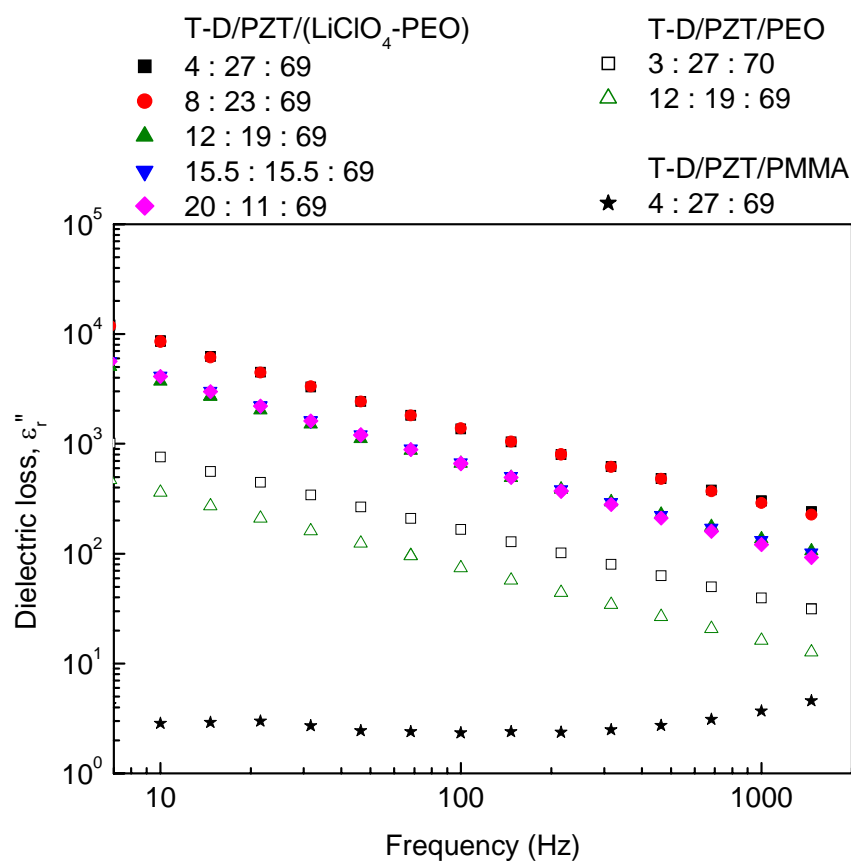


Figure 5.11 Dielectric losses of Terfenol-D/PZT/polymer composites, the matrices are PMMA, PEO and $\text{LiClO}_4\text{-PEO}$, as a function of frequency.

Beside the modelling on α_{p31} , Figure 5.12 also shows the theoretical fitting of α_{E31} with experimental results, they are reasonably good matching with each other, except that some deviations are found when H_{dc} higher than 1000 Oe. Same as in the previous discussion, due to the large ϵ' of $\text{LiClO}_4\text{-PEO}$ composite, 12% T-D/19% PZT/69% ($\text{LiClO}_4\text{-PEO}$) has smaller α_{E31} than 12% T-D/19% PZT/69% PEO.

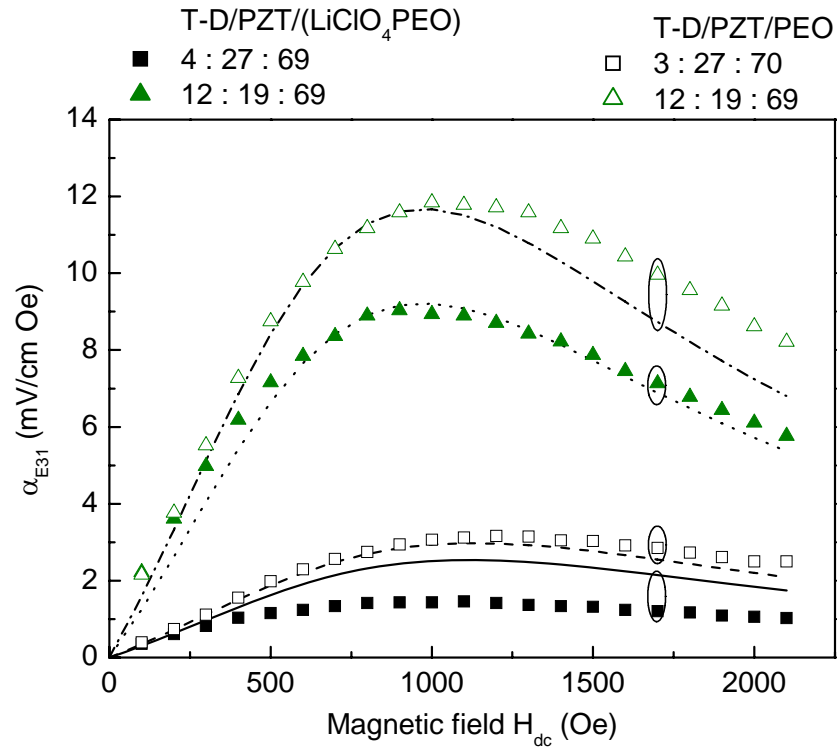


Figure 5.12 Magnetolectric voltage coefficients, α_{E31} of Terfenol-D/PZT/polymer composites, the matrices are PEO and LiClO_4 -PEO, under 5 Oe at 100 Hz sinusoidal magnetic field as a function of biasing magnetic field. The lines denoted as theoretical modelling.

After the investigation of ME effect of the 3-phase composites with different polymer matrices, we can state that the composite with the most conducting LiClO_4 doped PEO matrix has the largest values of α_{P31} . Therefore, the composites with LiClO_4 doped PEO matrix were further investigated, by varying the volume fraction of inclusions phases with a fixed fraction of 69% matrix. As the content of T-D increases from 4 %

to 20%, there is no percolation effect observed in the composites, and the ME effects of all of them are attainable (Figure 5.13). The percolation limit of this series of samples are obviously higher than reported in others work [Nan, et al., 2002], they claimed that percolation would occurred when Terfenol-D content was more than 10% in the T-D/PZT/PVDF composites, therefore no ME effect was observed.

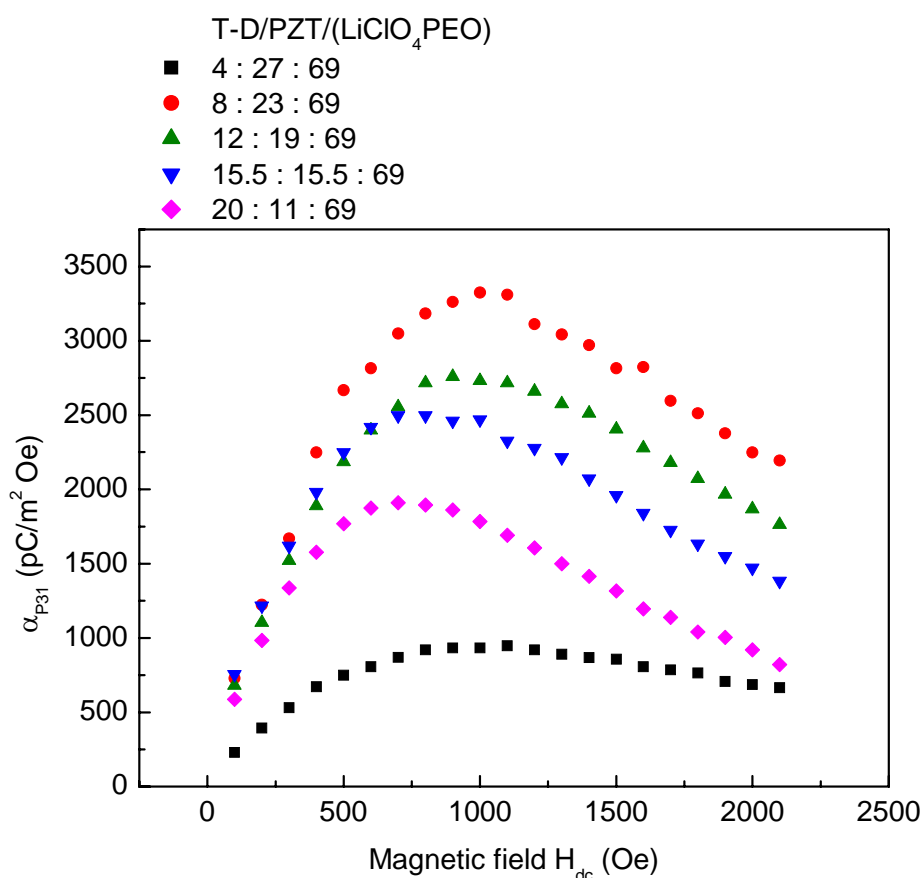


Figure 5.13 Magnetolectric coefficients, α_{p31} of Terfenol-D/PZT/LiClO₄-PEO composites, under 5 Oe at 100 Hz sinusoidal magnetic field as a function of biasing magnetic field.

Figure 5.13 shows that the 8% T-D/23% PZT/69% (LiClO₄-PEO) has the largest α_{p31} among all of the samples, its α_{p31} reaches a maximum of 3300 pC/m²·Oe at H_{dc} of 1000 Oe. The maximum α_{p31} of composites shift from higher H_{dc} to lower H_{dc} as the contents of T-D increased, this is expected in the theoretical model as represented by the factor $|G|$ of the composites. Finally, Figure 5.14 gives the corresponding frequency dependence of α_{p31} , of the composites, since the factor F are large at low frequency range, the α_{p31} of the composites at low frequency are much larger than at high frequency, so that these composites are more suitable for low frequency applications.

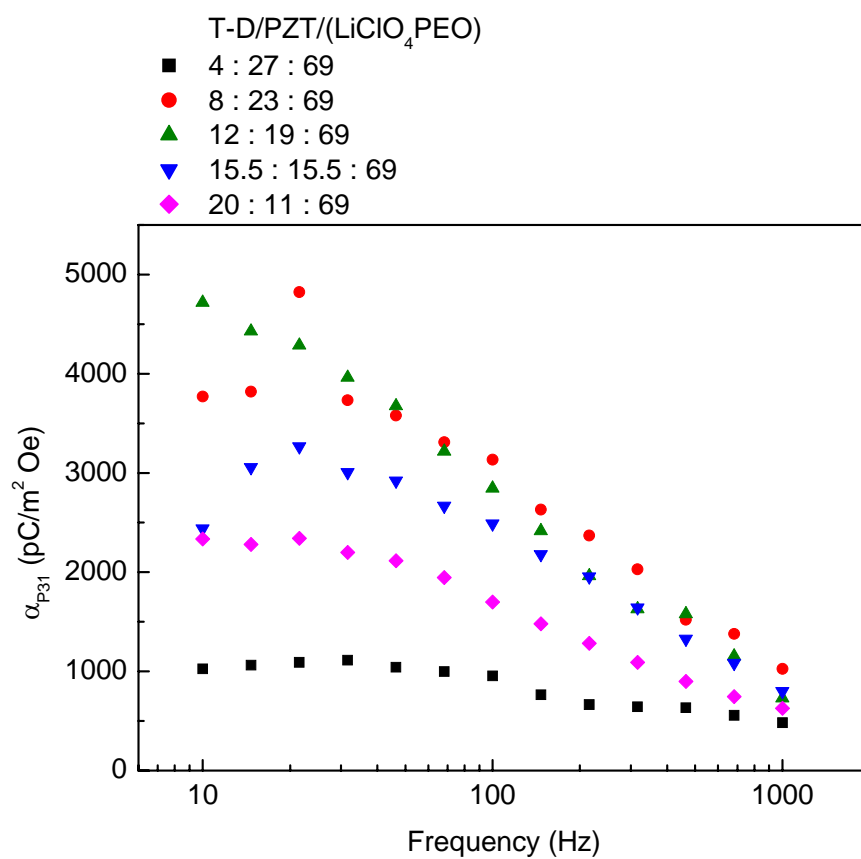


Figure 5.14 Magnetolectric coefficients, α_{p31} of Terfenol-D/PZT/(LiClO₄-PEO) composites, under 5 Oe sinusoidal magnetic fields superimposed with 1 kOe magnetic field in various frequencies.

Chapter 6 Conclusions

The electrical properties of PEO and LiClO₄ doped PEO were investigated, the conductivity of PEO will increase as absorption of moisture from ambient air, but it will saturated after overnight exposure in ambient. The conductivity of PEO can also be enhanced by doping of LiClO₄, the LiClO₄ doped PEO with molar ratio [ethylene oxide]:[Li] = 1.24x10³:1 has enhanced the conductivity of pure PEO by 1 to 2 order of magnitudes, the enhancement also depends on the frequency at measurements. The non-linear current-voltage relationship of PEO exhibits the characteristics of ionic conduction, accumulation of charges at electrolyte-blocking electrode interfaces can also be figured out by non-linear voltage drops along PEO. The charge accumulation has induced time dependent of d.c. conductivity, but not affecting the a.c. conductivity of PEO.

PZT/PEO composites were fabricated up to a PZT volume fraction of 34%. The pyroelectric coefficient of that sample is 120 μC/m²K, which is greatly enhanced compared with other PZT polymer composites with negligible conductivity. In addition, the piezoelectric coefficient d_{33} of that sample is found to be 170 pC/N as well. Similar to the pyroelectric coefficients, a significant enhancement in piezoelectric coefficients is observed. Moreover, d_{33} of PZT/(LiClO₄-PEO) sample with 20% of PZT is equal to

185 pC/N, this result can further confirm the relationship between conductivity of constituents and piezoelectric effect. Short poling process of the PZT/polymer electrolyte composites is also benefited by the ionic conducting matrices. These results are confirmed by the theoretical models which take the conductivities of the constituents into consideration. It is expected that both the study and applications of the sensors or actuators that make use of these composite materials will be benefited from the understanding of the role playing by the conductivity of the materials.

Samples of magnetostrictive Terfenol-D powder and piezoelectric PZT powder blended with three types of matrices, PMMA, PEO and LiClO₄-PEO were fabricated. Their ME coefficient were measured accordingly. Due to the relatively high conductivities of PEO and LiClO₄-PEO matrix, the ME responses of these composite films are significantly higher than the composite film with insulating PMMA matrix. For measurement at 100 Hz, 4% T-D/27% PZT/69% (LiClO₄-PEO) has about 10 times larger in ME coefficients ($\alpha_p = \frac{dP}{dH}$) than composites with PMMA matrix in the same inclusions content. 8% T-D/23% PZT/69% (LiClO₄-PEO) has the largest α_{p31} among all of the measured samples, its α_{p31} has reached a maximum of 3300 pC/m²·Oe at a bias magnetic field of 1000 Oe. The large ME coefficients implies a large signal output in a short-circuit measurement by using a charge amplifier. In other words, a composite

film with conductive matrix will produce enhanced ME signals compared with those using an insulating matrix.

On the other hand, the more reported ME voltage coefficient $\alpha_E = \frac{dE}{dH}$ has also been calculated, this is a coefficient that denote ME response in open circuit measurement, the α_{E31} of the 0-0-3 ME composites are ranged between 1 to 10 mV/cm·Oe. Due to the large permittivity of polymer electrolytes composites, the calculated α_{E31} of composites is largest with PMMA matrices, but smallest with LiClO₄-PEO matrices. The experimental results of α_{P31} and α_{E31} are found to be consist with theoretical model which is purposely developed for 0-0-3 ME composites system.

References

Abdullah, M.J. and Das-Gupta, D.K. "Electrical-Properties of Ceramic Polymer Composites". *Ieee Transactions on Electrical Insulation*, Vol.25 (3), pp.605-610 (1990).

Anderson, J.C. *Dielectrics*. Chapman and Hall, London (1964).

Armand, M. "Polymer solid electrolytes - an overview". *Solid State Ionics*, Vol.9-10 (Part 2), pp.745-754 (1983).

Armand, M.B. *Current State of PEO-Based Electrolyte*. Polymer electrolyte reviews. J. R. MacCallum and C. A. Vincent. London ; New York, Elsevier Applied Science. Vol.1, pp.1. (1987).

Armstrong, W.D. "A General Magneto-Elastic Model of Terfenol-D Particle Actuated Composite Materials". *Journal of Intelligent Material Systems and Structures*, Vol.13 (2-3), pp.137-141 (2002).

Bailey, F.E. and Koleske, J.V. *Polyethylene oxide*. Academic Pr., New York (1976).

Bartolotta, A., Di Marco, G. and Carini, G. "Elastic and anelastic behavior in poly (ethylene) oxide complexed with cesium salt". *Solid State Ionics*, Vol.58 (1-2), pp.55-60 (1992).

Bohnke, O. and Bohnke, C. "Polymer-Based Solid Electrochromic Cell for Matrix-Addressable Display Devices". *Journal of The Electrochemical Society*, Vol.138 (12), pp.3612-3617 (1991).

Cai, N., Zhai, J., Nan, C.W., Lin, Y. and Shi, Z. "Dielectric, ferroelectric, magnetic, and magnetoelectric properties of multiferroic laminated composites". *Physical Review B*, Vol.68 (22), pp.224103 (2003).

Callister, W.D. *Materials science and engineering : an introduction*. Wiley, New York

(2003).

Chan, H.L.W., Chen, Y. and Choy, C.L. "A Poling Study of Pzt/P(Vdf-Trfe) Copolymer 0-3-Composites". *Integrated Ferroelectrics*, Vol.9 (1-3), pp.207-214 (1995).

Chan, H.L.W., Ng, P.K.L. and Choy, C.L. "Effect of poling procedure on the properties of lead zirconate titanate/vinylidene fluoride-trifluoroethylene composites". *Applied Physics Letters*, Vol.74 (20), pp.3029-3031 (1999).

Chen, Y., Snyder, J.E., Schwichtenberg, C.R., Dennis, K.W., Falzgraf, D.K., McCallum, R.W. and Jiles, D.C. "Effect of the elastic modulus of the matrix on magnetostrictive strain in composites". *Applied Physics Letters*, Vol.74 (8), pp.1159-1161 (1999).

Choy, S.H., Li, W.K., Li, H.K., Lam, K.H. and Chan, H.L.W. "Study of BNKLBT-1.5 lead-free ceramic/epoxy 1-3 composites". *Journal of Applied Physics*, Vol.102 (11), pp.114111 (2007).

Cohen, E.R., Lide, D.R., Trigg, G.L. and American Institute of Physics. *AIP physics desk reference*. Springer, New York ; Hong Kong (2003).

Croce, F., Appetecchi, G.B., Persi, L. and Scrosati, B. "Nanocomposite polymer electrolytes for lithium batteries". *Nature*, Vol.394 (6692), pp.456-458 (1998).

Das-Gupta, D.K. "Pyroelectricity in Polymers". *Ferroelectrics*, Vol.118 (1-4), pp.165-189 (1991).

Deitzel, J.M., Kleinmeyer, J.D., Hirvonen, J.K. and Beck Tan, N.C. "Controlled deposition of electrospun poly(ethylene oxide) fibers". *Polymer*, Vol.42 (19), pp.8163-8170 (2001).

Fiebig, M. "Revival of the magnetoelectric effect". *Journal of Physics D: Applied Physics*, Vol.38 (8), pp.R123-R152 (2005).

Finn, C.B.P. *Thermal physics*. Stanley Thrones, Cheltenham [England] (1998).

Furukawa, T., Fujino, K. and Fukada, E. "Electromechanical Properties in Composites of Epoxy-Resin and Pzt Ceramics". *Japanese Journal of Applied Physics*, Vol.15 (11), pp.2119-2129 (1976).

Furukawa, T., Suzuki, K. and Date, M. "Switching process in composite systems of PZT ceramics and polymers". *Ferroelectrics*, Vol.68 (1), pp.33 - 44 (1986).

Furukawa, T., Yasuda, K. and Takahashi, Y. "Dielectric and conductive spectra of the composite of barium titanate and LiClO₄-doped polyethylene oxide". *IEEE Transactions on Dielectrics and Electrical Insulation*, Vol.11 (1), pp.65-71 (2004).

Gauthier, M., Belanger, A., Kapfer, B., Vassort, G. and Armand, M. *Solid polymer electrolyte lithium batteries*. Polymer electrolyte reviews. J. R. MacCallum and C. A. Vincent. London ; New York, Elsevier Applied Science. Vol.2, pp.285. (1987).

Gray, F.M. *Solid polymer electrolytes : fundamentals and technological applications*. VCH, New York (1991).

Gray, F.M. *Polymer electrolytes*. Royal Society of Chemistry, Cambridge (1997).

Grössinger, R., Duong, G.V. and Sato-Turtelli, R. "The physics of magnetoelectric composites". *Journal of Magnetism and Magnetic Materials*, Vol.320 (14), pp.1972-1977 (2008).

Hashin, Z. "The elastic moduli of heterogeneous materials". *Journal of Applied Mechanics*, Vol.29 pp.143-150 (1962).

Hom, C.L., Pilgrim, S.M., Shankar, N., Bridger, K., Massuda, M. and Winzer, S.R. "Calculation of quasi-static electromechanical coupling coefficients for electrostrictive ceramic materials". *IEEE Transactions on Ultrasonics, Ferroelectrics and Frequency Control*, Vol.41 (4), pp.542-551 (1994).

Jaffe, B., Cook, W.R. and Jaffé, H.L.C. *Piezoelectric ceramics*. Academic Press,

London (1971).

Kar-Gupta, R. and Venkatesh, T.A. "Electromechanical response of 1-3 piezoelectric composites: An analytical model". *Acta Materialia*, Vol.55 (3), pp.1093-1108 (2007).

Kirk, R.E. and Othmer, D.F. *Kirk-Othmer encyclopedia of chemical technology*. Vol.19, (1991).

Lam, K.S., Wong, Y.W., Tai, L.S., Poon, Y.M. and Shin, F.G. "Dielectric and pyroelectric properties of lead zirconate titanate/polyurethane composites". *Journal of Applied Physics*, Vol.96 (7), pp.3896-3899 (2004).

Marcos, J.I., Orlandi, E. and Zerbi, G. "Poly(ethylene oxide)-poly(methyl methacrylate) interactions in polymer blends: an infra-red study". *Polymer*, Vol.31 (10), pp.1899-1903 (1990).

Mathot, V.B.F. and Benoist, L. *Calorimetry and thermal analysis of polymers*. Hanser, Munich (1994).

McCrum, N.G., Read, B.E. and Williams, G. *Anelastic and dielectric effects in polymeric solids*. John Wiley & Sons, London (1967).

Nan, C.W., Bichurin, M.I., Dong, S., Viehland, D. and Srinivasan, G. "Multiferroic magnetoelectric composites: Historical perspective, status, and future directions". *Journal of Applied Physics*, Vol.103 (3), pp.031101 (2008).

Nan, C.W., Cai, N., Liu, L., Zhai, J., Ye, Y. and Lin, Y. "Coupled magnetic--electric properties and critical behavior in multiferroic particulate composites". *Journal of Applied Physics*, Vol.94 (9), pp.5930-5936 (2003).

Nan, C.W., Liu, L., Cai, N., Zhai, J., Ye, Y., Lin, Y.H., Dong, L.J. and Xiong, C.X. "A three-phase magnetoelectric composite of piezoelectric ceramics, rare-earth iron alloys, and polymer". *Applied Physics Letters*, Vol.81 (20), pp.3831-3833 (2002).

Natesan, B., Karan, N.K., Rivera, M.B., Aliev, F.M. and Katiyar, R.S. "Segmental

relaxation and ion transport in polymer electrolyte films by dielectric spectroscopy". *Journal of Non-Crystalline Solids*, Vol.352 (42-49), pp.5205-5209 (2006).

Physik_Instrumente

<http://www.physikinstrumente.com/en/products/prdetail.php?sortnr=400600.00>.
(2008).

Piezo_Kinetics *Manufacturer's data sheet*. (2007).

Ploss, B., Ploss, B., Shin, F.G., Chan, H.L.W. and Choy, C.L. "Pyroelectric activity of ferroelectric PT/PVDF-TRFE". *Ieee Transactions on Dielectrics and Electrical Insulation*, Vol.7 (4), pp.517-522 (2000).

Poon, Y.M. and Shin, F.G. "A simple explicit formula for the effective dielectric constant of binary 0-3 composites". *Journal of Materials Science*, Vol.39 (4), pp.1277-1281 (2004).

Reitz, J.R. and Milford, F.J. *Foundations of electromagnetic theory*. Addison-Wesley Pub. Co., Reading, Mass., (1960).

Riande, E. *Electrical properties of polymers*. Marcel Dekker, New York (2004).

Ryu, J., Priya, S., Uchino, K. and Kim, H.-E. "Magnetolectric Effect in Composites of Magnetostrictive and Piezoelectric Materials". *Journal of Electroceramics*, Vol.8 (2), pp.107-119 (2002).

Scrosati, B. *Applications of electroactive polymers*. Chapman & Hall, London (1993).

Shi, Z., Nan, C.W., Liu, J.M., Filippov, D.A. and Bichurin, M.I. "Influence of mechanical boundary conditions and microstructural features on magnetolectric behavior in a three-phase multiferroic particulate composite". *Physical Review B (Condensed Matter and Materials Physics)*, Vol.70 (13), pp.134417-134416 (2004).

Shukla, J.P. and Gupta, M. "Electrical-Conductivity of Some Amorphous Polymers". *Indian Journal of Pure & Applied Physics*, Vol.25 (5-6), pp.242-244 (1987).

Sigma-Aldrich *Specification Sheet*. (2007).

Skinner, D.P., Newnham, R.E. and Cross, L.E. "Flexible composite transducers". *Materials Research Bulletin*, Vol.13 (6), pp.599-607 (1978).

Smith, A.L. *Applied infrared spectroscopy: fundamentals, techniques, and analytical problem-solving*. Wiley, New York (1979).

Son, Y.H., Kweon, S.Y., Kim, S.J., Kim, Y.M., Hong, T.W. and Lee, Y.G. "Fabrication and Electrical Properties of PZT-PVDF 0-3 Type Composite Film". *Integrated Ferroelectrics*, Vol.88 (1), pp.44 - 50 (2007).

Stephan, M.A. and Nahm, K.S. "Review on composite polymer electrolytes for lithium batteries". *Polymer*, Vol.47 (16), pp.5952-5964 (2006).

Stuart, B. and Ando, D.J. *Modern infrared spectroscopy*. Published on behalf of ACOL (University of Greenwich) by Wiley, Chichester, England (1996).

Takahashi, Y., Sumita, I. and Tadokoro, H. "Structural studies of polyethers. IX. Planar zigzag modification of poly(ethylene oxide)". *Journal of Polymer Science: Polymer Physics Edition*, Vol.11 (11), pp.2113-2122 (1973).

Takahashi, Y. and Tadokoro, H. "Structural Studies of Polyethers, $-(\text{CH}_2)_m\text{-O}-$ n. X. Crystal Structure of Poly(ethylene oxide)". *Macromolecules*, Vol.6 (5), pp.672-675 (1973).

Van den Boomgaard, J., Van Run, A.M.J.G. and Van Suchtelen, J. "Magnetoelectricity in Piezoelectric-Magnetostrictive Composites". *Ferroelectrics*, Vol.10 pp.295-298 (1976).

Wagner, A. and Kliem, H. "Dispersive ionic space charge relaxation in solid polymer electrolytes. I. Experimental system polyethylene oxide". *Journal of Applied Physics*, Vol.91 (10), pp.6630-6637 (2002).

Wan, J.G., Liu, J.M., Chand, H.L.W., Choy, C.L., Wang, G.H. and Nan, C.W.

"Giant magnetoelectric effect of a hybrid of magnetostrictive and piezoelectric composites". *Journal of Applied Physics*, Vol.93 (12), pp.9916-9919 (2003).

Wong, C.K. and Shin, F.G. "Effect of electrical conductivity on poling and the dielectric, pyroelectric and piezoelectric properties of ferroelectric 0-3 composites". *Journal of Materials Science*, Vol.41 (1), pp.229-249 (2006).

Wong, C.K. and Shin, F.G. "Effect of inclusion deformation on the magnetoelectric effect of particulate magnetostrictive/piezoelectric composites". *Journal of Applied Physics*, Vol.102 (6), pp.063908 (2007).

Wong, C.K., Wong, Y.W. and Shin, F.G. "Effect of interfacial charge on polarization switching of lead zirconate titanate particles in lead zirconate titanate/polyurethane composites". *Journal of Applied Physics*, Vol.92 (7), pp.3974-3978 (2002).

Zeng, R., Kwok, K.W., Chan, H.L.W. and Choy, C.L. "Longitudinal and transverse piezoelectric coefficients of lead zirconate titanate/vinylidene fluoride-trifluoroethylene composites with different polarization states". *Journal of Applied Physics*, Vol.92 (5), pp.2674-2679 (2002).

Zhou, J.P., He, H.C., Shi, Z., Liu, G. and Nan, C.W. "Dielectric, magnetic, and magnetoelectric properties of laminated $\text{PbZr}_{0.52}\text{Ti}_{0.48}\text{O}_3/\text{CoFe}_2\text{O}_4$ composite ceramics". *Journal of Applied Physics*, Vol.100 (9), pp.094106-094106 (2006).

Zhou, Y. and Shin, F.G. "Magnetoelectric effect of mildly conducting magnetostrictive/piezoelectric particulate composites". *Journal of Applied Physics*, Vol.100 (4), pp.043910 (2006).